NAVAL POSTGRADUATE SCHOOL
Monterey, California

THESIS

EFFECT OF STRAIN AND STRAIN RATE ON THE MICROSTRUCTURE OF A SUPERPLASTICALLY DEFORMED Al-10%Mg-0.1%Zr ALLOY

by

Mark Edward Alcamo

June 1985

Thesis Advisor: T. R. McNelley

Approved for public release; distribution unlimited.

NAVAL POSTGRADUATE SCHOOL
Monterey, California

THESIS

EFFECT OF STRAIN AND STRAIN RATE ON THE MICROSTRUCTURE OF A SUPERPLASTICALLY DEFORMED Al-10%Mg-0.1%Zr ALLOY

by

Mark Edward Alcamo

June 1985

Thesis Advisor: T. R. McNelley

REPORT DOCUMENTATION PAGE

READ INSTRUCTIONS BEFORE COMPLETING FORM

1. REPORT NUMBER

2. GOVT ACCESSION NO.

3. RECIPIENT'S CATALOG NUMBER

4. TITLE (and Subtitle)
Effect of Strain and Strain Rate on the Microstructure of a Superplastically Deformed Al-10%Mg-0.1%Zr Alloy

5. TYPE OF REPORT & PERIOD COVERED
Engineer's Thesis; June 1985

6. PERFORMING ORG. REPORT NUMBER

7. AUTHOR(s)
Mark Edward Alcamo

8. CONTRACT OR GRANT NUMBER(s)

9. PERFORMING ORGANIZATION NAME AND ADDRESS
Naval Postgraduate School
Monterey, California 93943-5100

10. PROGRAM ELEMENT, PROJECT, TASK AREA & WORK UNIT NUMBERS

11. CONTROLLING OFFICE NAME AND ADDRESS
Naval Postgraduate School
Monterey, California 93943-5100

12. REPORT DATE
June 1985

13. NUMBER OF PAGES
122

14. MONITORING AGENCY NAME & ADDRESS(if different from Controlling Office)

15. SECURITY CLASS. (of this report)
Unclassified

15a. DECLASSIFICATION/ DOWNGRADING SCHEDULE

16. DISTRIBUTION STATEMENT (of this Report)
Approved for public release; distribution unlimited.

17. DISTRIBUTION STATEMENT (of the abstract entered in Block 20, if different from Report)

18. SUPPLEMENTARY NOTES

19. KEY WORDS (Continue on reverse side if necessary and identify by block number)
Superplasticity
Aluminum Alloys
Aluminum-Magnesium Alloys
Thermomechanical Processing

20. ABSTRACT (Continue on reverse side if necessary and identify by block number)

The deformation characteristics of two thermomechanically processed, high-Magnesium, Aluminum-Magnesium-Zirconium alloys were investigated. The processing included warm rolling at 300°C to 90-95% reduction. Tension testing was done at various temperatures and strain rates and superplastic elongations were observed for both alloys. Subsequently, samples of Al-10%Mg-0.1%Zr were tested at 300°C

to strains ranging from 8% to 267% as well as to fracture. Strain rates of 6.67×10^{-3} S^{-1} and 6.67×10^{-4} S^{-1} were used. These were examined via TEM to observe microstructural changes which occur during deformation. Quantitative analysis of the functional relationship between stress, strain, strain rate, and grain size for this alloy is done in an attempt to fit it's deformation response to current models for superplastic deformation.

Approved for public release; distribution unlimited.

Effect of Strain and Strain Rate on the Microstructure of a Superplastically Deformed Al-10%Mg-0.1%Zr Alloy

by

Mark Edward Alcamo
Lieutenant, U.S. Navy
B.S., U.S. Naval Academy, 1977

Submitted in partial fulfillment of the
requirements for the degrees of

MASTER OF SCIENCE IN MECHANICAL ENGINEERING

and

MECHANICAL ENGINEER

from the

NAVAL POSTGRADUATE SCHOOL
June 1985

ABSTRACT

The deformation characteristics of two thermomechanically processed, high-Magnesium, Aluminum-Magnesium-Zirconium alloys were investigated. The processing included warm rolling at 300°C to 90-95% reduction. Tension testing was done at various temperatures and strain rates and superplastic elongations were observed for both alloys. Subsequently, samples of Al-10%Mg-0.1%Zr were tested at 300°C to strains ranging from 8% to 267% as well as to fracture. Strain rates of 6.67×10^{-3} S^{-1} and 6.67×10^{-4} S^{-1} were used. These were examined via TEM to observe microstructural changes which occur during deformation. Quantitative analysis of the functional relationship between stress, strain, strain rate, and grain size for this alloy is done in an attempt to fit it's deformation response to current models for superplastic deformation.

TABLE OF CONTENTS

LIST OF TABLES

LIST OF FIGURES

ACKNOWLEDGEMENT

I would like to thank my advisor, Professor T. R. McNelley and Dr. E. W. Lee for their expert assistance and guidance in conducting this research, the Naval Air Systems Command and Mr. Richard Schmidt for their financial support and continued interest in superplastic Aluminum alloys. I would also like to acknowledge the two other thesis students, LCDR Thomas Hartmann and LT Dudley Berthold whose research concurrent with this work provided tremendous additional insight into the behavior of this alloy. Finally, I would like to thank Carol Cabanilla, who not only typed and helped me prepare this thesis for submission, but who also gave me support during the research.

I. INTRODUCTION

Superplasticity refers to the ability of certain materials to exhibit elongations of several hundred percent under certain conditions of strain rate and temperature. Examples of superplasticity were published as far back as 1912, when Bengough [Ref. 1] found a "special brass", an α / β brass, which exhibited an elongation of nearly 200% at 700°C. In 1934 Pearson [Ref. 2] demonstrated that certain two phase materials with a fine microstructure could achieve high elongations and because of that work he is often given credit for first demonstrating superplasticity. Two Russians, Bockvar and Sviderskaya [Ref. 3], published results of their extensive work with a superplastic Al-Zn alloy in 1945; there were numerous other articles written prior to 1960, but research of superplasticity was treated as more of a curiosity. Current interest in superplasticity was motivated by Underwood's review in 1962 [Ref. 4] of the work done in the USSR. Since that time considerable research has been done in the area, and elongations well in excess of one thousand percent are common in the literature. Initially, research was centered on structures attained in processing eutectic or eutectoid alloys, such as can be found in the Pb-Sn, Al-Cu, and Cu-Zn systems. It was felt that such compositions were essential to achieve a fine,

equiaxed, two phase microstructure. At elevated temperatures and low strain rates these structures deform by grain boundary sliding and superplastic elongations are frequently achieved, but commercial applications are limited. At room temperature these alloys are often either too brittle or too soft for structural uses. Frequently in two phase systems one of the phases is significantly harder than the other and during superplastic deformation the hard particles do not deform while the matrix does, resulting in cavitation. Additionally, the requirement for a low strain rate made these alloys infeasible for significant commercial use, and so the research was mainly of academic interest. Later, in the sixties and early seventies more focus was given to commercial use of superplastic deformation processes. Instead of finding alloys which displayed spectacular superplastic elongations but were technologically useless, more research was aimed at modifying important existing alloys to become capable of superplastic deformations. Because such materials exhibit a low flow stress as well as superplasticity, they have the potential to form complex shapes with a minimum amount of energy expended. Additionally, the fine microstructure needed for superplasticity at high temperatures is also often a benefit at service conditions; e.g, high strength and a smooth finish [Ref. 5]. Currently, numerous companies, such as Rockwell International [Ref. 6] and Pratt and Whitney [Ref. 7] use

superplastic deformation to manufacture certain components. In fact, in 1981, British Alcan Aluminum created a subsidiary, Superform Metals Limited, to focus on the use of superplastic forming for aluminum components. Certainly, the use of superplastic deformation is far from being in widespread use commercially; but as research continues and a better understanding of the mechanisms involved is gained, there is no doubt it will become a more common fabrication process.

The purpose of this thesis was to investigate the elevated temperature deformation response of two thermomechanically processed (TMP) high-Mg Al-Mg-Zr alloys. Previous research at the Naval Postgraduate School has demonstrated that thermomechanically processed high-Mg Aluminum alloys are capable of high strength with good ductility, and at elevated temperatures superplastic elongations were achieved by several of these alloys. Using transmission electron microscopy, McNelley and Garg [Ref. 8] found that the TMP used gives these alloys a fine microstructure, consisting of cellular or subgrain structures. Although a fine microstructure is considered a prerequisite for superplasticity via grain boundary sliding, conventional theories predict that low-angle subgrain structures such as found in these as-rolled microstructures should not accommodate grain boundary sliding; yet superplastic elongations are observed.

This work initially investigated two alloys: Al-8%Mg-0.1%Zr and Al-10%Mg-0.1%Zr. Tensile tests at room temperature, 250°C, and 300°C were conducted on each of these alloys at strain rates varying from 1.39×10^{-4} S^{-1} to 1.39×10^{-1} S^{-1}. Elongations in excess of 200% were achieved in both alloys. At this point it was decided more thoroughly to investigate the deformation response of the Al-10%Mg-0.1%Zr alloy concurrently with related work by Hartmann [Ref. 9] and Berthold [Ref. 10]. It was also at this time that the test specimen geometry was modified as explained in Chapter III. Tensile tests were then conducted at 300°C to six different strains prior to fracture at strain rates of 6.67×10^{-4} S^{-1} and 6.67×10^{-3} S^{-1}. These samples were examined using transmission electron microscopy (TEM) to observe microstructural changes which occur during deformation. Data obtained from the mechanical testing in conjunction with the TEM work is evaluated and compared with current theories of superplastic behavior.

II. BACKGROUND

There are currently several prominent theories to explain superplastic behavior. They are not in total agreement and none completely explains observed results. However, it is generally agreed there are certain requirements for superplasticity. These include: 1) a fine, equiaxed grain structure wit high angle grain boundaries; 2) a second phase which is comparable in strength to the matrix; 3) high t peratures (> 0.5 Tm); 4) low strain rates (generally < 10^{-2} S^{-1}); and 5) high strain rate sensitivity.

Typically, grain sizes less than 10 μm are required for superplastic behavior. The grain size effect on superplastic flow is generally taken to be of the form

$$\dot{\varepsilon} \propto \frac{D_{eff}}{d^p} f(\sigma) \qquad \text{(Eq. 2.1)}$$

where $\dot{\varepsilon}$ is the strain rate, p is the grain size exponent, d is the grain size during superplastic flow, D_{eff} is the effective diffusion coefficient, and $f(\sigma)$ is a function of flow stress, σ. This equation shows that for a constant $\dot{\varepsilon}$, as d increases, the flow stress must increase. In effect, grain growth during deformation may result in the material "strain hardening" during such superplastic flow. The higher strength would result from the greater diffusion distances

required because of the larger grains. At higher strength levels the mechanisms for superplasticity may no longer hold and dislocation generation, glide and climb become involved in the deformation. This strain hardening, therefore, results in decreased ductility.

Two processes frequently referred to when explaining superplastic behavior are: 1) Nabarro-Herring diffusion creep and 2) Coble diffusion creep. In Nabarro-Herring creep lattice diffusion is the rate-controlling process, $D_{eff} = D_L$ and the grain size exponent $p = 2$. For Coble creep, grain-boundary diffusion is the rate-controlling process, $D_{eff} \propto D_{gb}\, d^{-1}$ and $p = 3$. Neither of these processes adequately describes superplastic behavior, but experimental observations of D_{eff} and p have been made which coincide with these models [Ref. 5].

It is widely believed that the mechanism for superplastic behavior involves grain boundary sliding. This dictates the requirement for smooth, curved, high angle grain boundaries. Low angle subgrain structures (such as results from warm working) do not slide readily under shearing stresses because there is too much coherency in the lattice between subgrains. Grain boundary sliding would require breaking the majority of the bonds between the subgrains. Conventional superplastic theory says such a microstructure should not be superplastic. The vast majority of techniques used to achieve a microstructure capable of superplasticity have as

their last step recrystallization of the material to attain a fine, equiaxed microstructure. However, dynamic recrystallization may also be used. This results when the fine grain size is obtained early during the deformation process by means of coalescence of dislocation structures to form high-angle boundaries, as opposed to prior nucleation and growth of new, strain-free grains [Ref. 11].

A second phase is generally required for superplasticity as a means to inhibit grain growth. Because superplastic forming is done at high temperatures grain growth (resulting in strain hardening and suppression of the superplastic mechanism) must be restrained. A uniformly distributed, fine precipitate will help pin grain boundaries and retard grain growth as shown in the Zener-McLean relationship:

$$d \simeq \frac{4r}{3f} \qquad \text{(Eq. 2.2)}$$

where d is the size of grains whose boundaries are restrained by particles of radius r, and volume fraction, f. As the radius of the precipitate increases the mean distance between them increases, therefore, the finer the particles (assuming they are capable of pinning the grain boundaries), the smaller the grains. Additional alloying with grain refiners is frequently done, especially in aluminum, to inhibit grain growth. The second phase must be strong

enough to pin grain boundaries, but precipitates significantly stronger than the matrix will frequently result in cavitation. This is because the second phase does not deform with the matrix, and consequently cavities form at interphase boundaries. These may coalesce and cause fracture, or if they do not cause fracture their presence will greatly degrade the mechanical properties of the material. Because of this, cavitation in superplastic forming is of great concern and is currently undergoing much further study. Cavitation is generally reduced as the grain size is decreased [Ref. 12]. The presence of a finely distributed second phase is therefore necessary to prevent grain growth and stabilize the microstructure but it should be deformable with the matrix to prevent cavitation.

Superplastic deformation is a thermally activated process and will not occur readily until $T > 0.5T_m$. Diffusion controls the rate of deformation, and diffusion coefficients, having an exponential temperature dependence, are not sufficiently large except at relatively high temperatures. At such temperatures various creep mechanisms, all involving diffusion, become possible modes of deformation. The strain rate imposed in a stress-strain test must be low to give time for superplastic mechanisms to work. At higher strain rates, and therefore higher stresses, dislocation creep may become the controlling deformation mechanism.

Because plastic deformation is a thermally activated process, the flow stress at elevated temperatures is a function of strain, temperature, and also strain rate. A power law equation is often used to relate the flow stress (σ) to strain rate ($\dot{\varepsilon}$):

$$\sigma = k\dot{\varepsilon}^{m} \qquad \text{(Eq. 2.3)}$$

where k is a material and temperature dependent constant and m is the strain rate sensitivity coefficient. The value of m changes with temperature, strain, and strain rate. This expression has become prevalent in the literature to explain and predict superplastic behavior. The exponent m can be found as the instantaneous slope from a plot of log stress vs. log strain rate. It is generally felt such a plot should have a sigmoidal shape, with the three distinct regions resulting from three different mechanisms of deformation. It has been found that superplastic behavior may be observed for m values from 0.3 to 0.9. The higher the m value, the greater the elongation expected. (An m value of 1.0 would be a Newtonian fluid and would be perfectly superplastic.) The strain rate sensitivity coefficient can be thought of as a measure of the material's ability to resist further necking once it has started. The necking region can be thought of as a smaller tensile specimen in itself. With the necking localized within a small region the effective strain rate within that region is higher than for the sample

as a whole. With a high m value the increased strain rate $\dot{\varepsilon}$ will result in a higher flow stress for deformation within that region and if the necking region has hardened enough, further deformation will occur in another region. The larger the m value the longer the necking instability can be extended.

Figure 2.1 shows the three regions generally thought to be present during high temperature deformation. Region I is not always observed experimentally and some argue that it does not exist. There are generally three viewpoints concerning Region I [Ref. 13]:

1. It is actually an extension of Region II but due to grain growth there is an apparent change from Region II.
2. Region I represents the influence of a threshold stress below which no flow occurs.
3. A true change in mechanism occurs.

Region II, with the largest m values, is where the greatest elongations occur. A typical m value reported in the literature is 0.5. This gives a stress-strain rate relationship of

$$\dot{\varepsilon} \propto \sigma^2 \qquad \text{(Eq. 2.4)}$$

This is just rearrangement of the terms of the power law creep equation. The exponent 2 is referred to as 'n' and is simply equal to 1/m. As previously stated, the deformation mechanism in this region is generally accepted to be some form of grain boundary sliding. The most prevalent model to

explain the grain boundary sliding was proposed by Ashby and Verrall. They show the individual grains moving and changing their relative positions by grain boundary sliding with diffusional accommodation. Figure 2.2 [Ref. 14] shows the process. The strain rate equation predicted by their model can be summarized as:

$$\dot{\varepsilon} = K \frac{D_{eff}}{d^2} (\sigma - \sigma_o)^n \qquad \text{(Eq. 2.5)}$$

where n=1 and $D_{eff} \simeq D_L + (\delta/d) \cdot D_{GB}$, $\sigma_o = 0.72\Gamma/d$. δ is the effective cross section of the grain boundary for diffusional creep and Γ is the grain boundary energy of the alloy. From this, p=2 in equation 2.1 when $D_L >> (\delta/d) \cdot D_{GB}$ and p=3 when $(\delta/d) \cdot D_{GB} >> D_L$. This also contains a threshold term associated with extension of the grain boundaries to the point they can slide. A problem here is that for $\sigma >> \sigma_o$, n=1 is generally not observed. The term more frequently observed would be σ^2. When σ is above but near σ_o, the apparent n will still be greater than 1.0, although the $(\sigma - \sigma_o)$ term itself is applicable. Additionally, Nix [Ref. 15] has shown that this type of grain boundary sliding and accommodation cannot be occurring by diffusion processes alone. Because of this, there are several alternate models which focus on grain boundary sliding with slip accommodation which better explain some of the observed phenomenon.

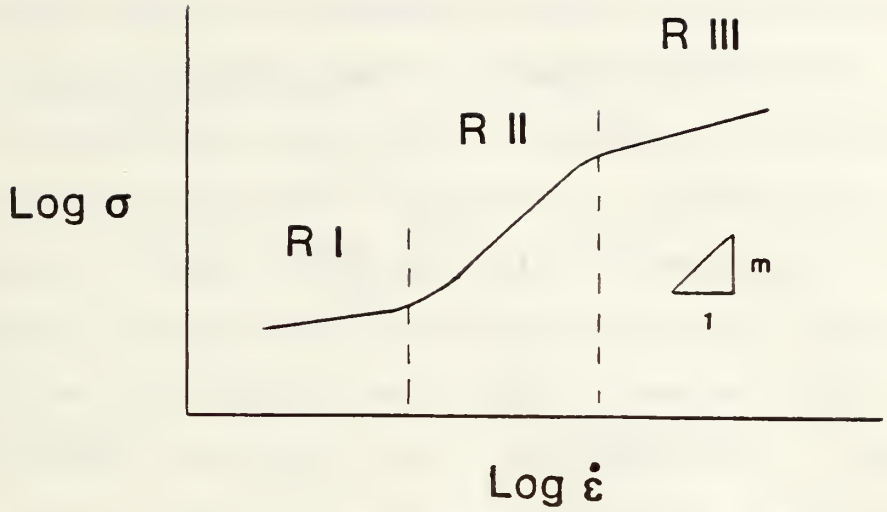

Figure 2.1 Typical plot of log σ vs. log $\dot{\varepsilon}$ obtained from constant strain rate data. In $\sigma = B\dot{\varepsilon}^{m}$, m, the slope, is the strain rate sensitivity coefficient.

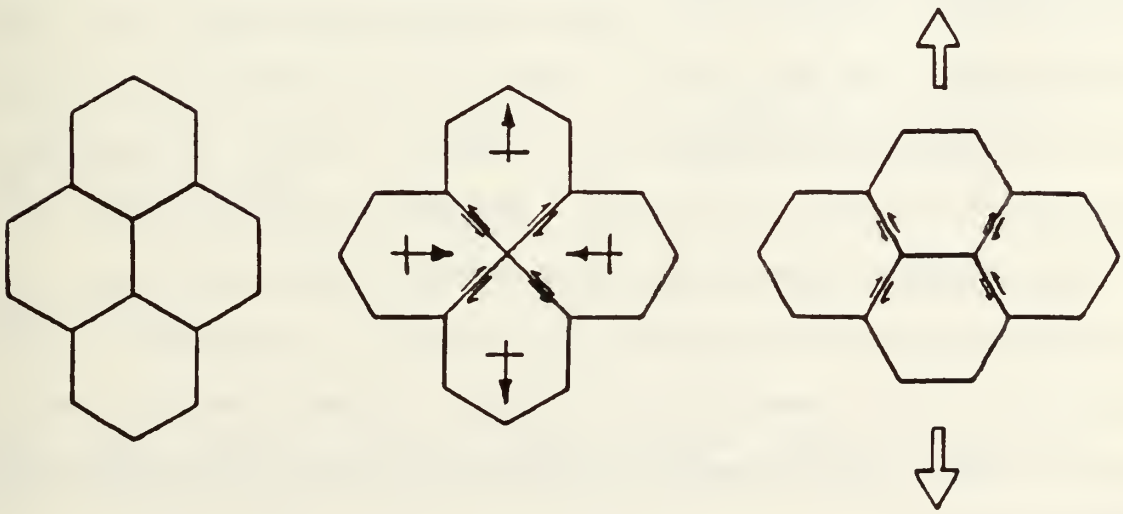

Figure 2.2 Illustration of the Ashby-Verrall model for grain boundary sliding with diffusional accommodation [Ref. 14].

At high stresses in Region III, it is generally accepted that the deformation mode is some form of dislocation creep [Ref. 16]. Grain boundary sliding with diffusional accommodation occurs too slowly to contribute significantly to the total deformation. The dominant dislocation creep mode occurs by dislocation glide and climb aided by vacancy diffusion. The basic theory was formulated by Weertman [Ref. 17]. The result is a lower strain rate sensitivity exponent in this region and the elongations are not as great. Using a power law equation (Eq. 2.3 or equivalently Eq. 2.4), $\dot{\varepsilon} \propto \sigma^n$ where n is around 4 to 5 for dislocation creep in pure metals. Equivalently, this gives a strain rate sensitivity coefficient, m, equal to 0.20 to 0.25. The rate controlling step in this model is dislocation climb. For solid solutions Weertman [Ref. 18] postulated that the solute atoms provide drag on the dislocations and glide becomes the rate controlling mechanism, resulting in an n value of 3. Sherby and Burke [Ref. 19] found, however, that many of the solid solutions they studied exhibited the power law relation formulated for pure metals, with n equal to 4-5. Table I summarizes the various strain rate relationships observed for elevated temperature deformation.

TABLE I

ELEVATED TEMPERATURE DEFORMATION MECHANISMS

$$\dot{\varepsilon} = K_1 \cdot \frac{D_{eff}}{d^p} \sigma^{n_1} + K_2 \cdot D_L \sigma^{n_2}$$

Exponent Values	Mechanism
$n_1 = 1$; $p = 2$	Nabarro-Herring Creep
$n_1 = 1$; $p = 3$	Coble Creep
*$n_1 = 2$; $p = 2$ to 3 ($m = 0.5$)	Grain Boundary Sliding with lattice ($p=2$) or grain boundary ($p=3$) diffusion accommodated
$n_2 \simeq 4\text{-}5$ ($m \simeq 0.20 - 0.25$)	Dislocation Creep for pure metals
$n_2 = 3$ ($m = 0.33$)	for solid solutions

*This most closely reflects the observed mechanism and is best modeled by Ashby and Verrall, except their model has $n_1 = 1$ ($m = 1.0$).

The first term dominates in Region II and can accommodate most of the prevalent models for superplasticity. The second term dominates at higher strain rates, Region III.

A. ALUMINUM MAGNESIUM ALLOYS

Aluminum alloys are technologically significant because they are light in weight, generally corrosion resistant, and have high strength with good ductility. The major alloying elements used with Aluminum are Copper, Silicon, Magnesium, Zinc and Manganese. Some of the more prevalent commercial alloys are the heat treatable Aluminum-Zinc-Magnesium alloys, such as 7075, and the Aluminum-Copper alloys, such as 2024.

Aluminum-Magnesium alloys are significant because Magnesium lowers the density and increases the strength, giving a higher strength to weight ratio. In the Aluminum-Magnesium alloy system the increased strength is mainly attributable to solid solution strengthening and work hardening. At higher Magnesium content precipitation strengthening contributes, but this precipitation should be kept fine and uniformly distributed. The maximum solubility of Magnesium in Aluminum is about 15% at the eutectic temperature of 451°C. The β phase is a relatively hard intermetallic with composition Mg_5Al_8. A problem with the β phase is at high Magnesium concentration it tends to precipitate on the grain boundaries. This creates a Magnesium-depleted zone adjacent to grain boundaries with a resultant microstructure more susceptible to intergranular corrosion and stress-corrosion cracking. Commercially, high strength Aluminum-Magnesium alloys are usually limited

to a Magnesium range of 4-6%. This is a result of the potential for microstructural instability (intergranular precipitation). Additionally, at concentrations near the solubility limit (about 15%) the alloy becomes too brittle for structural applications.

B. HIGH MAGNESIUM ALUMINUM ALLOY WORK AT NPS

Research on high Magnesium-Aluminum-Magnesium alloys began at the Naval Postgraduate School in 1976 when Ness [Ref. 20] tried to improve mechanical properties and refine the microstructure of an 18% Magnesium Aluminum-Magnesium alloy. Research in the thermomechanical processing of various high Magnesium alloys was continued by several students, including Grandon [Ref. 21], Speed [Ref. 22], Bingay [Ref. 23], Chesterman [Ref. 24], Shirah [Ref. 25], Glover [Ref. 26], and Johnson [Ref. 27]. The current thermomechanical processing sequence used for high Magnesium Aluminum-Magnesium alloys at NPS evolved from their research. The steps of the procedure are explained in Chapter III. Included in the processing is a 24-hour solution treatment at 440°C. A higher temperature could result in partial melting and a lower temperature may not result in the entire sample being in the single phase region. The upset forging is done at 440°C to provide hot working and the billet is then returned to 440°C in the furnace for one hour to ensure the entire sample is again isothermal prior

to an oil quench. It was found that the alloys would readily recrystallize if worked at temperatures above the solvus, so warm rolling is done just below the solvus at 300°C. The rolling is done within 24 hours of upset forging and quenching to avoid any possible Magnesium precipitation. Figure 2.3 shows the temperature range of interest in the processing. It wasn't until Becker's work in 1984 [Ref. 28] that these alloys were investigated for their mechanical properties at elevated temperatures and their superplastic response was found. Becker's research was principally with an Al-10%Mg-0.5%Mn alloy which exhibited an elongation of about 400% at 300°C at a strain rate of 1.4×10^{-3} S^{-1}. He also investigated an Al-8%Mg-0.4%Cu alloy which achieved about 300% elongation at 250°C.

Fractional amounts of elements such as Manganese, Copper, and Zirconium are frequently used as grain refiners and to homogenize the microstructure in various aluminum alloys. During deformation at elevated temperatures the particles formed from these elements, $MnAl_6$, $CuMg_4Al_6$, and $ZrAl_3$, act to pin the grain boundaries and prevent grain growth. As stated earlier, grain growth strengthens the material during elevated temperature flow during elevated temperature flow and is detrimental to superplasticity. Mills [Ref. 29] extended Becker's work on the Al-10%Mg-0.5%Mn over a larger temperature range and for more strain rates and found activation energies and strain rate sensitivity

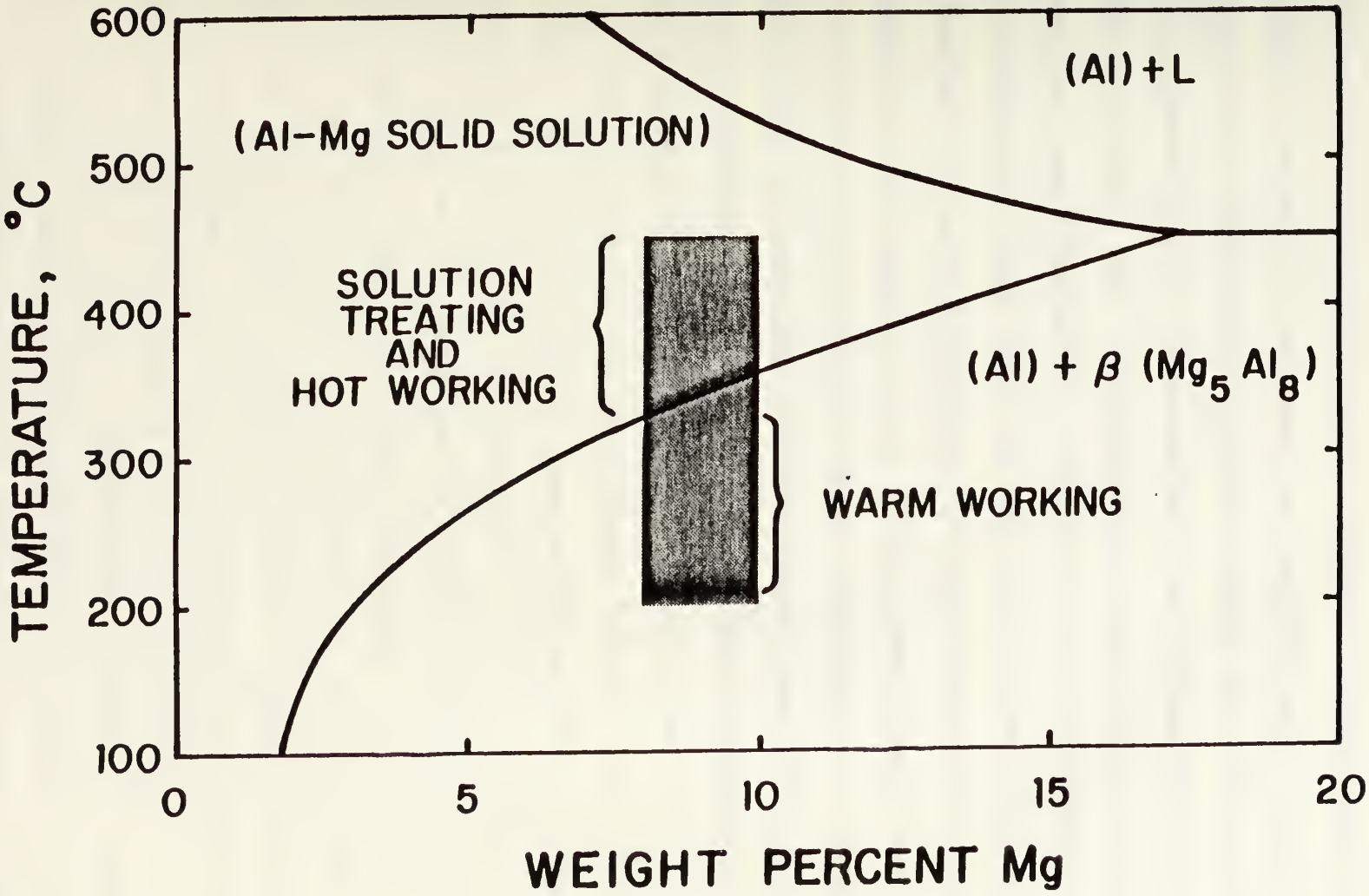

Figure 2.3 Portion of Al-Mg phase diagram showing region where material processing is done.

coefficients consistent with those in the literature. Self [Ref. 30] looked at several Aluminum-Magnesium alloys, including: 8%Mg, 8%Mg-0.4%Cu, 8%Mg-0.4%Cu-0.5%Mn, 10%Mg, 10%Mg-0.4%Cu, and 10%Mg-0.2%Mn. He found the use of Copper on an equal weight percentage as effective as the use of Manganese to promote superplasticity. The primary benefit of Manganese is as a grain refiner whereas Copper homogenizes the microstructure and has some grain refinement ability. Stengel [Ref. 31] continued the work of Becker and Mills on the Al-10%Mg-0.5%Mn alloy by using five different annealing treatments following warm rolling, including: one hour at 200°C, ten hours at 200°C, half hour at 250°C, one hour at 250°C or one hour at 440°C (to recrystallize the material). She found that annealing below the rolling temperature enhanced the superplasticity; with a one hour anneal at 200°C and subsequent testing at 300°C at a strain rate of 5.6×10^{-3} S^{-1} an elongation of 572% was achieved. However, recrystallization strengthened the microstructure and resulted in a decreased ductility. Berthold [Ref. 10] and Hartmann [Ref. 9], concurrently with this work, did extensive research on this Al-10%Mg-0.1%Zr alloy. Berthold concentrated on microstructural aspects, examining the microstructural changes during processing as well as after fracture at various temperatures and strain rates for as-rolled, annealed, and recrystallized samples. Hartmann did extensive mechanical testing at various temperatures and

strain rates for as-rolled, annealed, and recrystallized samples. He also utilized this data to determine activation energies and strain rate sensitivity coefficients.

This work focuses on the behavior of the alloy at 300°C. The variation of the strain rate sensitivity coefficient, m, with strain and strain rate is plotted and reasons for the variation are postulated. Tensile tests to six different elongations prior to fracture are done for two strain rates. The microstructural changes which occur during testing are followed using TEM. From the information gained using microscopy, a correlation is made of how σ , ε , $\dot{\varepsilon}$, d, and m vary with deformation. The data is evaluated as to how well it compares with current models for superplastic deformation mechanisms.

III. EXPERIMENTAL PROCEDURE

A. MATERIAL PROCESSING

The two alloys initially studied in this research were direct-chill cast at the ALCOA Technical Center. The ingots as received measured 152mm (6 in.) in diameter by 1016mm (40 in.) in length. The composition for each alloy is listed below [Ref. 32].

TABLE II

ALLOY COMPOSITION (WEIGHT PERCENT)

Serial Number	Si	Fe	Mg	Zr	Al
S572823	0.01	0.02	8.05	0.13	Balance
S572826	0.02	0.02	9.90	0.09	Balance

Billets of dimension 32mm X 32mm X 95mm (1.25 in. X 1.25 in. X 3.75 in.) were sectioned from the as-cast ingots. Following the procedures developed by Johnson [Ref. 27] and Becker [Ref. 28], these were then solution treated at 440°C for 24 hours, upset forged at 440°C on heated platens to approximately 28mm (1.1 in.), annealed at 440°C for 1 hour and then oil quenched. This hot working reduced the billet by approximately 70%, equivalent to a true strain of about 1.2. Warm rolling was then done at 300°C within 24 hours of upset forging in the manner described by Mills [Ref. 29].

Isothermal rolling was desired so each billet was placed in a furnace for about 30 minutes to heat from room temperature to 300°C before attempting the first pass. The samples were then heated for 8 to 10 minutes between passes to ensure isothermal rolling. Each billet was rolled to a thickness of about 1.8mm (0.07 in.) thickness. This took about 25 passes, resulting in a final warm reduction of approximately 94%, equivalent to a true strain of about 2.75. When the specimen geometry was changed, the sample thickness became 2.0 mm (0.08 in.) resulting in a warm reduction of approximately 92%. Figure 3.1 is a schematic diagram showing the steps in the thermomechanical processing. Figure 3.2 illustrates the processing sequence from ingot to fabricated test specimen.

B. SPECIMEN FABRICATION

For the initial testing of these two alloys the specimens were prepared as described by Becker [Ref. 28]. Each sheet was cut into blanks of dimension 64mm (2.5 in.) long and 14.3mm (0.5625 in.) width and these were endmilled to give gage dimensions of 3.1mm (0.12 in.) width and 15.2mm (0.6 in.) length. This gives a gage width to length ratio of 1 to 5. Figure 3.3 shows this specimen geometry. This design emphasized a gradual specimen shoulder at the ends of the gage section to prevent stress concentrations which could cause premature fracture. Elongations were based on

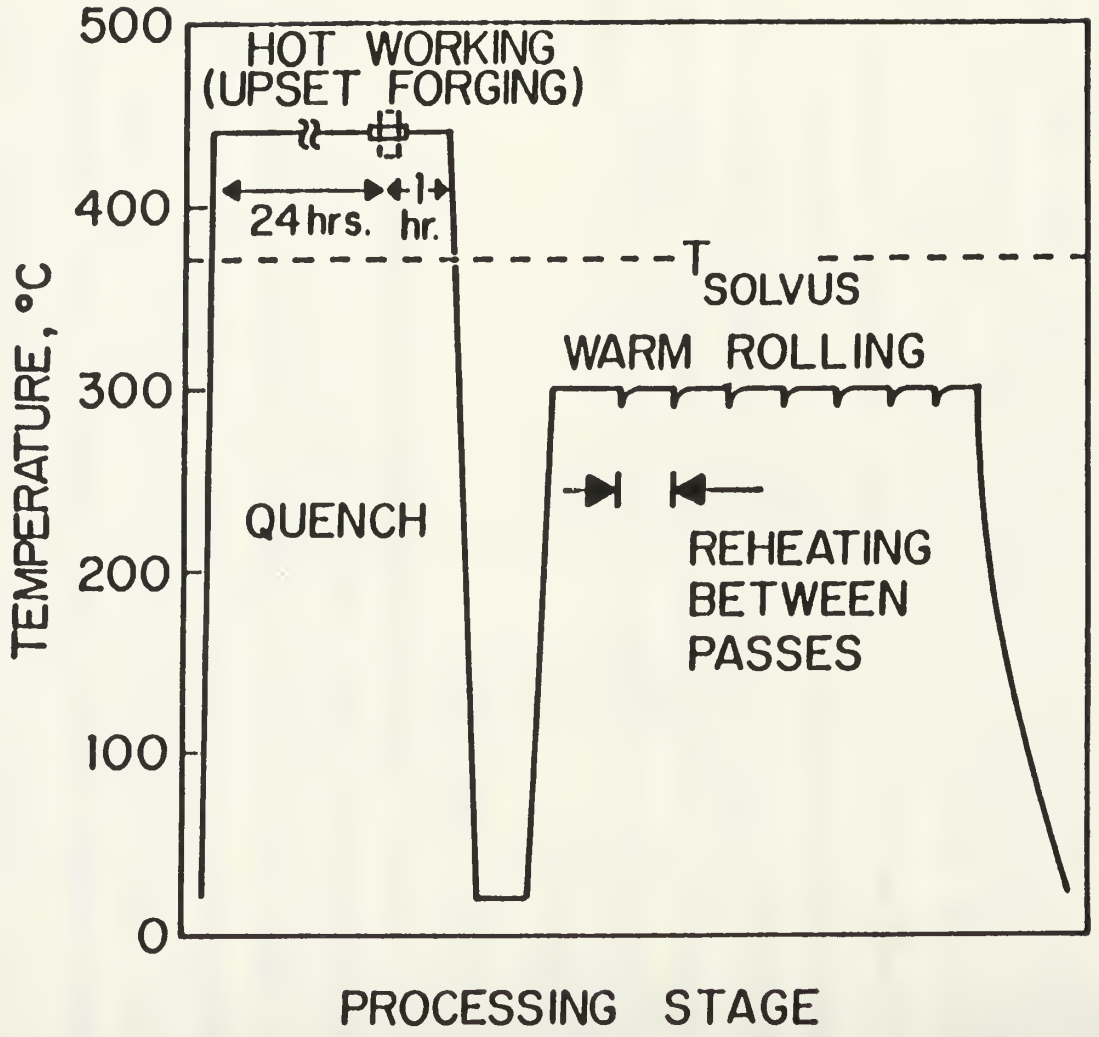

Figure 3.1 Schematic diagram of thermomechanical processing.

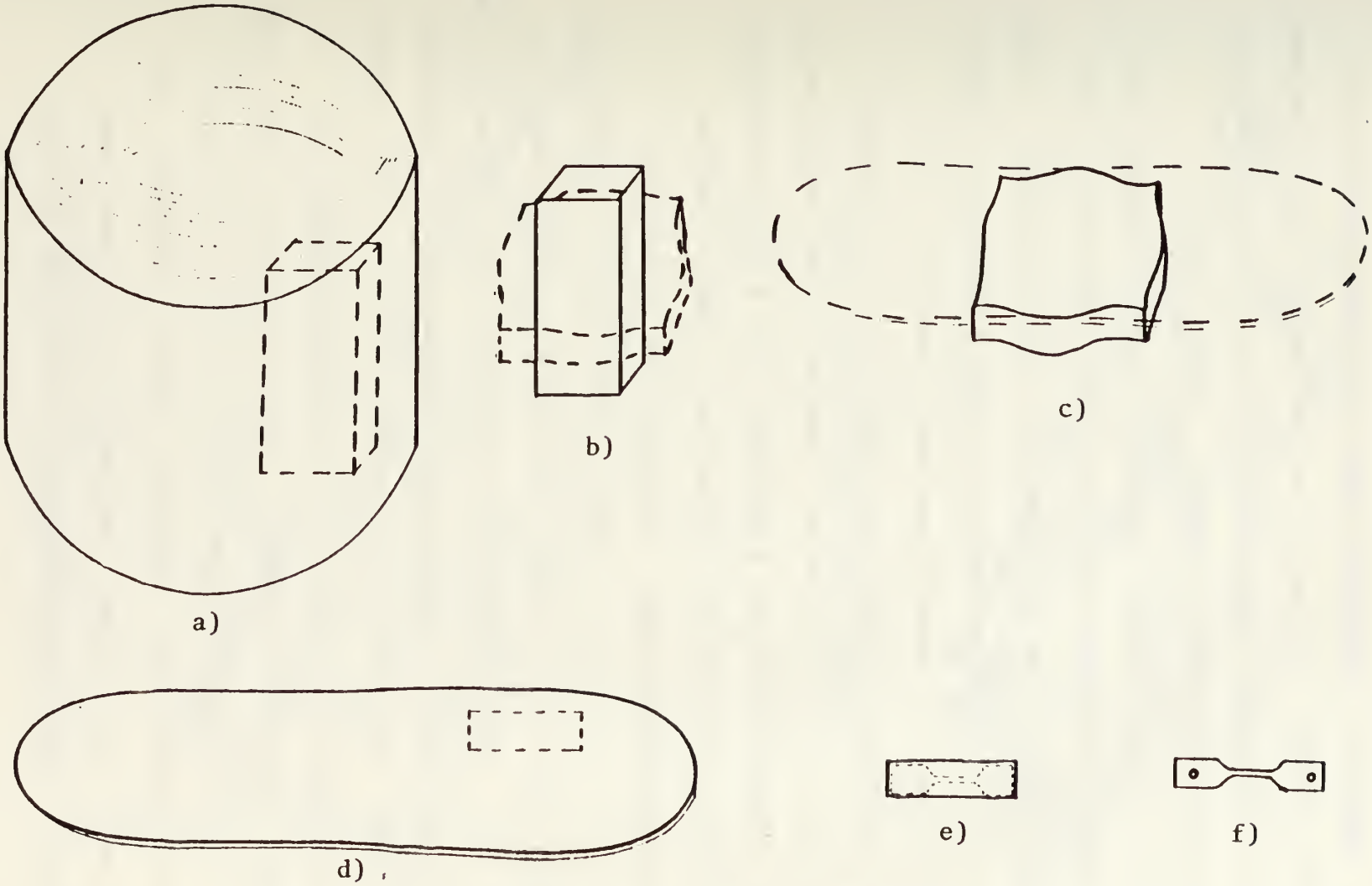

Figure 3.2 Schematic illustration of processing sequence from a) billet cut out of ingot, b) upset forged, c) warm rolled, d) blanks cut out, and e) machined to sample dimension.

a gage length of 15.2mm (0.6 in.), but measurements were taken end to end. Gage marks were not used on the specimens because at elevated temperatures they are not well defined or they may disappear altogether.

After initial testing of these alloys it was decided that further, in depth testing would be done only on the Al-10%Mg-0.1%Zr alloy in conjunction with Hartmann. At this time it was decided to change the sample geometry to make it more comparable to current specimen geometries used for tension testing of superplastic materials. At elevated temperatures the ductility of a sample is less sensitive to stress concentrations and a geometry with a better-defined gage section (sharper shoulders) can be used. The new geometry changed the gage dimensions to 5.1mm (0.20 in.) width and 12.7mm (0.5 in.) length. This gives a gage width to length ratio of 1 to 2.5. The new geometry is shown in Figure 3.4. With this specimen geometry shoulder-to-shoulder measurements before and after testing were used to determine elongations. This eliminated errors in calculations caused by elongation in the tabs of the sample which were not accounted for with the previous sample geometry. Also, with the previous design the samples were milled by the student in sets of 5 on a small Tensilkut machine. However, after the geometry was changed, the sample blanks were taken to the machine shop to be endmilled to the proper specimen

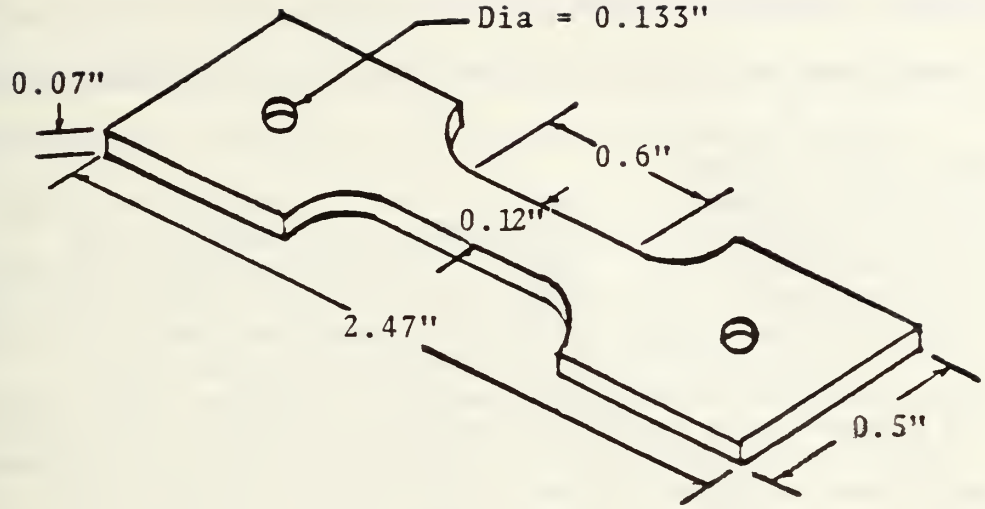

Figure 3.3 Old specimen geometry.

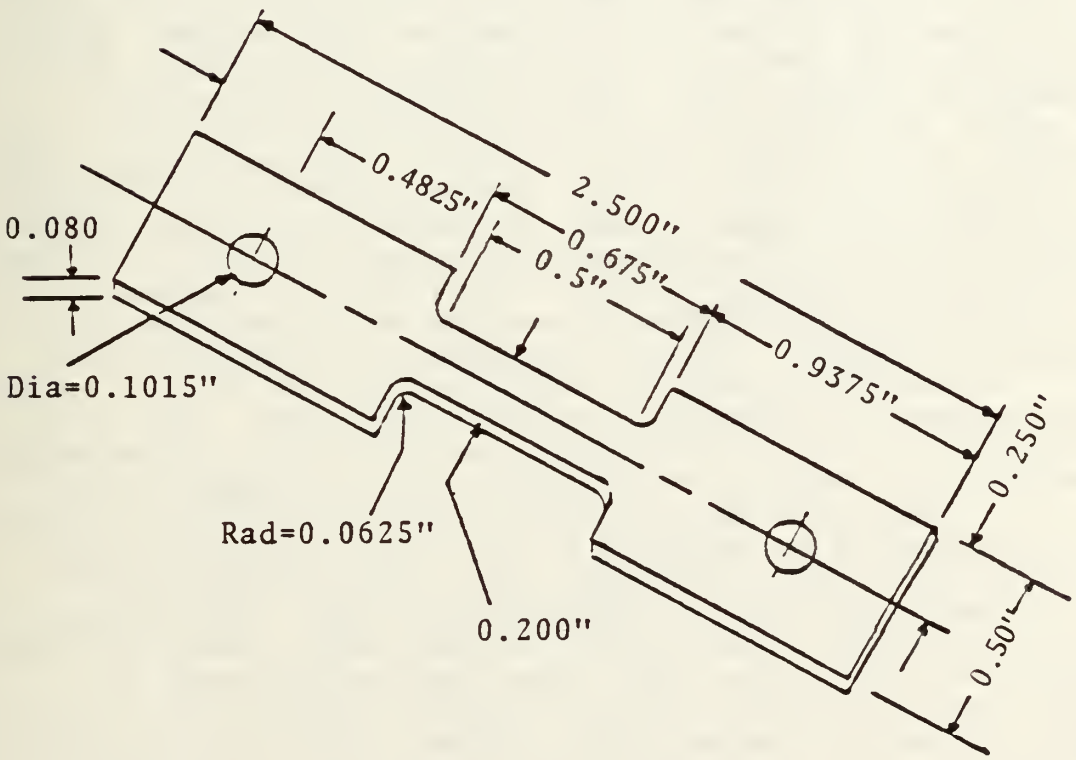

Figure 3.4 New specimen geometry.

dimensions. These specimens were produced to a much closer tolerance than could be achieved with the Tensilkut machine.

C. SPECIMEN TESTING

Initial testing for both alloys was done at room temperature, 250°C, and 300°C, with strain rates from 1.39 X 10^{-1} S^{-1} to 1.39 X 10^{-4} S^{-1}. An electromechanical Instron machine was used for tensile testing; the testing procedure was similar to that described by Self [Ref. 30]. Test specimens were placed in wedge-action grips and held in place by pins passing through the wedges. The wedges were slid into a grip assembly which is screw mounted on pull rods connected to the Instron machine. The wedges, grip assemblies and pull rods were produced by Applied Test Systems, Inc. and are made of Inconel 718 specifically for use at elevated temperatures. Elevated temperature testing was conducted using a Marshall model 2232 three-zone clamshell furnace. Furnace temperature is controlled by three separate controllers, one for each zone. The three thermocouples used for controlling the zone temperatures were brought in through the side of the furnace and had glass fiber insulation wrapped around them. The thermocouple to control the upper zone was located about six inches above the thermocouple entrance point and approximately one inch in from the heating elements. The control thermocouple for the bottom zone was located in a

corresponding location below the entrance point, and the thermocouple for controlling the middle zone was just approximately one inch in from the entrance point.

Additional insulation was used at several locations both inside and outside of the furnace. Glass insulation of one inch thickness was used throughout except where noted. Flue effects were reduced by using insulation mounted inside the furnace at the top and bottom where the pull rods go through, such that the insulation wraps around the pull rods when the furnace is closed. Also, on the outside top and bottom of the furnace ceramic plates were slid in place almost flush around the pull rods after the furnace was closed. Pads of insulation with a slot and hole cut for the pull rods were also placed on the top and bottom of the furnace to help minimize heat loss. Two or three pads were used on top and one pad was used on the bottom; the bottom pad was secured to the furnace by wrapping Nichrome wire around it and the furnace. Thin strips of asbestos-impregnated paper and glass fiber insulation were placed inside the furnace doors on the closing surfaces.

Three thermocouples were installed inside the furnace to directly monitor the specimen temperature. Two thermocouples were brought through the top of the furnace alongside the upper pull rod. Asbestos-impregnated paper and glass fiber insulation was wrapped around the pull rod and thermocouple couple and this was secured with Nichrome wire.

One of these thermocouples was placed in contact with the upper tab of the sample to directly monitor the temperature of the specimen. The second was placed near, but not touching, the middle of the gage section of the sample. The third thermocouple was brought up through the bottom of the furnace and was secured to the bottom pull rod in a similar manner as above. It was placed in contact with the lower tab of the sample. The furnace controllers were adjusted such that these three thermocouples were all within 1% of the desired testing temperature. The furnace was heated for 24 hours prior to conducting a sequence of tests for a given temperature to ensure the temperature had settled out to the desired testing temperature. After a sample was mounted the furnace was closed back up and the three thermocouple temperatures were monitored until they were back within the desired range for testing. It would usually take about one hour for the temperatures to reach equilibrium and then the tensile test would begin. The crosshead speeds ranged from 0.0508mm/min (0.002 in/min) to 127mm/min (5 in/min). For the original specimen geometry this provided strain rates from $5.55 \times 10^{-5}\ S^{-1}$ to $1.39 \times 10^{-1}\ S^{-1}$. For the new specimen geometry this provided strain rates from $6.67 \times 10^{-5}\ S^{-1}$ to $1.67 \times 10^{-1}\ S^{-1}$.

D. DATA REDUCTION

Elongation was determined by measurement of the test specimen before and after tension testing. For the original geometry these measurements were taken end-to-end and a gage length of 15.2mm (0.6 in.) was used to determine elongation.

$$\% \text{ Elongation} = (L_f - L_o) / 0.6$$

$$(L_o = 2.5 \text{ in.})$$

For the new geometry these measurements were taken shoulder-to-shoulder and a gage length of 12.7mm (0.5 in.) was used to determine elongation.

$$\% \text{ Elongation} = (G_f - G_o) / 0.5$$

$$(G_o = 0.625 \text{ in.})$$

The Instron strip chart recorded the applied load (lbs.) vs. chart motion. The magnification ratio between chart speed and crosshead speed varied from 10-100 for these tests. For accurate determination of stress-strain strain behavior, values of 40, 50 or 100 were used.

From the strip chart, raw data points of chart displacement and load were taken from the curve and put in data files to be reduced. A "floating slope" was used on the strip chart from which measurements were taken. This was used to remove such variables as grip adjustment and elasticity of the sample as well as Instron components themselves. The input data file would also have the

magnification factor, the Instron full load scale setting, and the specimen's initial dimensions. A computer program was used to convert this data to engineering stress, engineering strain, true stress, and true strain. The following basic formulas were used:

$$\sigma_{eng} = P/A_o \qquad \text{(Eq. 3.1)}$$

$$e = (L_f - L_o)/L_o \qquad \text{(Eq. 3.2)}$$

$$\sigma_{true} = \sigma_{eng}\,(1 + e) \qquad \text{(Eq. 3.3)}$$

$$\varepsilon = \ln\,(1 + e) \qquad \text{(Eq. 3.4)}$$

where e is engineering strain and ε is true strain and σ_{eng} is engineering stress and σ_{true} is true stress. Since these relationships for true stress and true strain are only valid up until the onset of necking, true stress vs. true strain plots show those points past the onset of necking as a dashed line.

There was routinely a discrepancy between the measured elongation and the elongation computed using the raw data from the strip chart. This discrepancy was as high as 20% in some cases but averaged about 10% difference. Some of the factors contributing to this error were:

1. Deciding on the point of fracture from the strip chart. For the highly superplastic samples the load at fracture was perhaps only a fraction of a pound.
2. Grip seating. The wedges are slid into the grip assembly and as the load increases the wedges could be seated more securely within the grip assembly. The strip chart would record this as elongation of the sample.

3. Elongation of the sample outside of the gage section. The computer reduction was based on a gage length of either 0.6 in. for the original specimen geometry or 0.5 in. for the new geometry. The chart records crosshead movement and cannot distinguish gage length elongation from elongation outside the gage length.

After the geometry was changed it was decided to adjust the computer reduced data to coincide exactly with the measured elongation. This was accomplished with a simple correction factor which equaled the ratio of measured elongation to computed elongation. A typical value for this correction factor would be 0.900. The correction was accomplished with a simple computer program.

E. COMPUTER PROGRAMS

Data reduction programs were written in Fortran and were run on the IBM 3033 at the Naval Postgraduate School. All plotting was accomplished using EASYPLOT, an interactive computer plotting routine available on the IBM 3033. The programs used to reduce and correct the raw data along with sample input data files are included in Appendix C.

F. METALLOGRAPHY

Using transmission electron microscopy a comparison done of microstructures at various strains prior to fracture (approximately 8%, 14%, 20%, 45%, 160%, and 260%) for strain rates of $6.67 \times 10^{-4}\ S^{-1}$ and $6.67 \times 10^{-3}\ S^{-1}$. Gage sections of the specimens were polished using 240 to 600 grit paper to a thickness of about .254mm (0.01 in.). Discs of 3mm

diameter were punched out and these were electro-polished using a TENUPOL 2 polisher. An electrolytic solution of two parts methanol and one part nitric acid maintained at about -20°C was used to thin the specimen. The samples were thoroughly rinsed in methanol after thinning. Microscopy was done on a JEOL (JEM-100 CX II) Electron Microscope. Kodak Electron Microscope film 4487 was used.

G. GRAIN SIZE DETERMINATION

Grain sizes were determined by using the mean-linear-intercept ($\bar{L}$) method. An 8 cm X 8 cm grid was used with micrographs with a magnification of 5000 diameters. Equation 3.5 was used to determine the mean intercept length.

$$\bar{L} = \frac{1}{N_L} \qquad \text{(Eq. 3.5)}$$

where $\bar{L}$ is the mean intercept length and N_L is the number of intercepts of grain boundaries or substructure per unit length of test line [Ref. 33]. Measurements from one to three micrographs representative of the specimen were used to determine an average $\bar{L}$.

IV. RESULTS AND DISCUSSION

A. INITIAL MECHANICAL TEST RESULTS

Tensile testing was done as described in Chapter III on the Al-8%Mg-0.1%Zr and Al-10%Mg-0.1%Zr alloys, processed by warm rolling, and stress-strain data was obtained. Tables III and IV summarize the data obtained for these two alloys. Appendix A contains a complete set of plots for engineering stress vs. engineering strain and true stress vs. true strain for these alloys.

Both the 8% and the 10% alloys show good room temperature properties and ductilities are about 10% for each. This is considered sufficient for most applications of high-strength Aluminum and is comparable to the superplastic Al-Mg-Cu alloys previously researched at NPS. It is a significant improvement over the 3-4% ductilities exhibited by the superplastic Al-Mg-Mn alloys studied previously. Ductilities of less than 5% indicate in sufficient toughness for most applications. It has been reported that Copper additions to high strength Al-Mg alloys are less desirable because of an increase in susceptibility to pitting corrosion. The ultimate tensile strength of each of these alloys is about 450 MPa which is comparable to all the alloys previously researched. Overall, there is little significant difference in room temperature response of these two alloys.

TABLE III MECHANICAL TEST DATA OF Al-8%Mg-0.1%Zr ALLOY

Temp (C)	Strain Rate (sec^{-1})	UTS (MPA)	True Strain at 0.1 True Plastic Strain (MPA)	Ductility (Percent Elong.)
20	1.39×10^{-2}	427.2	426.3	12.3
	1.39×10^{-3}	467.6	*	9.5
250	1.39×10^{-1}	228.8	226.1	33.0
	1.39×10^{-2}	205.1	204.3	54.5
	1.39×10^{-3}	131.7	131.1	141.8
	1.39×10^{-4}	86.5	83.2	161.0
300	1.39×10^{-1}	169.8	161.3	46.2
	1.39×10^{-2}	125.8	125.7	118.3
	1.39×10^{-3}	82.2	78.7	181.7
	1.39×10^{-4}	45.4	40.4	223.8

*Specimen fractured prior to 0.1 true strain.

TABLE IV MECHANICAL TEST DATA OF Al-10%Mg-0.1%Zr ALLOY

Temp (C)	Strain Rate (sec^{-1})	UTS (MPA)	True Stress at 0.1 True Plastic Strain (MPA)	Ductility (Percent Elong.)
20	1.39×10^{-2}	456.6	448.9	11.7
	1.39×10^{-3}	450.6	*	9.5
250	1.39×10^{-1}	218.9	216.4	69.0
	1.39×10^{-2}	155.4	153.7	112.2
	1.39×10^{-3}	103.4	101.3	163.3
	1.39×10^{-4}	39.3	34.8	219.2
300	1.39×10^{-1}	157.6	147.7	123.8
		145.2	143.8	98.3
		141.4	132.5	48.3
	1.39×10^{-2}	85.5	83.2	288.7
		90.9	86.3	177.0
	5.56×10^{-3}	65.9	59.8	345.0
		71.0	69.1	140.5
	1.39×10^{-3}	48.7	46.2	331.7
		42.2	38.0	301.7
		46.8	45.1	201.7
		45.6	38.1	199.0
	5.56×10^{-4}	30.1	28.7	442.7
		36.4	32.2	312.5
	1.39×10^{-4}	17.4	16.4	298.8
		23.0	18.7	266.2
		23.8	18.1	230.0

In view of the TMP used on these alloys, it is not surprising these alloys exhibit such similar room temperature characteristics. As previously stated, the main strengthen-ing mechanisms for these alloys is solid solution strengthening and work hardening which comes from warm rolling to about 94% reduction or 2.75 true strain. Figure 4.1 from McNelley and Garg [Ref. 8] shows that as the true strain increases the amount of Magnesium in solution decreases until it reaches the solubility limit of about 7% for the 300°C rolling temperature. Although this figure illustrates results for a 10% Mg alloy, there is undoubtedly a similar pattern for an 8% alloy. Therefore, both alloys would have about the same amount of Magnesium in solution and both have experienced about the same amount of strain hardening from the rolling procedure. Using the lever rule it is found the 8% alloy should have about 3.5 weight pct. of β phase, while the 10% alloy has about 10.5 weight pct. of β phase. Because of the TMP used there is little strengthening from the β precipitation.

At elevated temperatures the ductility of the 10% Magnesium alloy is clearly superior to that of the 8% alloy. While an elongation of over 200% was achieved by the 8% alloy at 300°C, the 10% alloy exhibited in excess of 300% ductility at 300°C and at a strain rate ten times faster (1.39×10^{-3} vs. 1.39×10^{-4} S^{-1}). Figures 4.2 through 4.7 summarize the mechanical test data for these two alloys.

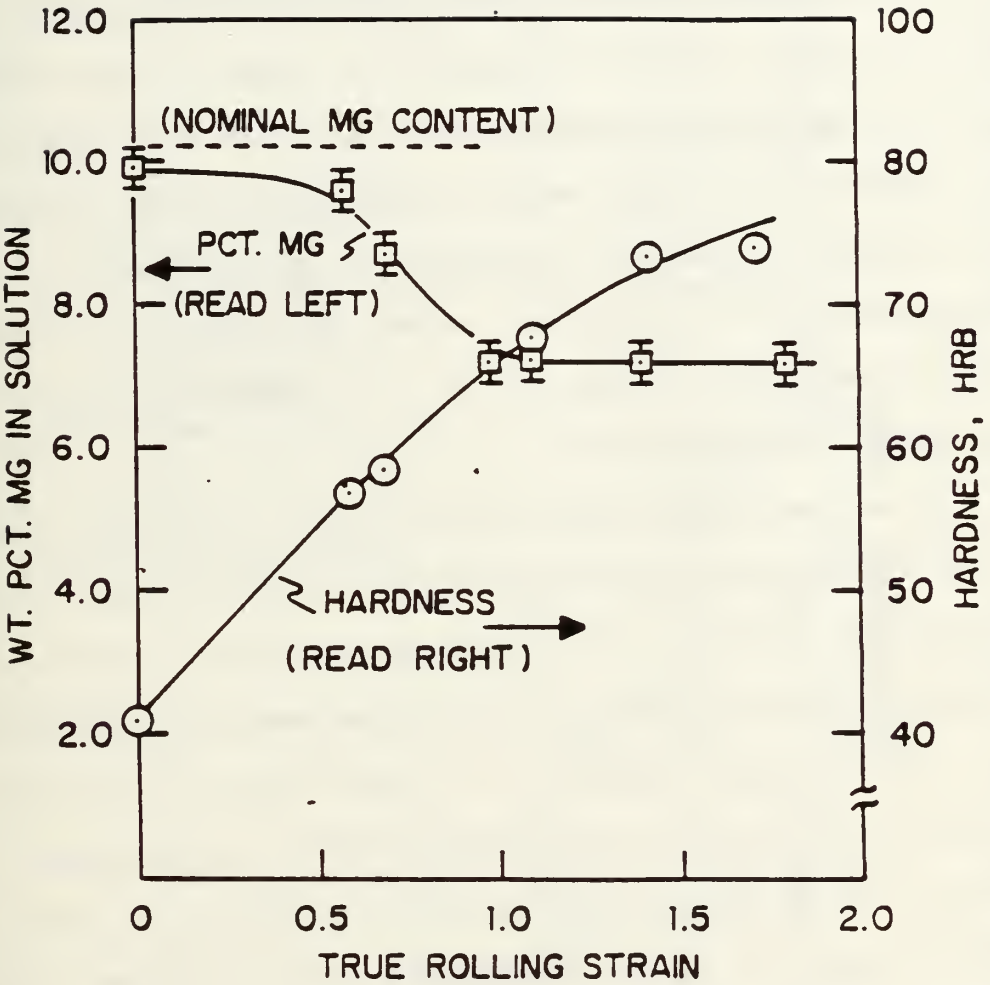

Figure 4.1 Weight percent Mg in solution vs. true rolling strain for Al-10%Mg binary alloy, showing increase in hardness and precipitation of Mg from solution during warm rolling at 300°C. From McNelley and Garg [Ref. 8].

Figures 4.2 and 4.3 are true stress vs. true strain plots at 300°C for these alloys. Figures 4.4 and 4.5 plot ductility data for these materials at 250°C and 350°C while 4.6 and 4.7 plot stress vs. strain rate data corresponding to the ductility data. In this temperature regime, the lower Mg alloy (8% Mg) is both stronger and less ductile. Both as well exhibit an initial strain hardening during deformation. This initial hardening is thought to result from an unstable microstructure in both cases, where the grain size increases during deformation (refer to Eq. 2.1, $1/d^p$ dependence predicted for Region II).

The decreased strength and increased ductility attained in the 10% Mg alloy compared to the 8% Mg material is consistent with previous work by Becker and Self. This is thought to arise from the differing amounts of the intermetallic β (Mg_5Al_8) available to stabilize the structure against grain growth during deformation. If, as noted previously, the Mg content of the solid solution is the equilibrium value for 300°C, then there will be lesser volume fraction of β in the 8% alloy. Hence, grain structure will tend to be more coarse with higher strength and lesser extent of Region II, again as indicated by equation 2.1.

The importance of the Zirconium addition is not clear at this point. The Zirconium is non-uniformly distributed as found by Berthold. Interaction between the β_{Zr} ($ZrAl_3$) and the β_{Mg} (Mg_5Al_8), the efectiveness of the β_{Zr} in

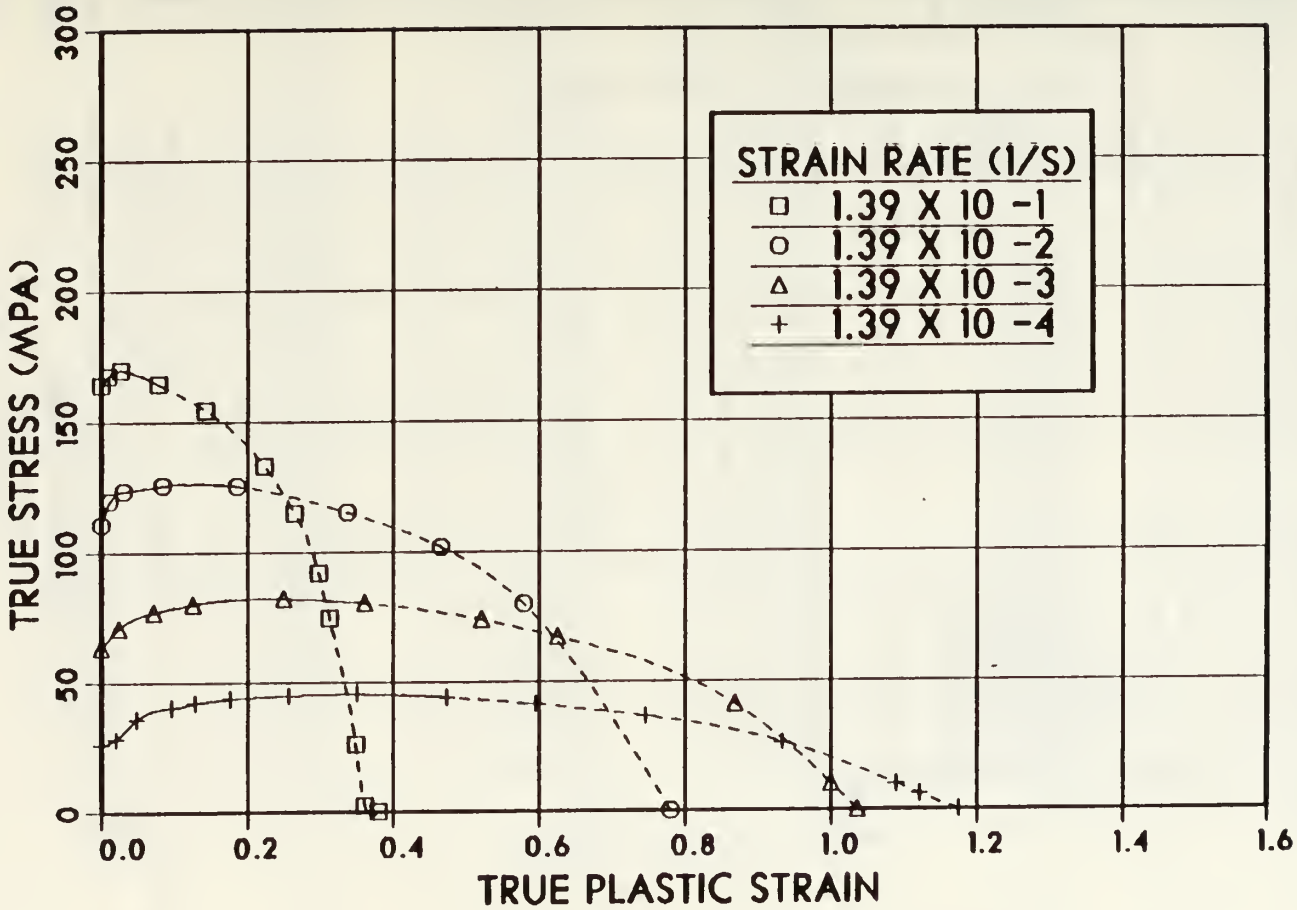

Figure 4.2 True stress vs. true plastic strain for tests conducted at 300°C on Al-8%Mg-0.1%Zr. Solution treated, hot worked, oil quenched, and warm rolled at 300°C to 94% reduction. Dashed lines indicate straining beyond the onset of necking.

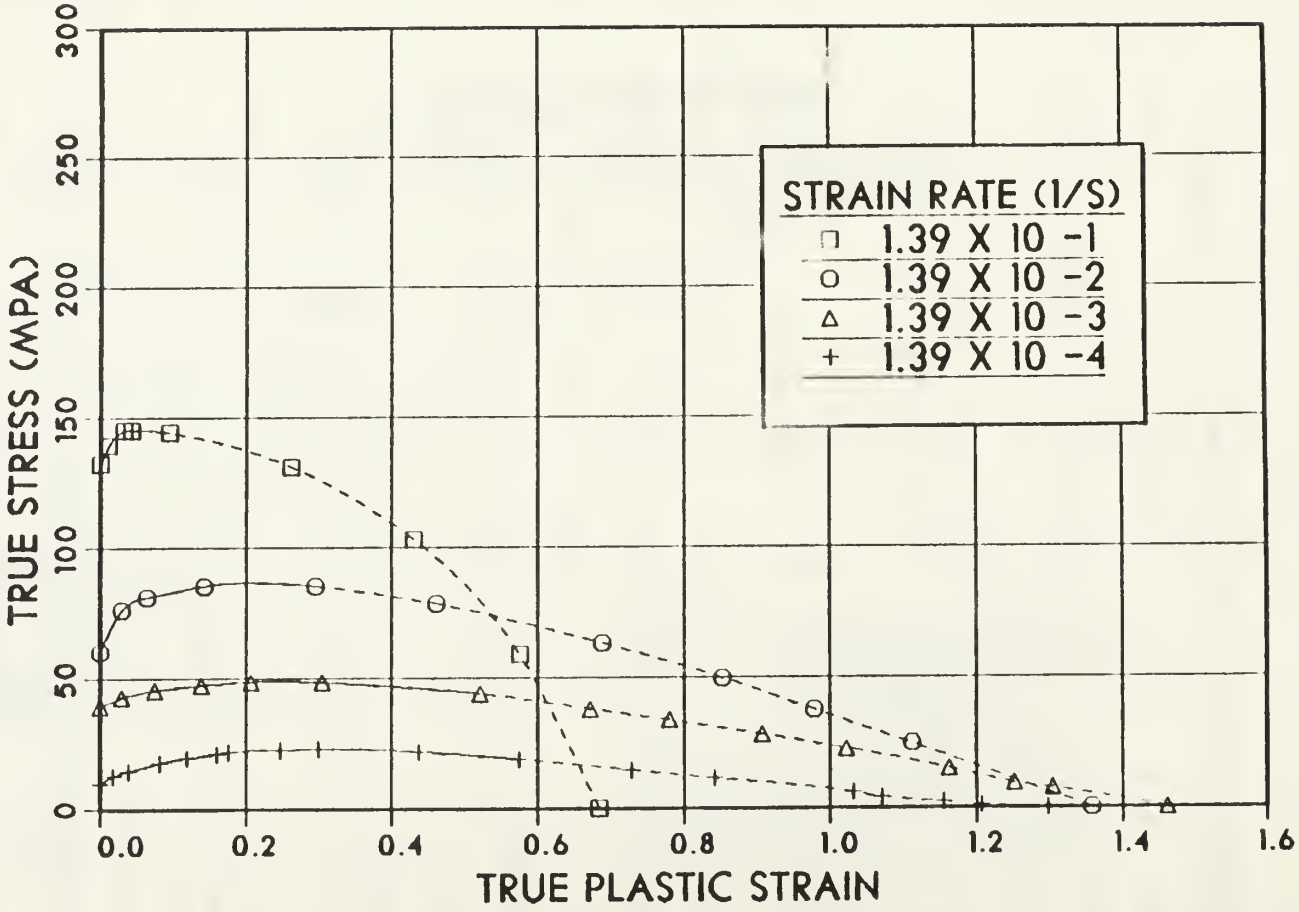

Figure 4.3 True stress vs. true plastic strain for tests conducted at 300°C on Al-10%Mg-0.1%Zr. Solution treated, hot worked, oil quenched, and warm rolled at 300°C to 94% reduction. Dashed lines indicate straining beyond the onset of necking.

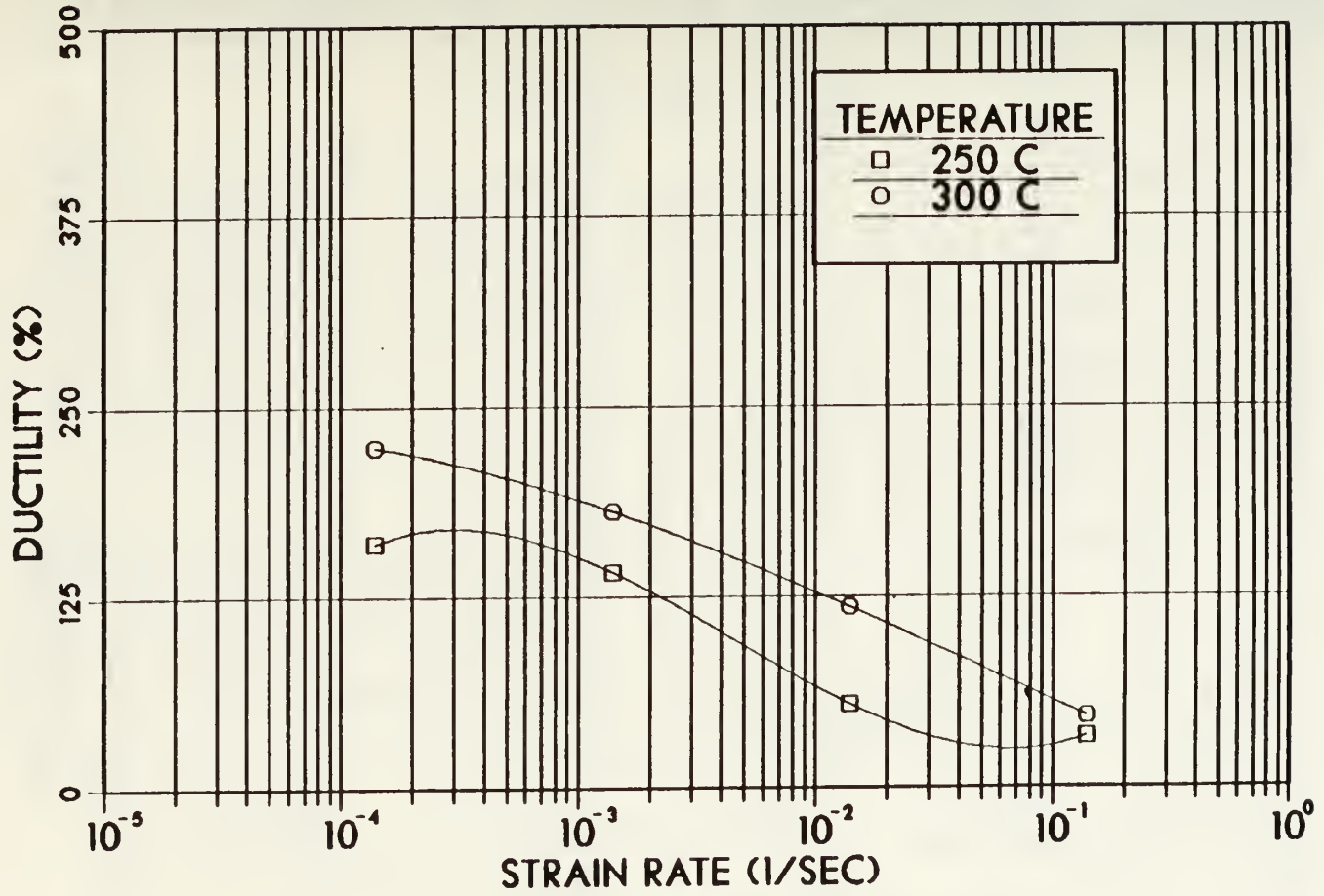

Figure 4.4 Ductility vs. strain rate for tests conducted at 250°C and 300°C on Al-8%Mg-0.1%Zr. Solution treated, hot worked, oil quenched, and warm rolled at 300°C to 94% reduction.

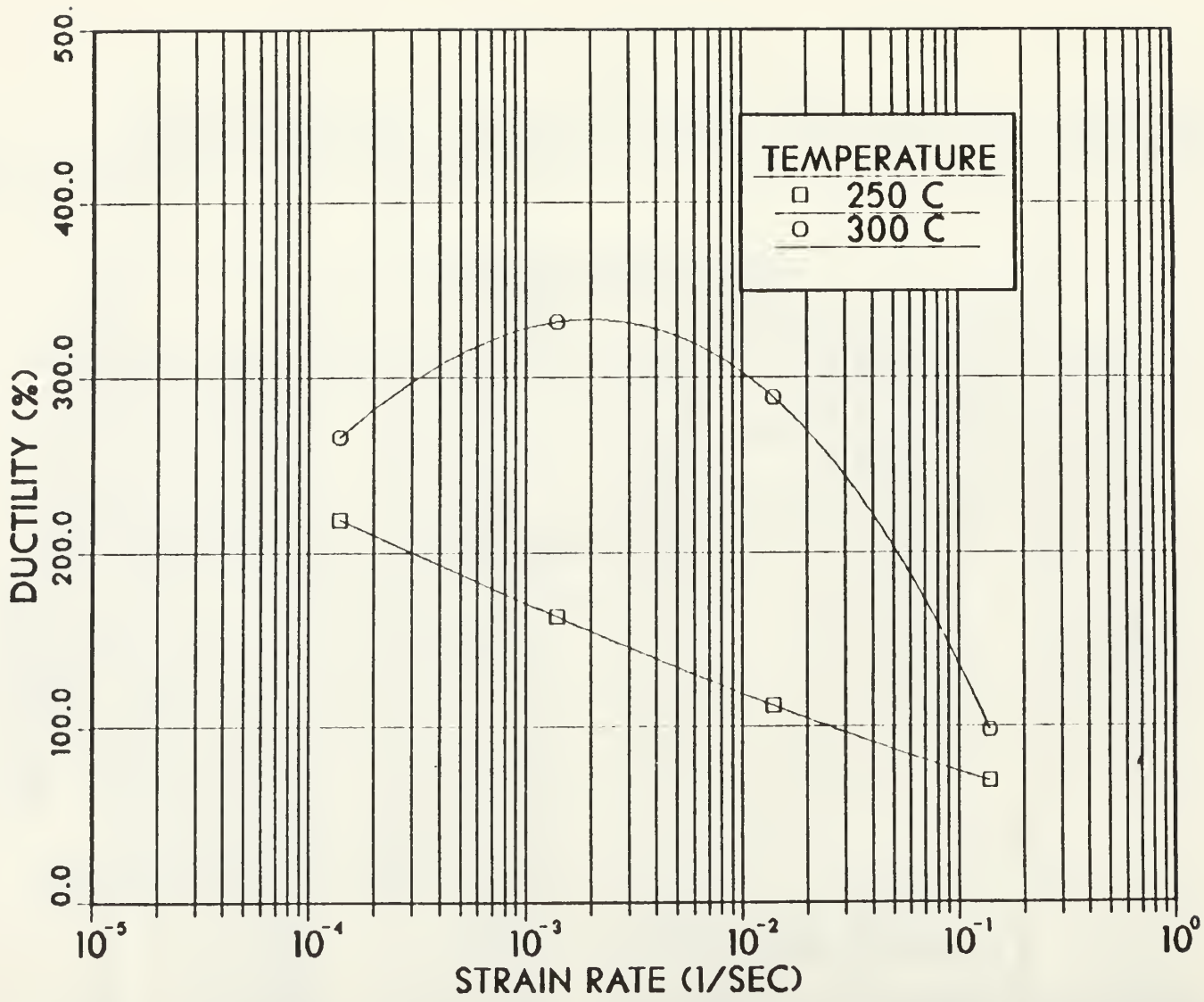

Figure 4.5 Ductility vs. strain rate for tests conducted at 250°C and 300°C on Al-10%Mg-0.1%Zr. Solution treated, hot worked, oil quenched, and warm rolled at 300°C to 94% reduction.

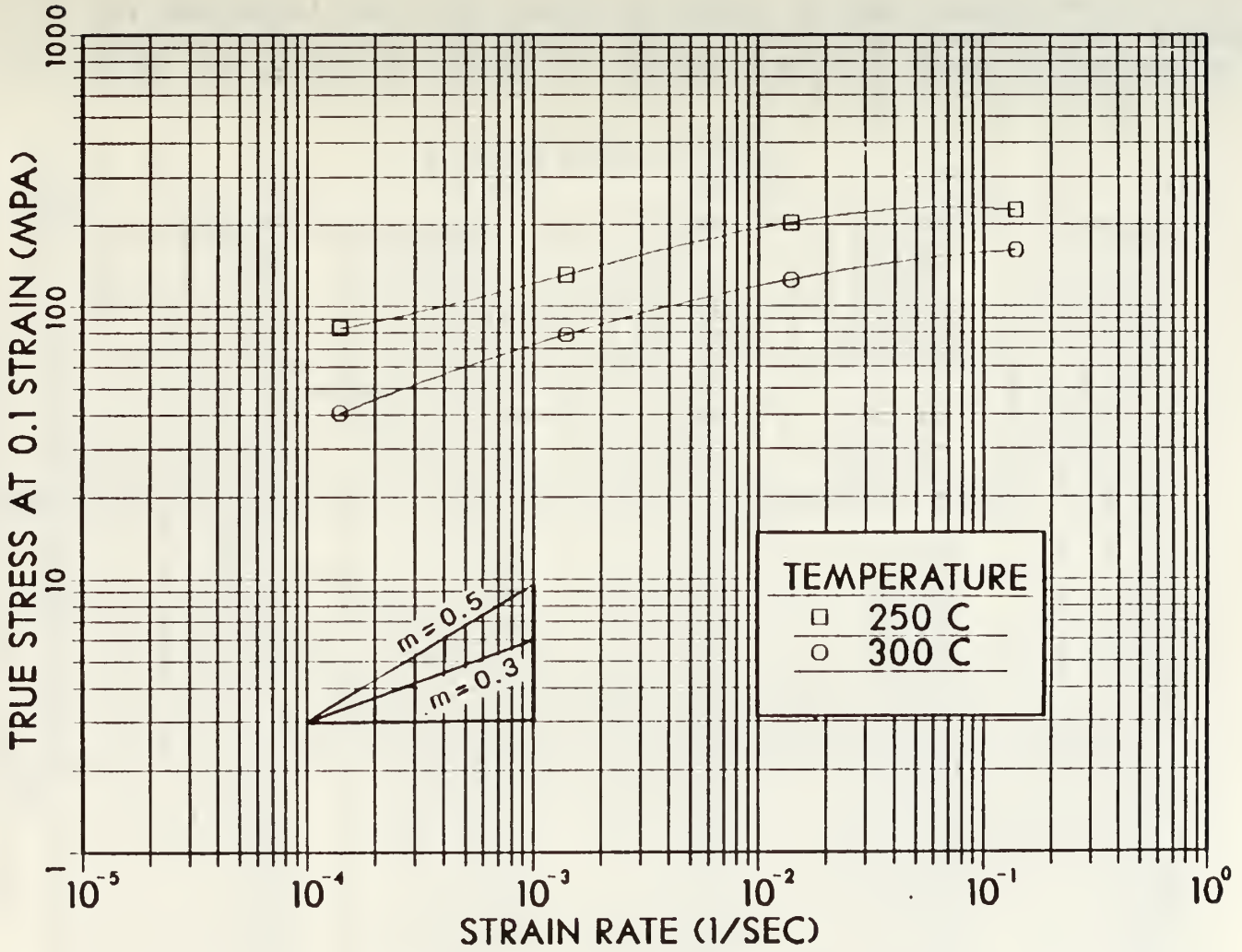

Figure 4.6 True stress at 0.1 strain vs. strain rate for tests conducted at 250°C and 300°C on Al-8%Mg-0.1%Zr. Solution treated, hot worked, oil quenched, and warm rolled at 300°C to 94% reduction.

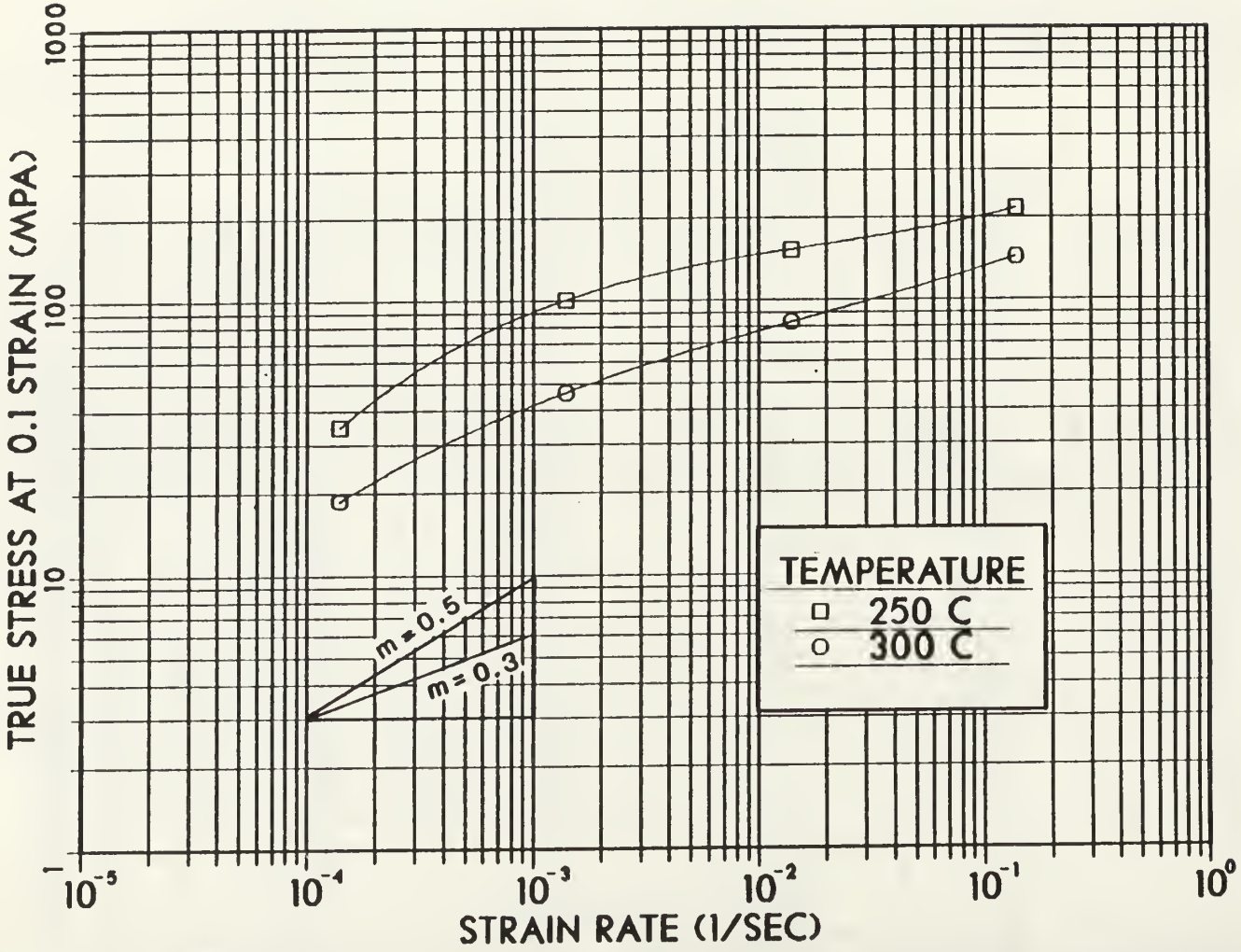

Figure 4.7 True stress at 0.1 strain vs. strain rate for tests conducted at 250°C and 300°C on Al-10%Mg-0.1%Zr. Solution treated, hot worked, oil quenched, and warm rolled at 300°C to 94% reduction.

retarding microstructural coarsening and the relative importance of the Zr and Mg content all need further microstructural analysis.

B. EFFECT OF SPECIMEN GEOMETRY, DATA SCATTER

As explained in Chapter III, the specimen geometry was changed after initial testing of these two alloys to more closely resemble specimen geometries used in superplastic testing in other laboratories. After changing the specimen geometry, a series of tests were conducted at 300°C with similar strain rates for specimens of both geometries. The newer geometry consistently gave better ductilities, as expected, due to the lower length to width ratio of the gage section. Figures 4.8 and 4.9 are plots of ductility vs. strain rate for the old and new geometry specimens, respectively. Multiple tests at many of the strain rates show the significant data scatter experienced throughout this research. Data scatter such as seen here is of concern, there are even a few tests where there is over 100% difference in results. It can be argued that experimental error might account for some of the data scatter, particularly when ductilities fall significantly lower than others. The data scatter, however, also reflects the statistical nature of the mechanisms involved in the deformation. Any material flaws: voids, impurities, or inordinate constituent particle or grain sizes might accelerate the deformation processes

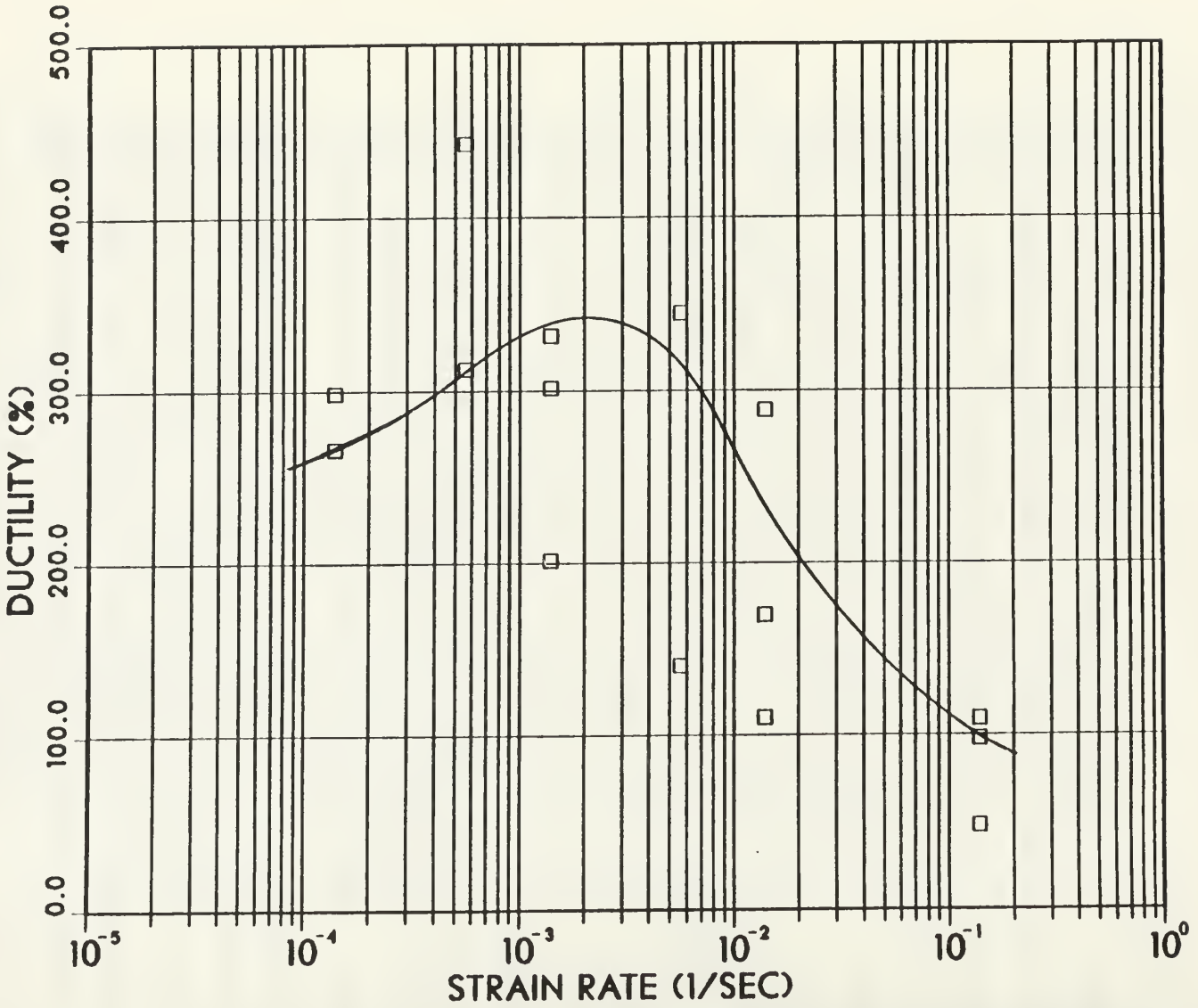

Figure 4.8 Ductility vs. strain rate for tests conducted at 300°C for old geometry samples of Al-10%Mg-0.1%Zr. Solution treated, hot worked, oil quenched, and warm rolled at 300°C to 94% reduction.

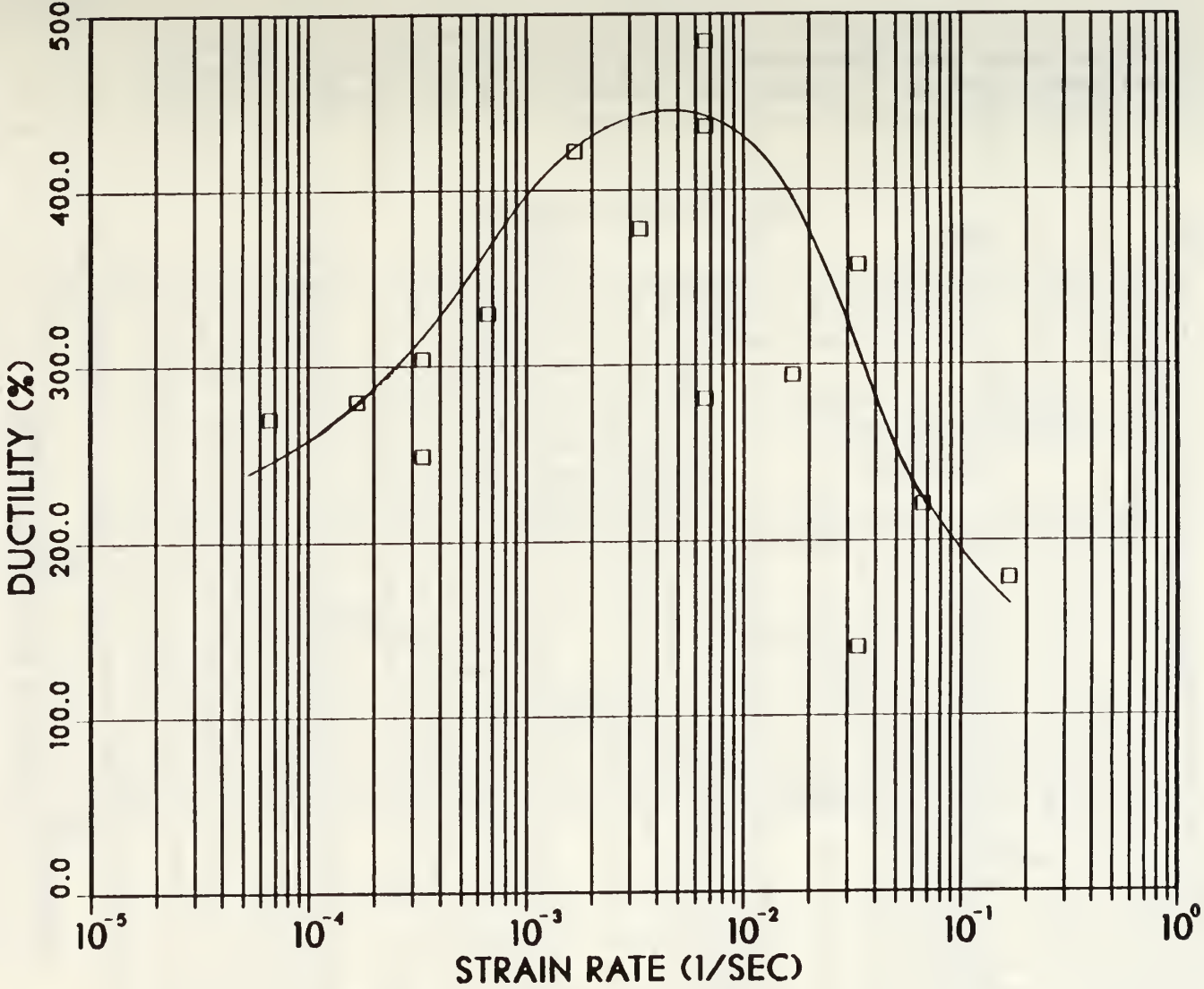

Figure 4.9 Ductility vs. strain rate for tests conducted at 300°C for new geometry samples of Al-10%Mg-0.1%Zr. Solution treated, hot worked, oil quenched, and warm rolled at 300°C to 92% reduction.

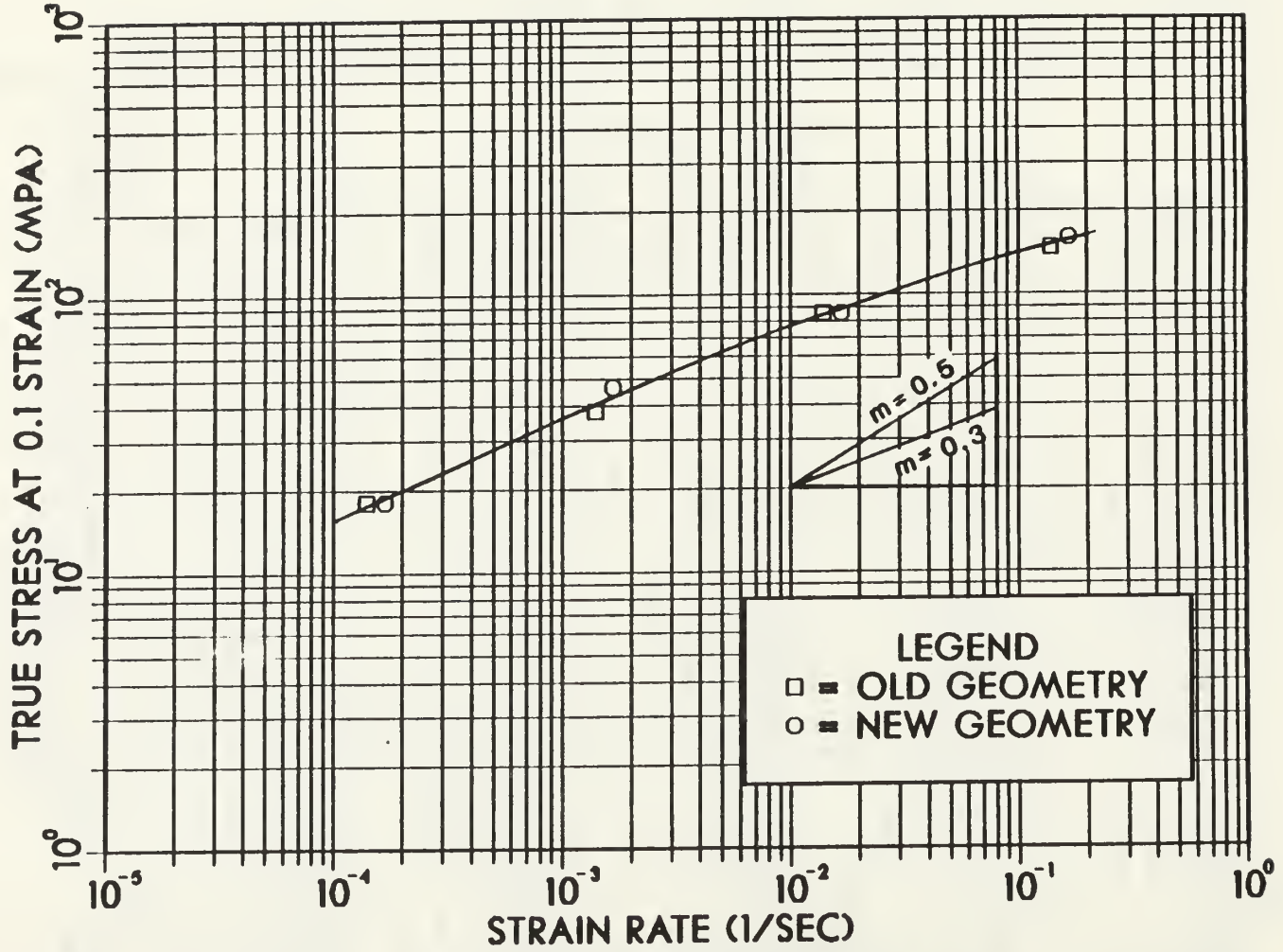

Figure 4.10 True stress at 0.1 true strain vs. strain rate for tests conducted at 300°C on Al-10%Mg-0.1%Zr samples of each geometry. Solution treated, hot worked, oil quenched, and warm rolled at 300°C to 94% and 92% reductino, respectively.

locally and result in significantly less ductility than would be for a "perfect" specimen. Besides getting better ductilities with the new specimen geometry, it also appears there has been a small shift to higher strain rates for maximum ductility. It is not known whether such a shift is real or whether it reflects the data scatter involved. Of course, because the data scatter is significant, it must be further studied as more knowledge of the mechanisms involved is gained. Figure 4.10 shows a comparison of flow stresses at 0.1 true strain vs. strain rates for each of the specimen geometries. As can be seen, one curve can fit both sets of data, meaning the strengths are the same, as expected.

C. TESTING OF Al-10%Mg-0.1%Zr AT 300°C

1. Mechanical Test Data

Concurrently with Berthold [Ref. 10] and Hartmann [Ref. 9] further research of the Al-10%Mg 0.1%Zr alloy was initiated. This research focused on the materials response when deformed at 300°C. Eleven different strain rates were tested and results are summarized in Table V. Appendix B contains a complete set of plots developed during this series of experiments. The true stress vs. true strain curves are similar to those shown in Figures 4.2 and 4.3, with early strain hardening followed by a region of straining at relatively constant stress prior to the onset of necking. It is significant to note that over a range of

TABLE V MECHANICAL TEST DATA OF Al-10%Mg-0.1%Zr ALLOY TESTED AT 300°C

Strain Rate (sec^{-1})	UTS (MPA)	True Stress at 0.1 True Plastic Strain (MPA)	Ductility (Percent Elong.)
1.67×10^{-1}	161.4	159.2	178.8
	165.7	160.4	110.4
6.67×10^{-2}	126.7	124.4	220.6
3.33×10^{-2}	114.6	107.9	356.6
	119.2	111.9	139.4
1.67×10^{-2}	102.5	87.1	294.0
	94.1	86.0	201.6
6.67×10^{-3}	83.6	64.9	484.4
	92.5	48.3	280.6
3.33×10^{-3}	68.4	51.9	377.8
1.67×10^{-3}	54.3	39.5	422.0
	61.2	46.3	241.6
6.67×10^{-4}	42.6	29.4	330.0
3.33×10^{-4}	32.3	24.5	304.0
	42.4	29.1	248.6
1.67×10^{-4}	27.0	18.1	317.6
	30.7	17.4	279.6
6.67×10^{-5}	22.5	14.0	270.0

strain rates from 3.33×10^{-4} S^{-1} to 3.33×10^{-2} S^{-1} elongations were all at least 300%. Technologically significant is the high strain rate, 10^{-1} S^{-1} (10 pct. per second) at which ductility in excess of 200% is observed.

Using this same data, a study was done on how the strain rate sensitivity coefficient, m, changes with strain. All previous research at NPS based calculation of m on the slope of the log (σ) at 0.1 true strain verses the log ($\dot{\varepsilon}$). The literature frequently quotes values for m, but it is seldom stated what value of true strain was used in the calculations. This is because the flow stress often is constant over a large range of strain. This being true, it does not matter what value of true strain is used and m is the same throughout this region. Figure 4.11 shows how the log σ vs. log $\dot{\varepsilon}$ plot is made. As can be seen, any constant strain value, after initial strain hardening, can be used and the curve will be the same, if the flow stress is constant. This is not observed with this alloy. There is significant hardening up to $\varepsilon \approx 0.1$ and then gradual hardening up to the onset of necking. Plotting true stress vs. strain rate on logarithmic axes for several values of true strain reveals that the coefficient m clearly decreases with increased strain as well as demonstrating the strain hardening.

It is important to note that this type of analysis can only be done for true strains before the onset of

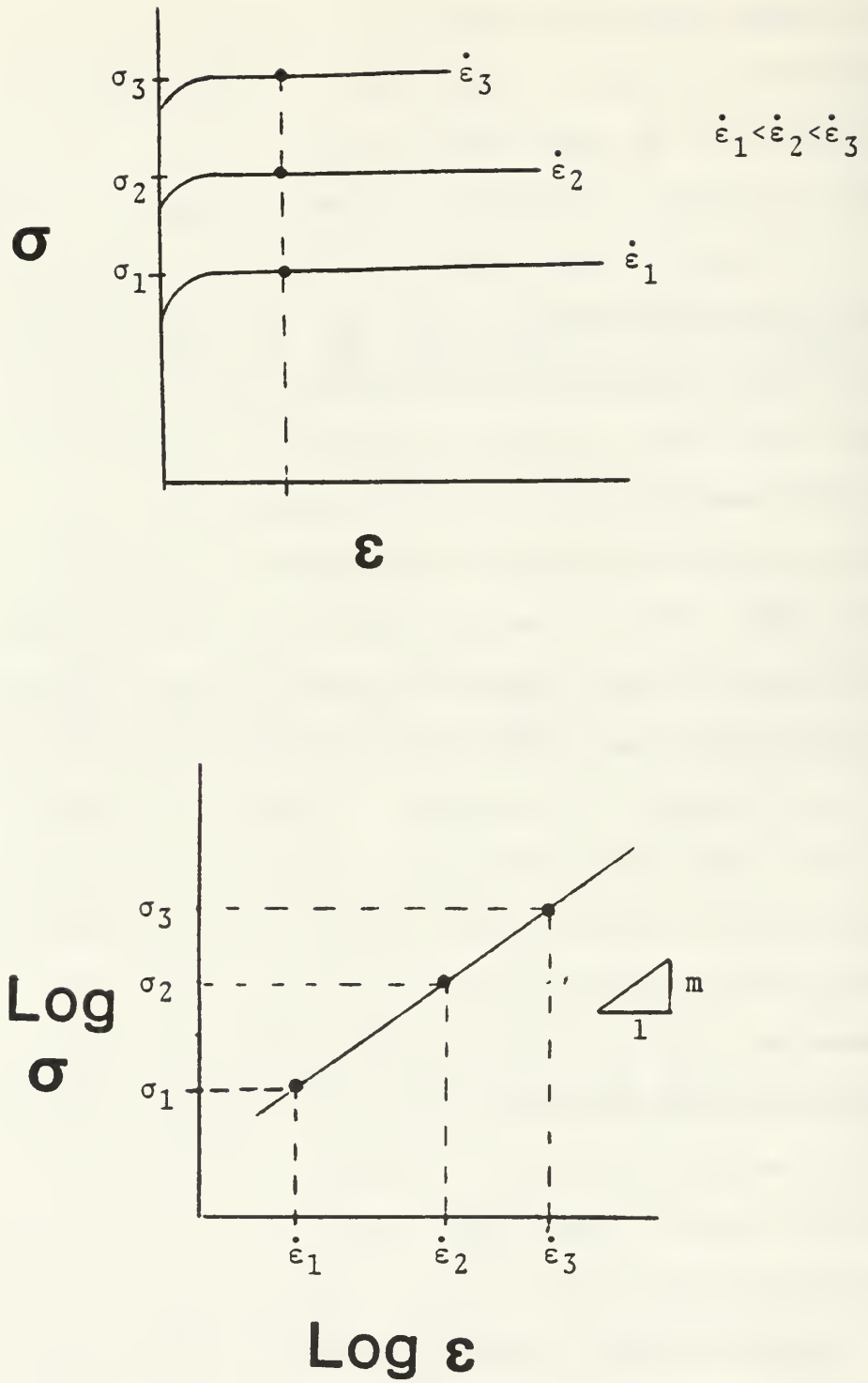

Figure 4.11 Schematic diagrams illustrating determination of m: a) true stress vs. true strain for various strain rates; b) log σ vs. $\dot{\varepsilon}$ log, with $\sigma = B\dot{\varepsilon}^{m}$, m = slope.

necking. At the onset of necking the equations for true stress and true strain (Eqs. 3.3 and 3.4) are no longer valid and calculations would have to reflect the reduced area at the neck. For this analysis, true stress vs. strain rate was plotted on logarithmic axes for true strains of 0.02, 0.05, 0.1, 0.2, and 0.5. Figure 4.12 shows the curves for 0.02, 0.1, and 0.5 true strain. Plots for all the strains are included in Appendix B. The m value found for 0.02 strain is about 0.38 and for the 0.5 strain plot (at lower strain rates), it is about 0.29. It should be noted that for most materials m varies between 0.02 and 0.2 for temperatures between 0 absolute and 0.9 T_m [Ref. 34].

Several other observations may be made. At low strain rates, rapid strain hardening is seen due to the grain growth. Micrographs presented later will reinforce this point. For a strain rate of $6.67 \times 10^{-5}\ S^{-1}$, the strength more than doubles from 8 MPA to 21 MPA going from true strain of 0.02 to 0.5. Conversely, the strain hardening at a strain rate of $1.67 \times 10^{-1}\ S^{-1}$ is only about 9%, from 147 MPA at 0.02 true strain to 160 MPA at 0.2 true strain. It is also readily apparent that the shape of the curves are different. Recalling Figure 2.1, a log σ vs. log $\dot{\varepsilon}$ plot for superplastic materials generally is sigmoidal in nature. For this alloy, Regime I is not apparent for the strain rates tested. If lower strain rates were tested, still more rapid strengthening due to grain growth very

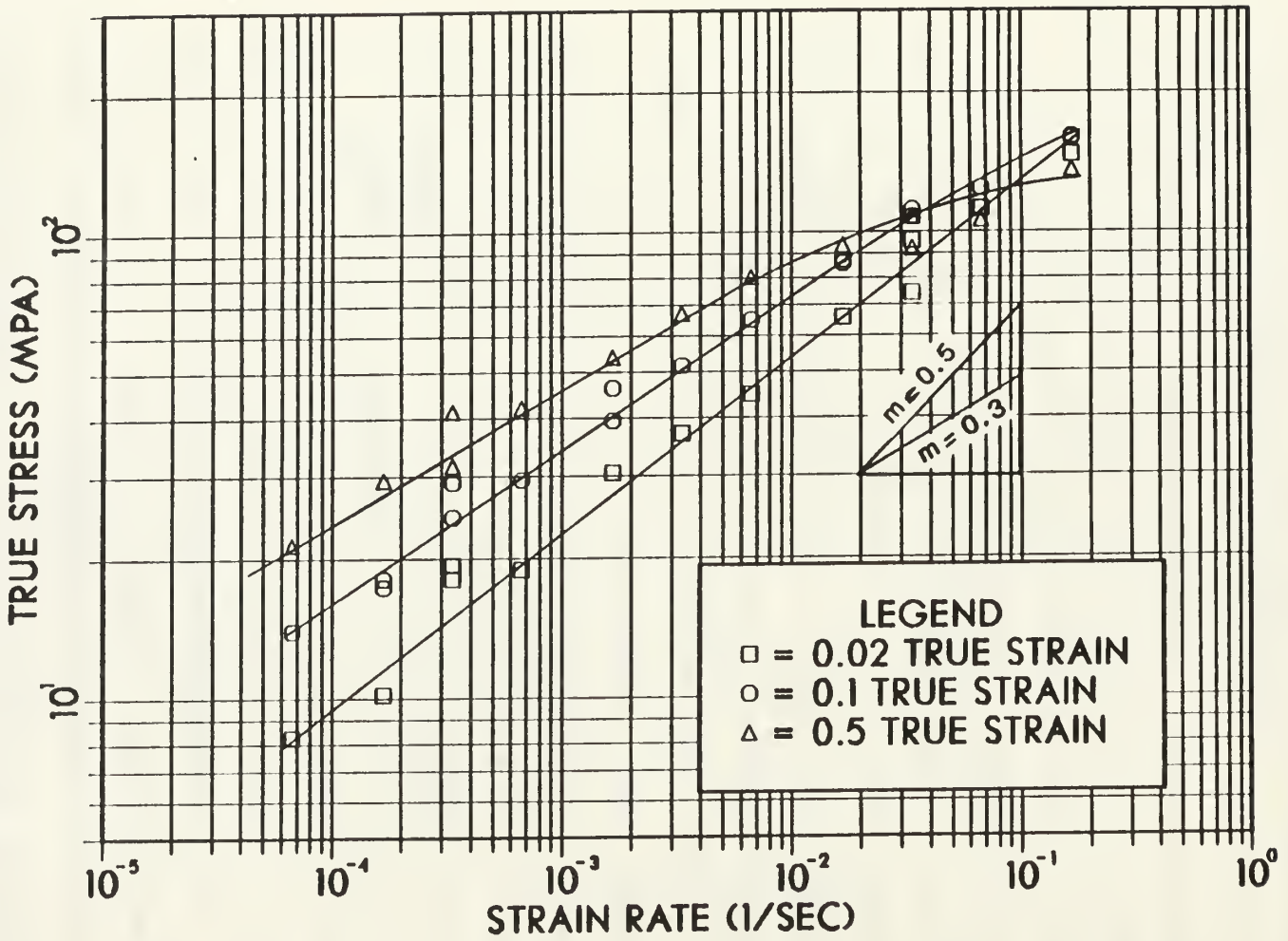

Figure 4.12 True stress at 0.02, 0.1, and 0.5 strain vs. strain rate for tests conducted at 300°C on Al-10%Mg-0.1%Zr. Solution treated, hot worked, oil quenched, and warm rolled at 300°C to 92% reduction.

likely would lead to tailing off of the curve. However, as pointed out earlier, Regime I may reflect a threshold stress below which flow will not occur, or Regime I may not exist at all.

It is also seen that Regime III becomes more apparent as the strain increases. Regime III represents a change in the mechanism of deformation. In Regime II the flow process is more diffusionally accommodated, whereas in Regime III the stresses are higher, dislocations are generated and the mechanism of deformation likely is dislocation creep. The curve for 0.02 strain appears fairly linear through all strain rates tested, whereas for the 0.5 strain curve there is a distinct transition to a region where m is about 0.17, signifying a change in the deformation mechanism to dislocation creep, although the corresponding n of 5.9 is slightly larger than either Weertman model would predict. It would appear that if tests were conducted at higher strain rates the change of mechanism would become apparent at lower strains. Figure 4.13 shows the strain rate sensitivity coefficient m vs. true strain.

It is concluded that the coarsening of the substructure which occurs with strain strengthens the material and also acts to suppress superplastic response. In effect the growth shrinks the strain rate regime over which high elongations can be achieved. This is undesirable because an important goal in the design of superplastic alloys is to be

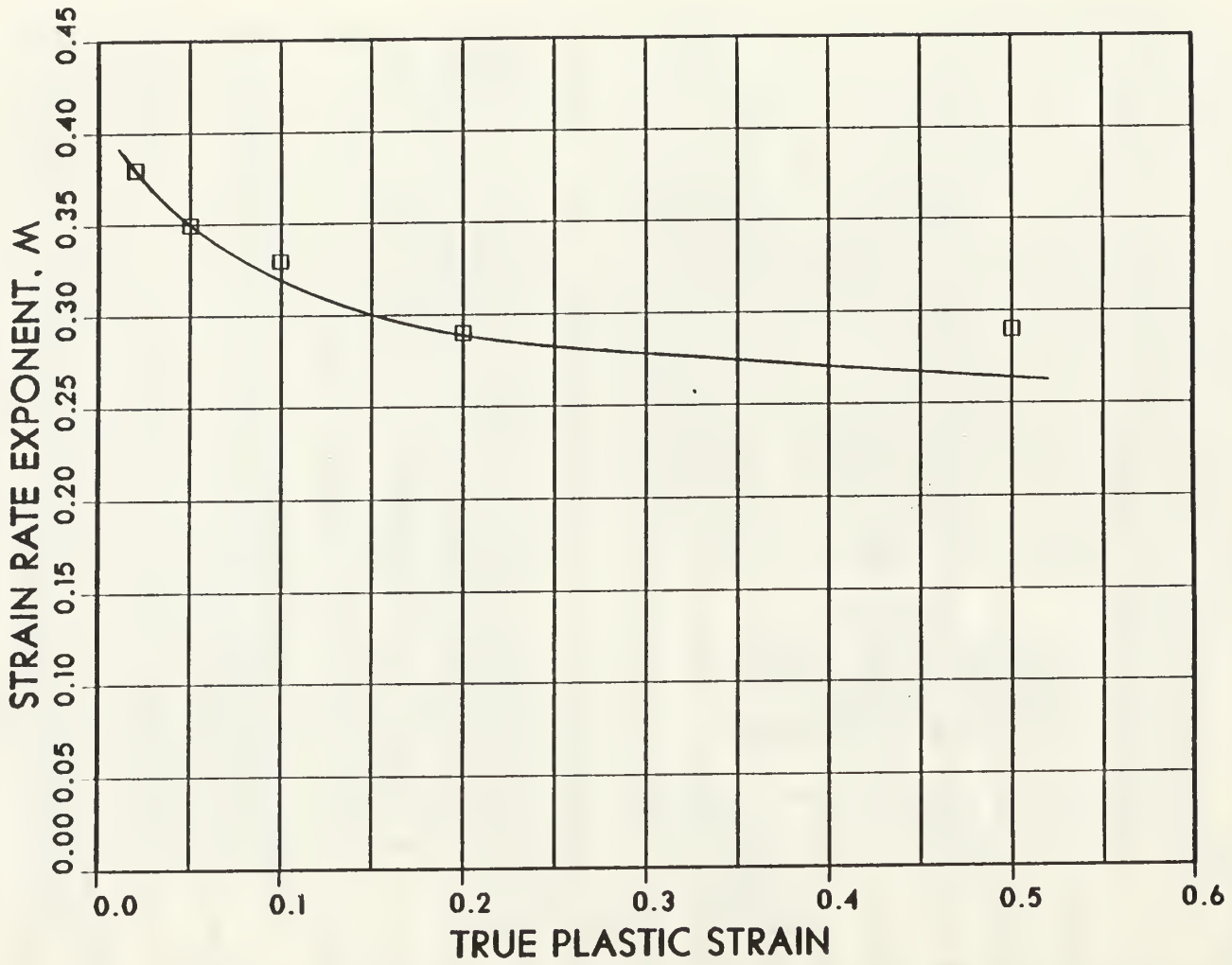

Figure 4.13 Strain rate coefficient, m vs. true plastic strain for tests conducted at 300°C on Al-10%Mg-0.1%Zr. Solution treated, hot worked, oil quenched, and warm rolled at 300°C to 92% reduction.

able to deform the material at the highest possible strain rate. The grain growth in this alloy decreases this strain rate region where good superplastic response can be attained.

Recalling from Table I, the mechanism for superplasticity is assumed to follow a constitutive law of the form:

$$\dot{\varepsilon} = K D_{eff} \frac{\sigma^n}{d^2} \qquad \text{(Eq. 4.1)}$$

where n is experimentally found to be about 2. This is equivalent to

$$\sigma = C\dot{\varepsilon}^m \qquad \text{(Eq. 4.2)}$$

where ε, T, and d are constant and $C = \frac{d^2}{K D_{eff}}$. From this

$$m_{true} = \left.\frac{\partial(\ln \sigma)}{\partial(\ln \dot{\varepsilon})}\right|_{\varepsilon,T,d} \qquad \text{(Eq. 4.3)}$$

However, if d is not constant, using constant strain rate tests to determine m will not be accurate. A better method would be to use a step strain rate test as described, for example, by Meyers and Chawla [Ref. 34]. In this test the strain rate is instantaneously changed from $\dot{\varepsilon}_1$, to $\dot{\varepsilon}_2$ and the two corresponding flow stresses, σ_1 and σ_2 are obtained by extrapolation and used to find m_{true} from Eq. 4.3.

If the change in strain rate is instantaneous and d is, in fact, constant, the resultant m value from this test would be higher than the apparent value obtained here. Figure 4.14 illustrates this. If the processing could be modified to attain a stable microstructure, the current procedure would exhibit a higher value for m.

2. Microstructural Analysis

It was seen in previous work at NPS [Refs. 28, 29, 30 and 31] that there is considerable change in the microstructure of these alloys from the as-rolled condition to that at fracture. Berthold [Ref. 10] showed the same to be true for this alloy. It was therefore decided to conduct a series of tests at 300°C where samples were pulled to various strains prior to fracture and then examined via TEM. This was done at two strain rates to determine the effect of strain rate on the microstructure as well. At a strain rate of 6.67×10^{-3} S^{-1} samples were pulled to elongations of 8.4%, 20.0%, 45.6% 103.2%, 162%, and 267%. For a strain rate of 6.67×10^{-4} S^{-1} (10 times slower) samples were pulled to elongations of 8.6%, 13.8%, 43.2%, 100.2%, 157.4%, and 263.8%. Figure 4.15 shows the samples pulled at 6.67×10^{-3} S^{-1}. Additionally, a sample was placed in the 300°C furnace, heated for one hour and then examined via TEM. The microstructure of this sample demonstrated the changes which take place from the time an as-rolled sample is placed in the furnace until just prior to testing.

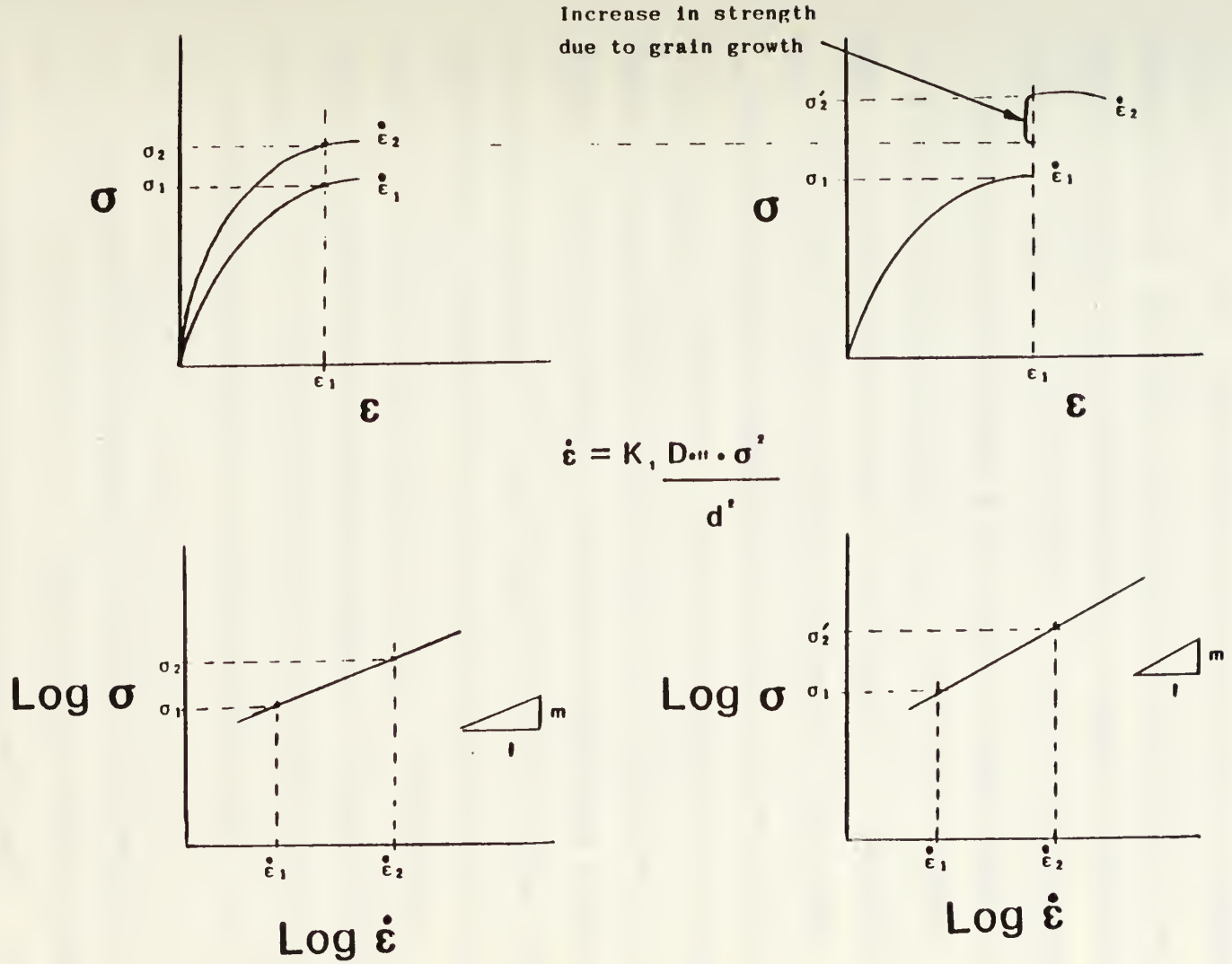

Figure 4.14 Two methods to determine m: a) and b) use 2 different samples and 2 strain rates; c) and d) use one sample with a shift in strain rates. The second method shows how the grain growth increases σ_2, giving a higher m value.

Another sample was heated for two hours at 300°C and then examined via TEM to determine the effect of time at temperature without straining. It must be noted that a rigorous quantitative study of the microstructures was not attempted; i.e., analysis of grain misorientations and percent recrystallization were not done. Observations of changes in the microstructure are from more of a qualitative viewpoint.

Figure 4.16 shows the significant recovery which takes place within the hour it takes for the sample to reach 300°C. The as-rolled condition has a high dislocation density, the grains cannot be distinguished and the substructure is diffuse; by the time the sample is heated to 300°C for one hour it has recovered sufficiently to distinguish a fine subgrain structure. The mean intercept length for this substructure was determined to be 1.9 μm. The sample which was heated for two hours showed no discernible change in microstructure from that heated one hour. This follows the previous research on Aluminum-Magnesium alloys that found the alloys did not recrystallize unless heated above the solvus, which is about 350°C for the 10% Mg-Al alloys.

Figures 4.17 through 4.20 are a progression of micrographs showing the change in microstructure as it is strained. They show the microstructures at about 8%, 45%, 160% and 265% elongation for strain rates of 6.67×10^{-3} S^{-1} and 6.67×10^{-4} S^{-1}, respectively. The faster strain rate

micrographs are at the top of each page. It is readily apparent that by 45% elongation there is a significant difference in the size scale of each microstructure. The slower strain rate has resulted in a considerably coarser microstructure. Whereas annealing at 300°C results in initial recovery with little subsequent coarsening, additional straining results in noticeable coarsening, and much more so at the slower strain rate where more time is available for the grain growth to take place. It appears the microstructure is undergoing recrystallization, but the recrystallization is not of the conventional nucleation and growth process where new, strain-free grains form and grow through dislocated regions. Instead, it appears that the microstructure recovers continuously until the relatively low-angle subgrain structure becomes in many areas essentially a high-angle grain structure. These structures then continue to grow into adjacent regions. The micrographs in Figure 4.21 is from a sample pulled to fracture at a strain rate of 6.67×10^{-4} S^{-1}. Significant dislocation activity is still apparent and it is seen these are able to cut through substructure boundaries, meaning that they are relatively low-angle boundaries. It is not known from what source these dislocation were generated. They may be a result of accommodation by slip of grain boundary sliding. Using micrographs from each sample, the microstructure size was measured at the various strains and Figure 4.22 is a

plot of the results. Between 150 and 300 intercepts were counted at each strain so still more microscopy would need to be done to try to draw definitive numerical conclusions. The trend, however, is clear. There is appreciable grain growth during testing with this alloy, especially at lower strain rates. At 6.67×10^{-3} S^{-1} where grain growth was less, an elongation of 485% was achieved. At 6.67×10^{-4} S^{-1} where grain growth was more severe, an elongation of 330% was achieved.

Berthold's [Ref. 10] microscopy on the as-received structure showed $ZrAl_3$ particles (β_{Zr}) as large as 10 μm. All the Zirconium should have been in solution to be precipitated out during TMP as fine β_{Zr} particles which would then pin the grain boundaries. As result of the high Mg content in this alloy, primary β_{Zr} formed in the liquid and grew because of rapid diffusion in the liquid state. These primary particles, having formed at such high temperature, are stable and resistant to resolutioning. There is, therefore, less Zr available to form fine $ZrAl_3$ to serve more effectively to pin boundaries and stabilize the grain size.

3. The Grain Size Exponent

The data available was utilized to attempt to determine the grain size exponent in Eq. 4.1 applicable here. For $p = 2$, lattice (or bulk) diffusion is indicated as the rate controlling process in the deformation mechanism. The

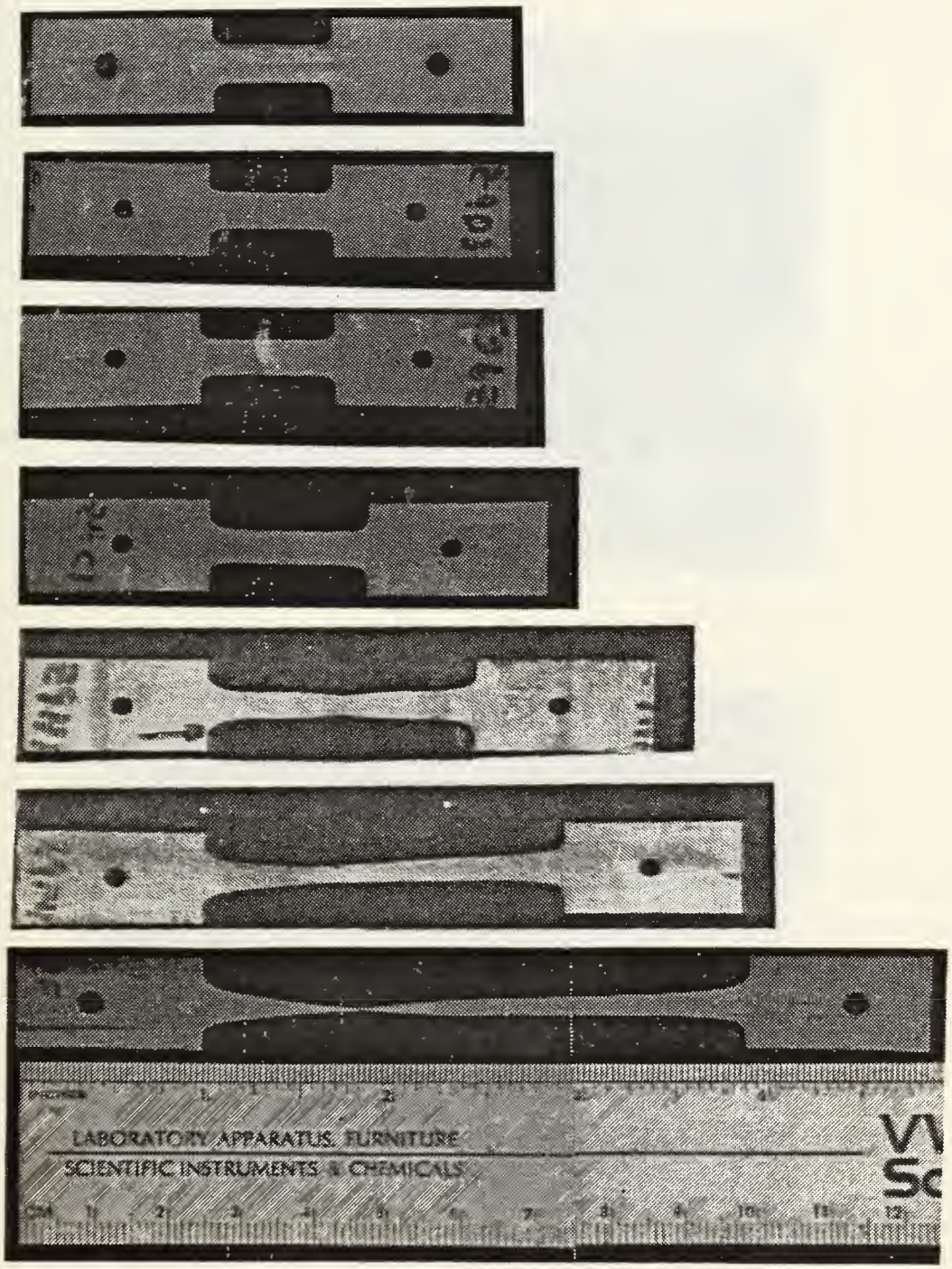

Figure 4.15 Samples of Al-10%Mg-0.1%Zr pulled to various elongations at 6.67 X 10^{-3} S^{-1}, including: unstrained, 8%, 20%, 45%, 160%, 265% and to fracture (485%).

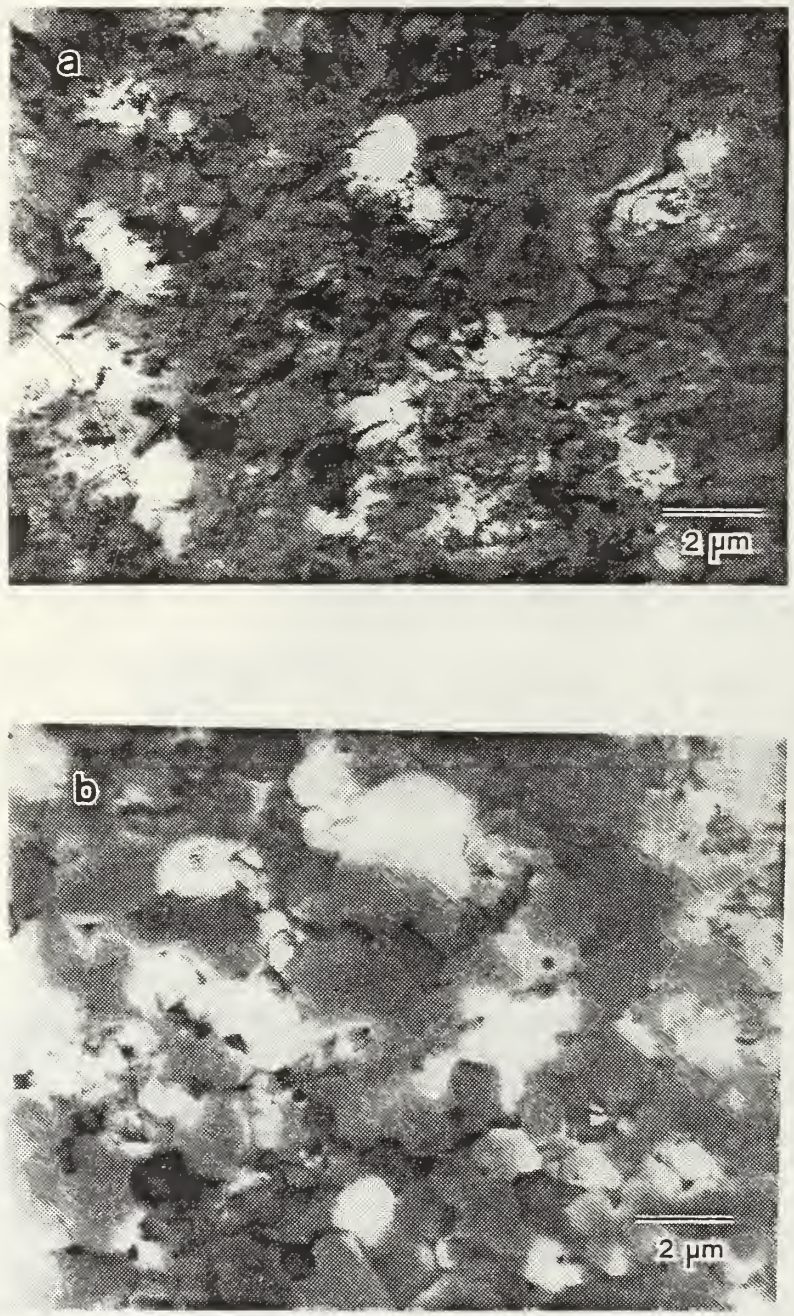

Figure 4.16 Transmission electron micrographs of Al-10%Mg-0.1%Zr for as-rolled condition (a) and after 1 hour heating to 300°C (b).

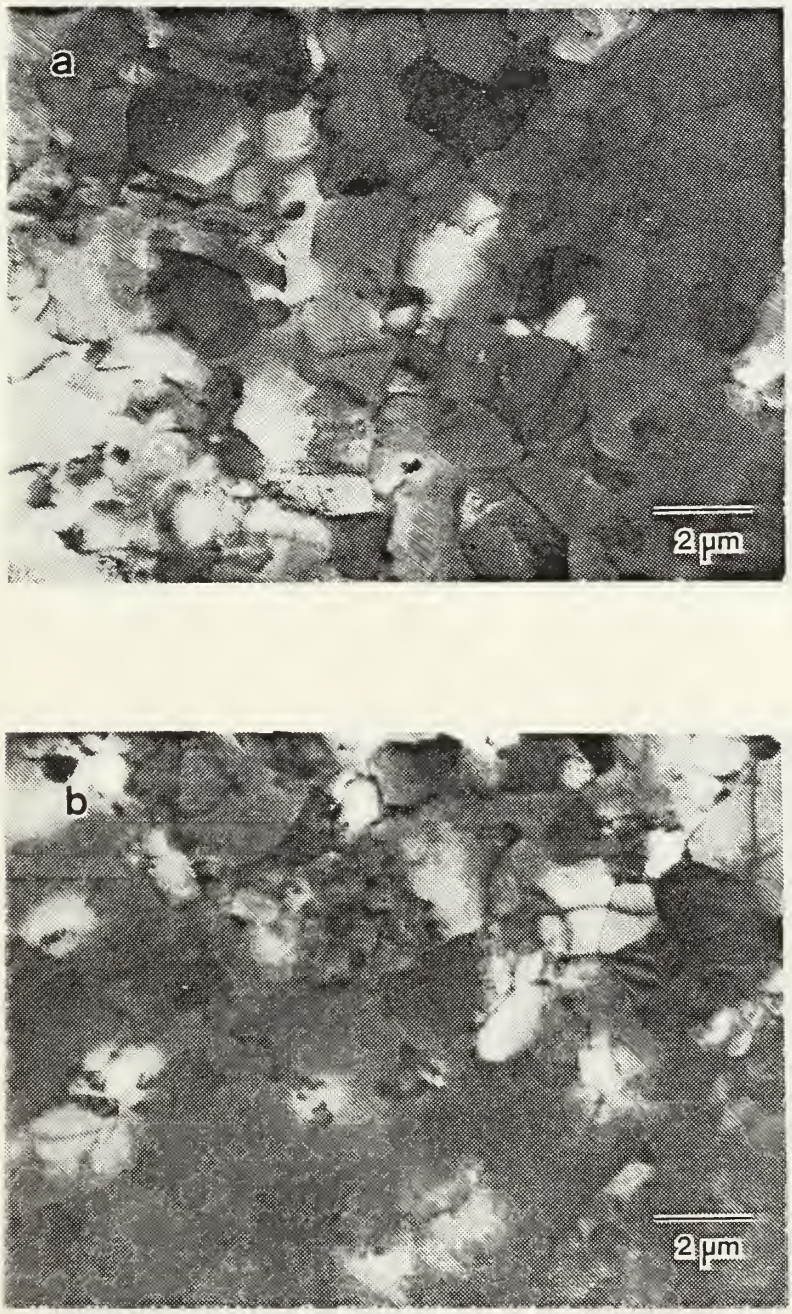

Figure 4.17 Transmission electron micrographs of Al-10%Mg-0.1%Zr after elongation to 8% strain at 6.67×10^{-3} S^{-1} (a) and 6.67×10^{-4} S^{-1} (b).

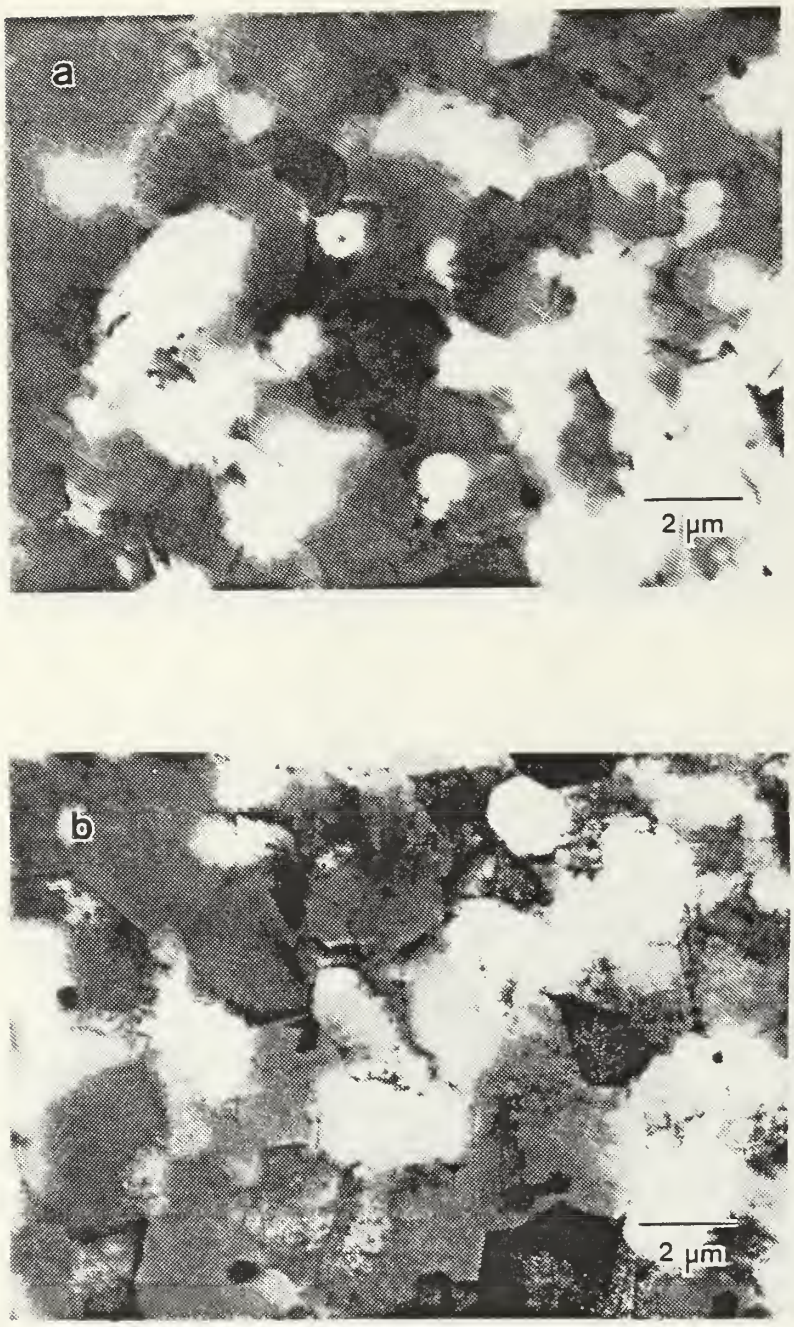

Figure 4.18 Transmission electron micrographs of Al-10%Mg-0.1%Zr after elongation to 45% strain at 6.67×10^{-3} S^{-1} (a) and 6.67×10^{-4} S^{-1} (b).

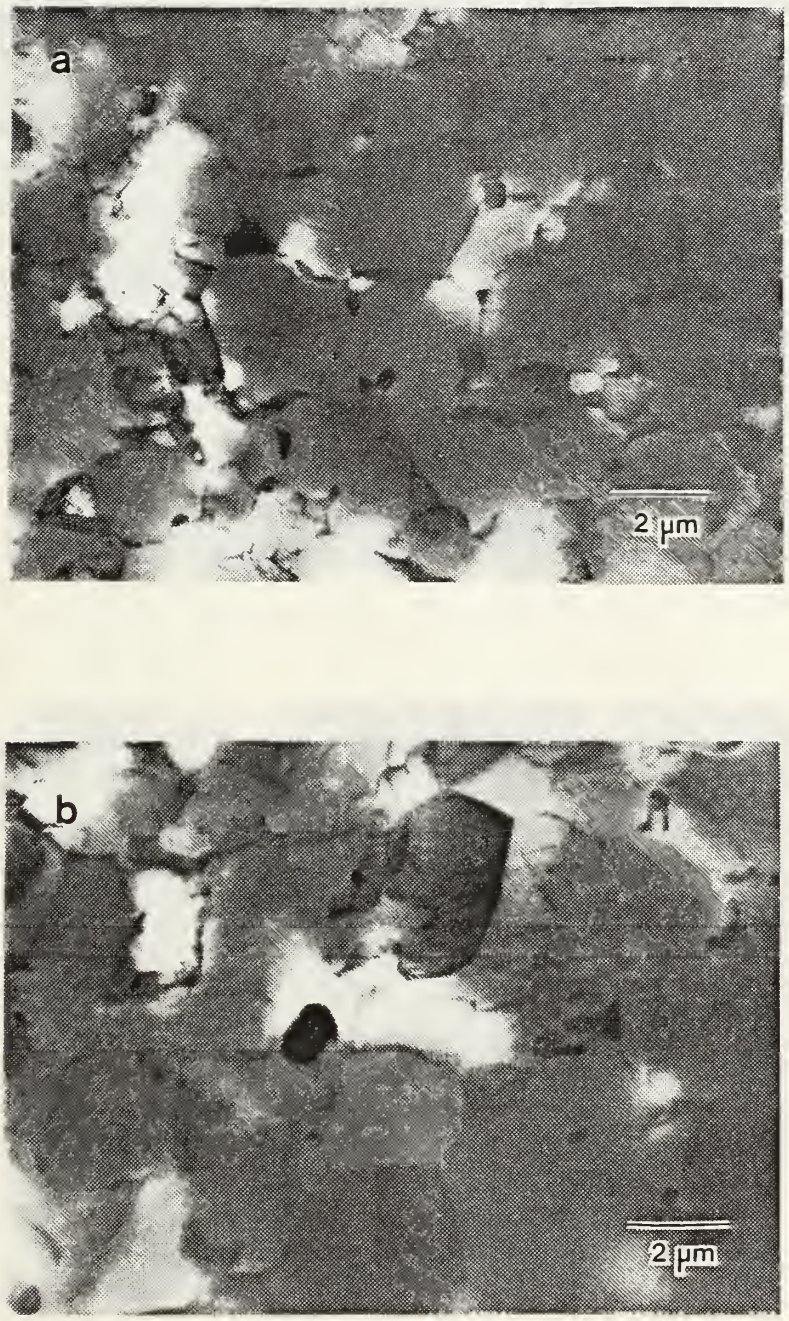

Figure 4.19 Transmission electron micrographs of Al-10%Mg-0.1%Zr after elongation to 160% strain at 6.67×10^{-3} S^{-1} (a) and 6.67×10^{-4} S^{-1} (b).

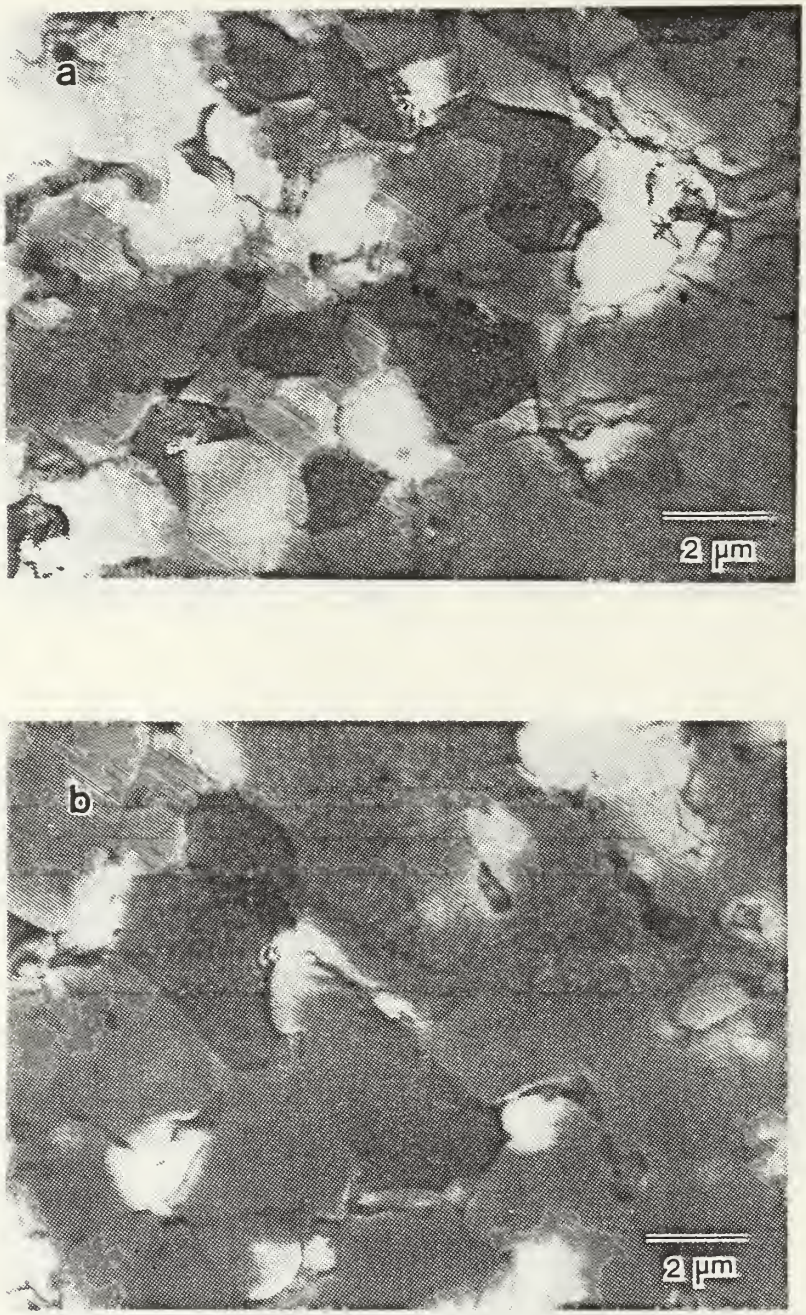

Figure 4.20 Transmission electron micrographs of Al-10%Mg-0.1%Zr after elongation to 260% strain at 6.67×10^{-3} S^{-1} (a) and 6.67×10^{-4} S^{-1} (b).

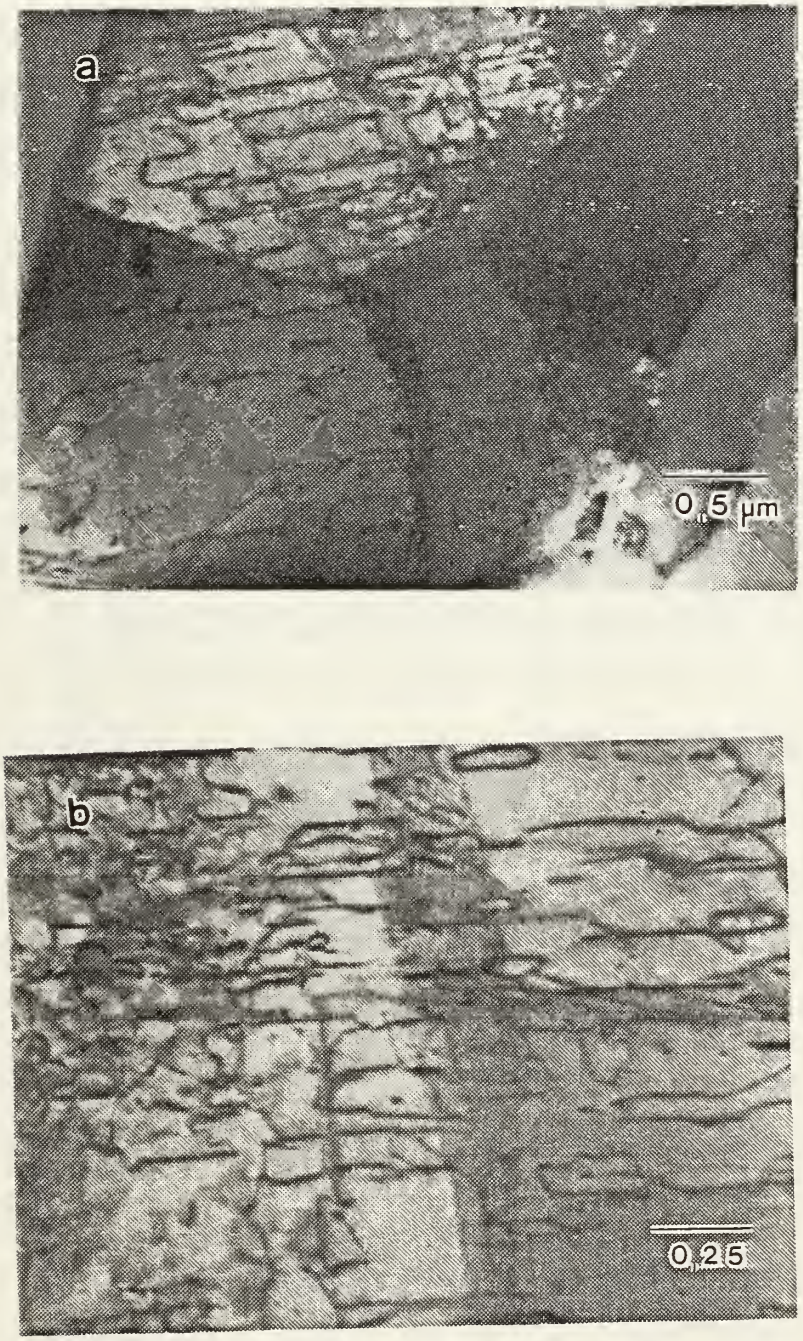

Figure 4.21 Transmission electron micrographs of Al-10%Mg-0.1%Zr after fracture with straining at 6.67 X 10^{-4} S^{-1}, showing dislocations in grain or subgrain interiors.

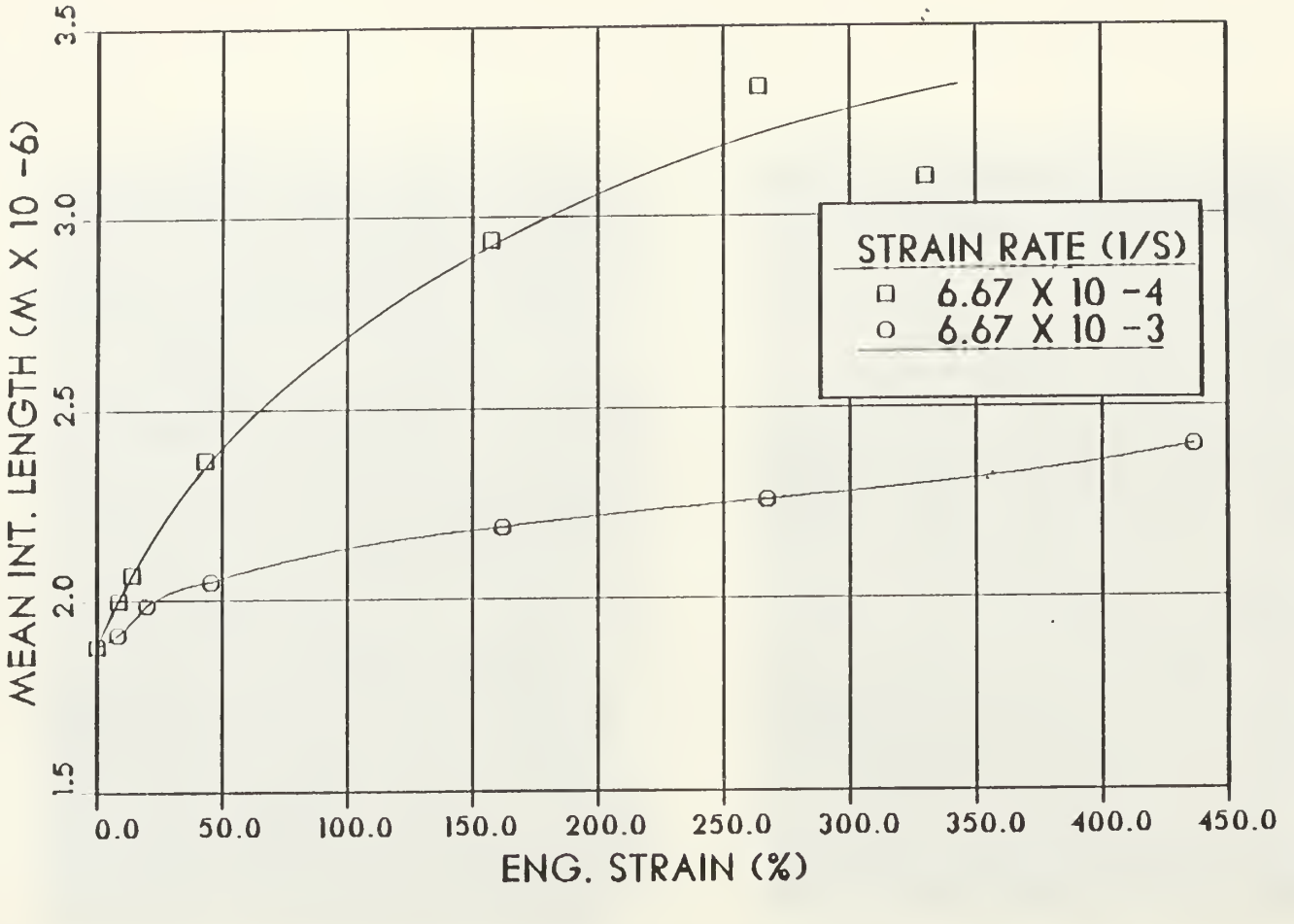

Figure 4.22 Mean intercept length vs. engineering strain for tests conducted at 300°C on Al-10%Mg-0.1%Zr. Solution treated, hot worked, oil quenched, and warm rolled to 92% reduction.

exponent on d becomes 3 when grain boundary diffusion is rate controlling. This added dependence on d comes from the D_{eff} coefficient as discussed in Chapter II. Using the true stress data for each of the tested strain rates (refer to Figure 4.12), with the data of mean intercept length vs. true strain (Figure B.11 from Figure 4.22), a plot of true stress vs. mean intercept length was constructed. This is shown in Figure 4.23. It should be noted that the true stress data could not be taken directly from the data used to generate Figure 4.12 because the true strain rate changes with strain. The greater the strain, the lower the true strain rate and therefore the true stress at the given strain rate is higher than would be taken directly from the data. Additionally, to extract a value of p from the data an exponent of 2 was assumed for the flow stress σ. This derivation also assumes the grain size, d, is directly proportional to the mean intercept length.

From Eq. 4.1, with the exponent on d an unknown, p, it can be shown that:

$$\log \sigma = 1/2 \log C + p/2 \log d \qquad \text{(Eq. 4.4)}$$

where $C = \text{constant} = \dot{\varepsilon}/KD$

Therefore the slope of log σ vs. log d should be equal to p/2. The curves in Figure 4.23 are obviously not linear, however, some useful data can be extracted. For the slower

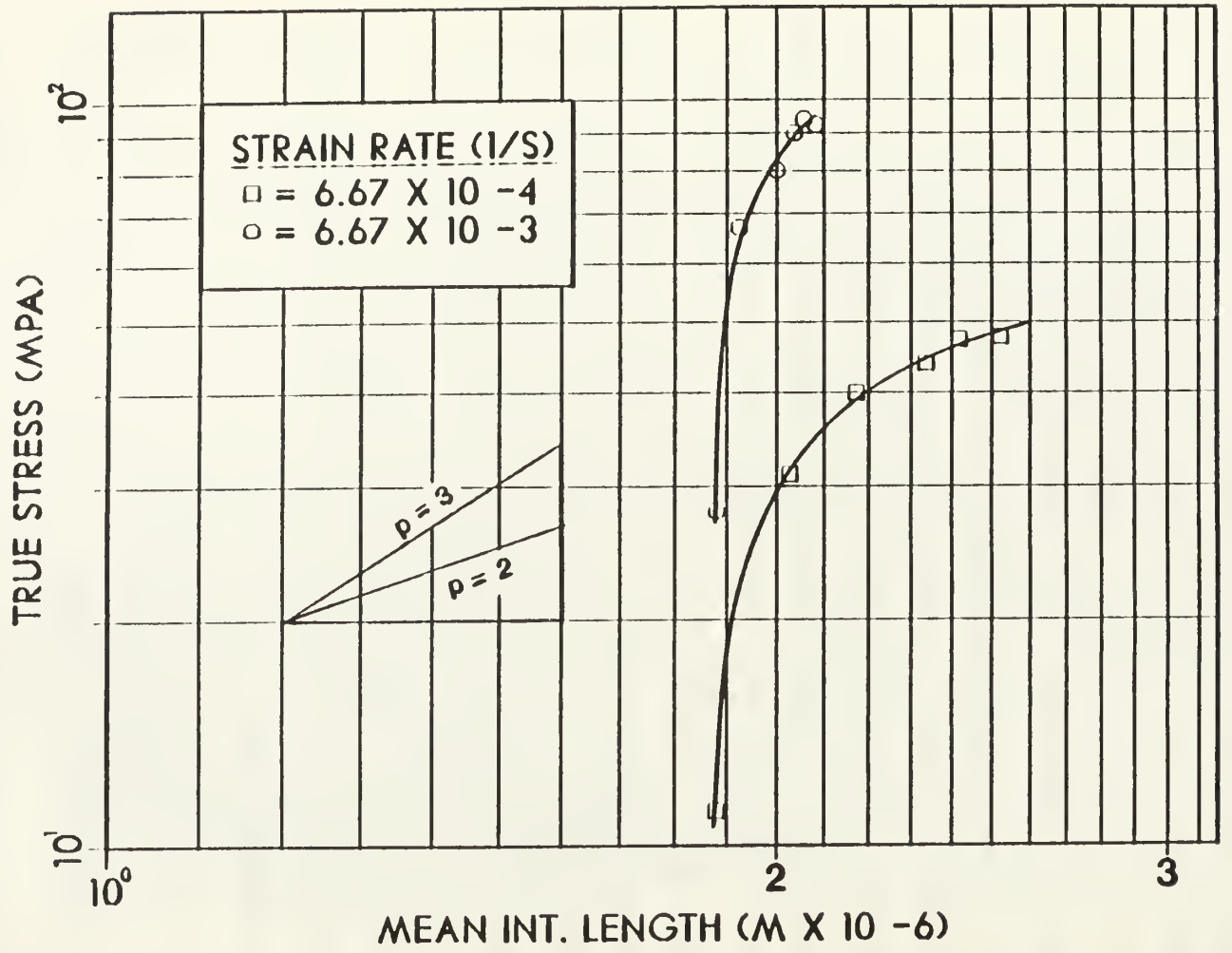

Figure 4.23 True stress vs. mean intercept length for tests conducted at 300°C on Al-10%Mg-0.1%Zr. Solution treated, hot worked, oil quenched, and warm rolled to 92% reduction.

strain rate where more significant grain growth is apparent, a fairly good linear fit can be made over the last four data points. If this is done, a slope of 1.27 gives a value for p equal to 2.54. This is almost exactly in between the two modeled values of 2 and 3. Using this approach it would be difficult to plot any further data because, although mean intercept length data is available, localized necking begins to occur beyond the maximum strain of 0.5 used for this plot. It might be speculated that the slope would continue to decrease to about 1 where p would equal 2, but no such conclusion can be drawn. Nothing can be gained from the curve for the faster strain rate because the data points are too clustered together. It should be noted that the first point on each plot can be termed a hybrid. The yield strength, which is difficult to determine, is used with the mean intercept length found from the sample heated to 300°C for 1 hour. The point is included to show the trend of the curves.

In summary, this set of experiments showed significant grain growth in this alloy when tested at 300°C, and the lower the strain rate, the greater the grain growth. This microstructural instability was also evident in Hartmann's work [Ref. 9]. He found values for activation energy signifying lattice diffusion from test temperature of 150°C up to about 275°C, and then again above 350°C. In the temperature range around 300°C to 350°C there are

dramatic microstructural changes; ie., continuous recrystallization, and then conventional recrystallization which resulted in an anomalously low or even negative activation energies. It has been shown here that the behavior of this alloy fits the most prevalent model for a superplastic mechanism of deformation, expressed as Eq. 4.1, with a stress dependence of 2 and grain size exponent likely 2 as well. This model is thought to be most applicable to a fine, equiaxed grain structure with high-angle grain boundaries. The TMP used on this alloy, however, results in an elongated grain structure with a dislocation substructure initially. When testing at 300°C it appears the microstructure undergoes recovery, continuous recrystallization and grain growth processes and the resultant mechanical behavior follows that modeled for a classical superplastic material.

V. CONCLUSIONS AND RECOMMENDATIONS

The following conclusions are drawn from this research:

1. The greatest elongations for this alloy are exhibited when tested at temperatures around 300°C. This is below the solvus for Mg and it appears the high dislocation density, subgrain structure of the as-rolled condition undergoes a continuous recrystallization process resulting in a microstructure of mixed high and low angle grains.

2. Grain coarsening is seen in the alloy when tested at 300°C. This results in strain hardening of the alloy and is detrimental to the superplastic elongations achieved.

3. The functional relationship between stress, strain, strain rate and grain size for this alloy can be considered consistent with current models used to describe a superplastic deformation mechanism.

4. The Al-10%Mg-0.1%Zr alloy showed consistently greater elongations than the Al-8%Mg-0.1%Zr alloy. The poorer elongations exhibited by the 8% alloy were a result of too much of the magnesium going back into solution at around the 300°C temperature range.

The following recommendations for further study are made:

1. Investigate changes in the processing to result in more of the Zirconium being finely dispersed throughout the microstructure in an attempt to stabilize the microstructure.

2. Conduct step strain rate tests to measure the effect of the grain growth on the strain rate sensitivity of the alloy.

3. Investigate room temperature mechanical behavior of the alloy after it has been deformed at elevated temperatures.

4. Further research into the deformation mechanism observed for this alloy with a view toward determining the role of dislocation type processes.

LIST OF REFERENCES

1. Bengough, G. D., Journal of the Institute of Metals, Vol. 7, p. 123, 1912.

2. Pearson, C. E., Journal of the Institute of Metals, Vol. 54, p. 111, 1934.

3. Bockvar, A. A. and Sviderskaya, Z. A., "Izvest. Akad. Nauk SSSR," Ordel Tekhn. Nauk, Vol. 9, p. 821, 1945.

4. Underwood, L. F., "A Review of Superplasticity and Related Phenomena," Journal of Metals, pp. 914-919, 1962.

5. Sherby, O. D. and Wadsworth, J., "Development and Characterization of Fine-Grain Superplastic Materials," Deformation, Processing, and Structure, pp. 354-384, 1982.

6. Hamilton, C. H. and Stacker, G. W., Metal Progr., Vol. 109, p. 34, 1976.

7. Moore, J. B., Tequesta, J., and Athey, R. L., U.S. Patent No. 3,951,967, 1976.

8. McNelley, T. R. and Garg, A., "Development of Structure and Mechanical Properties in Al-10.2%Mg by Thermo-mechanical Processing," Scripta Metallurgical, Vol. 18, pp. 917-920, 1984.

9. Hartmann, T. S, Mechanical Characteristics of a Superplastic Aluminum-10%Mg-0.1%Zr Alloy, M.S. Thesis, Naval Postgraduate School, Monterey, California, June 1985.

10. Berthold, D. B., Effect of Temperature and Strain Rate on the Microstructure of a Deformed, Superplastic Al-10%Mg-0.1%Zr Alloy, M.S. Thesis, Naval Postgraduate School, Monterey, California, June 1985.

11. Lloyd, D. J. and Moore, D. M., "Aluminum Alloy Design for Superplasticity," Superplastic Forming of Structure Alloys, Conference Proceedings of TMS-AIME, pp. 147-172, June 1982.

12. Stowell, M. J., "Cavitation in Superplasticity," Superplastic Forming of Structure Alloys, Conference Proceeding of TMS-AIME, pp. 321-336, June 1982.

13. Gifkins, R. C., "Mechanicsm of Superplasticity," Superplastic Forming of Structural Alloys, Conference Proceedings of TMS-AIME, pp. 3-26, June 1982.

14. Ashby, M. F. and Verrall, R. A., "Diffusion-Accommodated Flow and Superplasticity," Acta Metallurgica, Vol. 21, pp. 149-163, 1973.

15. Nix, W. D., "On Some Fundamental Aspects of Superplastic Flow," ASM Metals/Materials Technology Series, 1984 ASM Superplastic Forming Symposium, pp. 1-12, 22 March 1984.

16. Langdon, T. G., "Experimental Observation in Superplasticity," Superplastic Forming of Structural Alloys, Conference Proceedings of TMS-AIME, pp. 27-40, June 1982.

17. Weertman, J., Journal of Applied Physics, Vol. 26, p. 1213, 1955.

18. Weertman, J., Journal of Applied Physics, Vol. 28, p. 362, 1957.

19. Sherby, O. D. and Burke, P. M., "Mechanical Behavior of Crystalline Solids at Elevated Temperatures," Progress in Materials Science, Vol. 13, p. 325, 1968.

20. Ness, F. G., Jr., High Strength to Weight Aluminum-18 Weight Percent Magnesium Alloy Through Thermomechanical Processing, M.S. Thesis, Naval Postgraduate School, Monterey, California, December 1976.

21. Grandon, R. A., High Strength Aluminum-Magnesium Alloys: Thermomechnical Processing, Microstructure and Tensile Mechanical Properties of High Strength Aluminum-Magnesium Alloy, M.S. Thesis, Naval Postgraduate School, Monterey, California, March 1980.

22. Speed, W. G., An Investigation into the Influence of Thermomechanical Processing on Microstructure and Mechanical Properties of High Strength Aluminum-Magnesium Alloys, M.S. Thesis, Naval Postgraduate School, Monterey, California, December 1977.

23. Bingay, C. P., Microstructural Response of Aluminum-Magnesium Alloys to Thermomechanical Processing, M.S. Thesis, Naval Postgraduate School, Monterey, California, December 1977.

24. Chesterman, C. W., Jr., Precipitation, Recovery and Recrystallization Under Static and Dynamic Conditions for High Magnesium Aluminum-Magnesium Alloys, M.S. Thesis, Naval Postgraduate School, Monterey, California, March 1980.

25. Shirah, R. H., The Influence of Solution Time and Quench Rate on the Microstructure and Mechanical Properties of High Magnesium Aluminum-Magnesium Alloys, M.S. Thesis, Naval Postgraduate School, Monterey, California, December 1981.

26. Glover, T. L., Effects of Thermomechanical Procesing of Aluminum-Magnesium Alloys Containing High Weight Percent Magnesium, M.S. Thesis, Naval Postgraduate School, Monterey, California, December 1977.

27. Johnson, R. B., The Influence of Alloy Composition and Thermomechanical Processing Procedure on Microstructural and Mechanical Properties of High Magnesium Aluminum-Magnesium Alloys, M.S. Thesis, Naval Postgraduate School, Monterey, California, June 1980.

28. Becker, J. J., Superplasticity in Thermomechanically Processed High-Magnesium Aluminum Magnesium Alloys, M.S. Thesis, Naval Postgraduate School, Monterey, California, March 1984.

29. Mills, M. E., Superplasticity in Thermomechanically Processed Aluminum-10.2%Mg-0.52%Mn Alloy, M.S. Thesis, Naval Postgraduate School, Monterey, California, September 1984.

30. Self, R. J., The Effect of Alloy Additions on Superplasticity in Thermomechanically Processed High Magnesium Aluminum Magnesium Alloys, M.S. Thesis, Naval Postgraduate School, Monterey, California, December 1984.

31. Stengel, A. R., Effects of Annealing Treatments on Superplasticity in a Thermomechanically Processed Aluminum-10.2%Mg-0.52%Mn Alloy, M.S. Thesis, Naval Postgraduate School, Monterey, California, December 1984.

32. Alcoa Technical Center, Ltr, August 1984.

33. Underwood, E. E., Quantitative Sterelogy, Addison-Wesley, 1970.

34. Meyers, M. N. and Chawla, K. K., Mechanical Metallurgy, Principles and Applications, Prentice-Hall, Inc., 1984.

APPENDIX A: GRAPHS FROM INITIAL TESTING OF Al-10%Mg-0.1%Zr AND Al-8%Mg-0.1%Zr ALLOYS

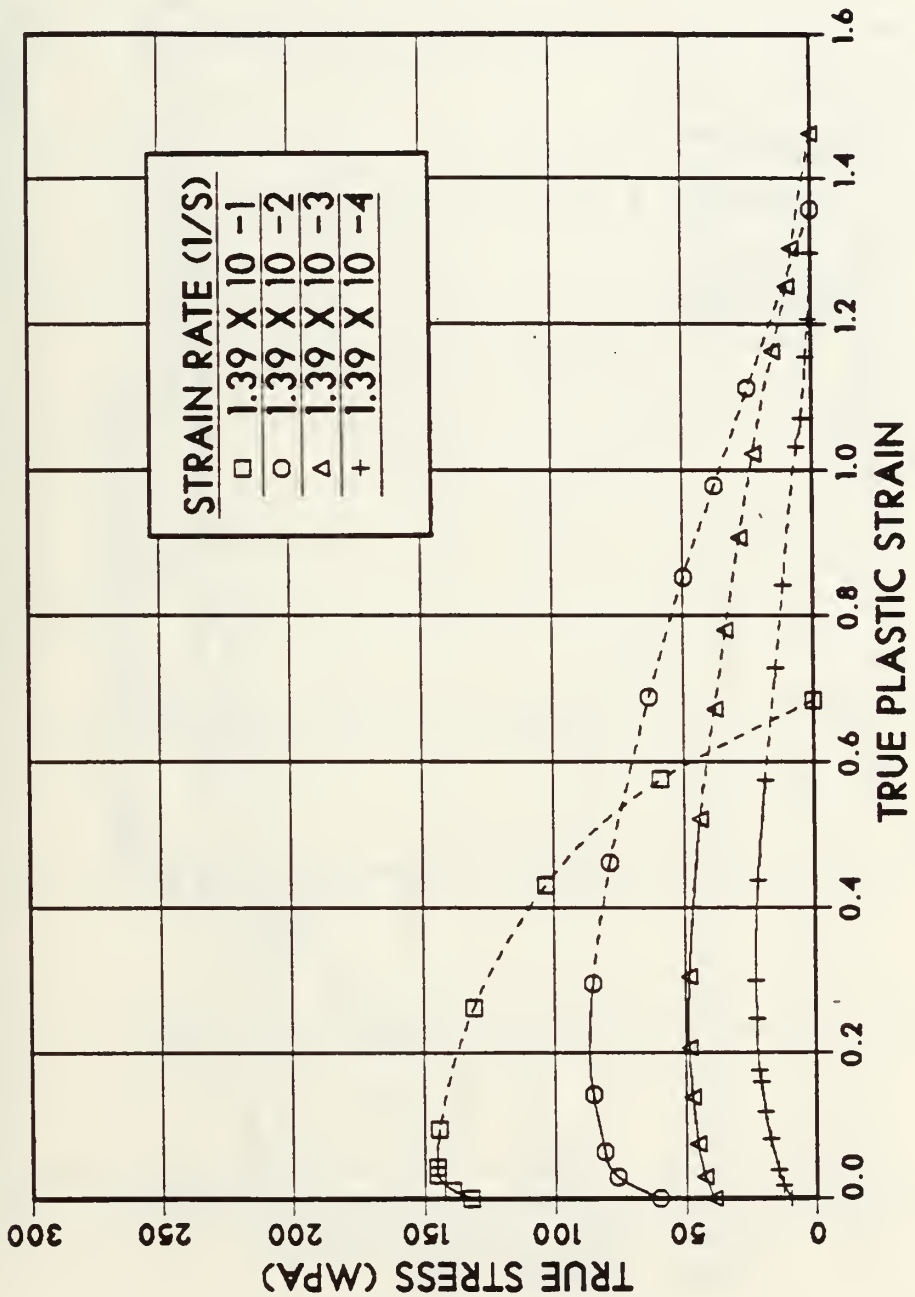

Figure A.1 True stress vs. true plastic strain for tests conducted at 300°C on Al-10%Mg-0.1%Zr. Solution treated, hot worked, oil quenched, and warm rolled at 300°C to 94% reduction. Dashed lines indicate straining beyond the onset of necking.

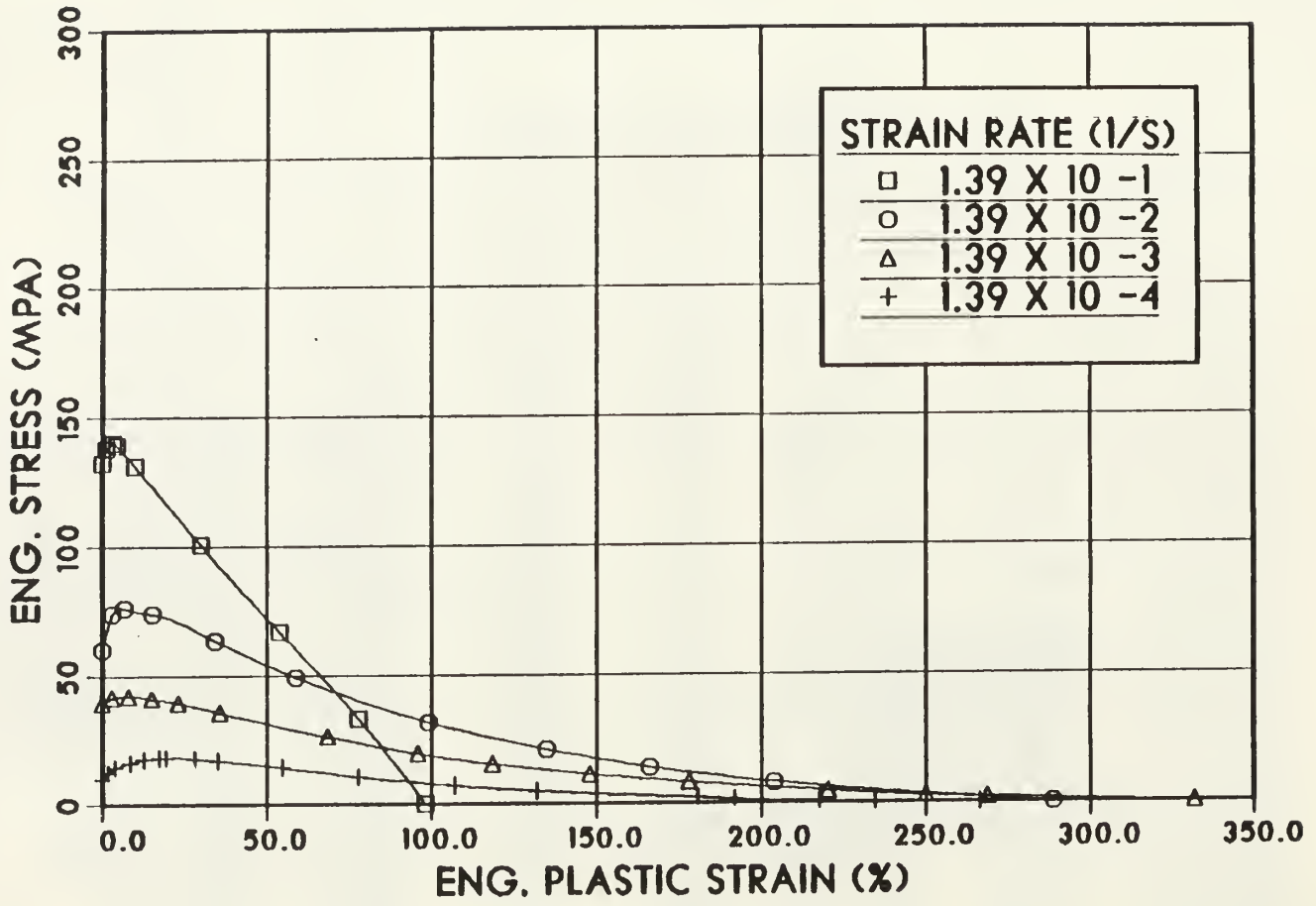

Figure A.2 Engineering stress vs. engineering plastic strain for tests conducted at 300°C on Al-10%Mg-0.1%Zr. Solution treated, hot worked, oil quenched, and warm rolled at 300°C to 94% reduction.

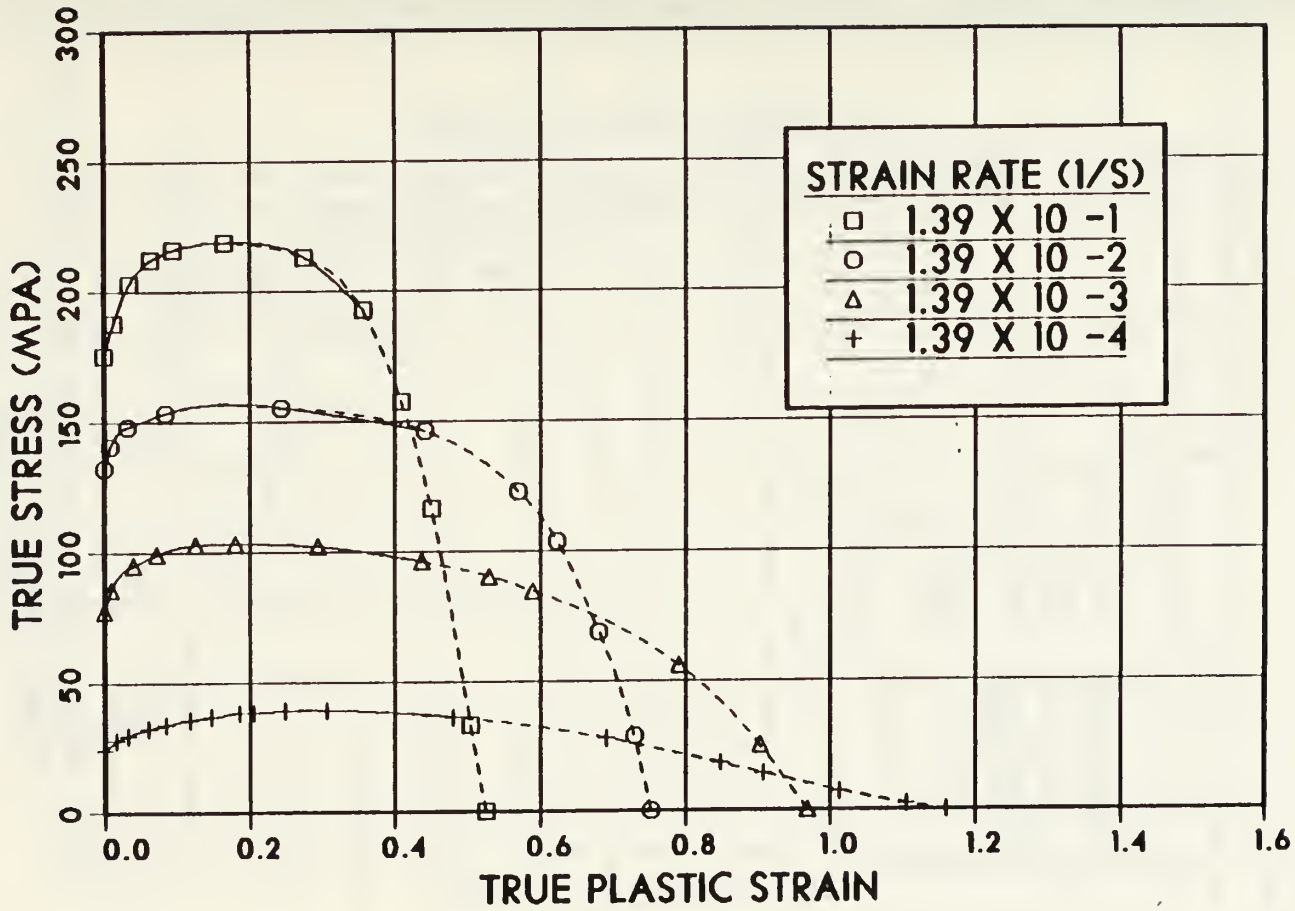

Figure A.3 True stress vs. true plastic strain for tests conducted at 250°C on Al-10%Mg-0.1%Zr. Solution treated, hot worked, oil quenched, and warm rolled at 300°C to 94% reduction. Dashed lines indicate straining beyond the onset of necking.

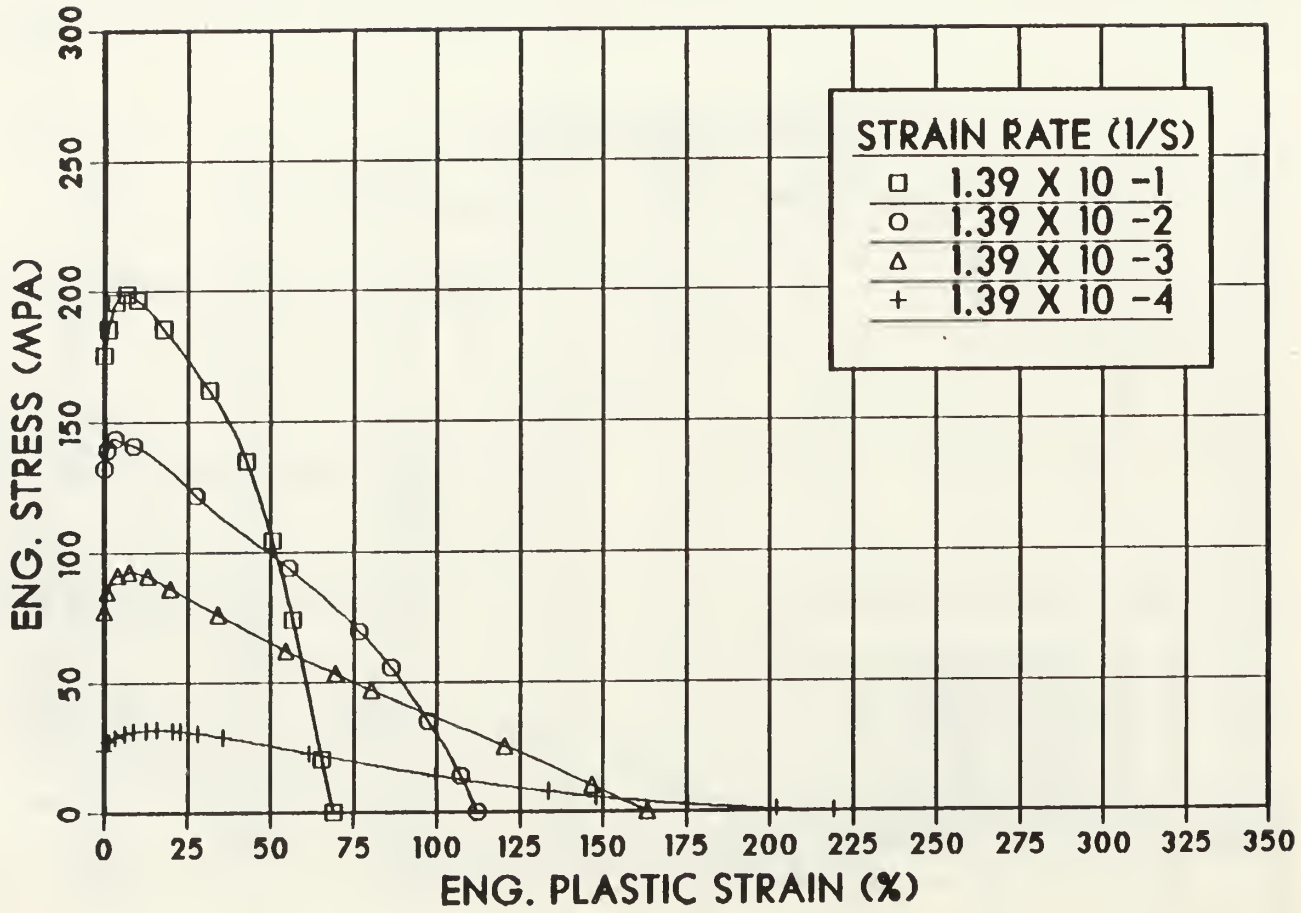

Figure A.4 Engineering stress vs. engineering plastic strain for tests conducted at 250°C on Al-10%Mg-0.1%Zr. Solution treated, hot worked, oil quenched, and warm rolled at 300°C to 94% reduction.

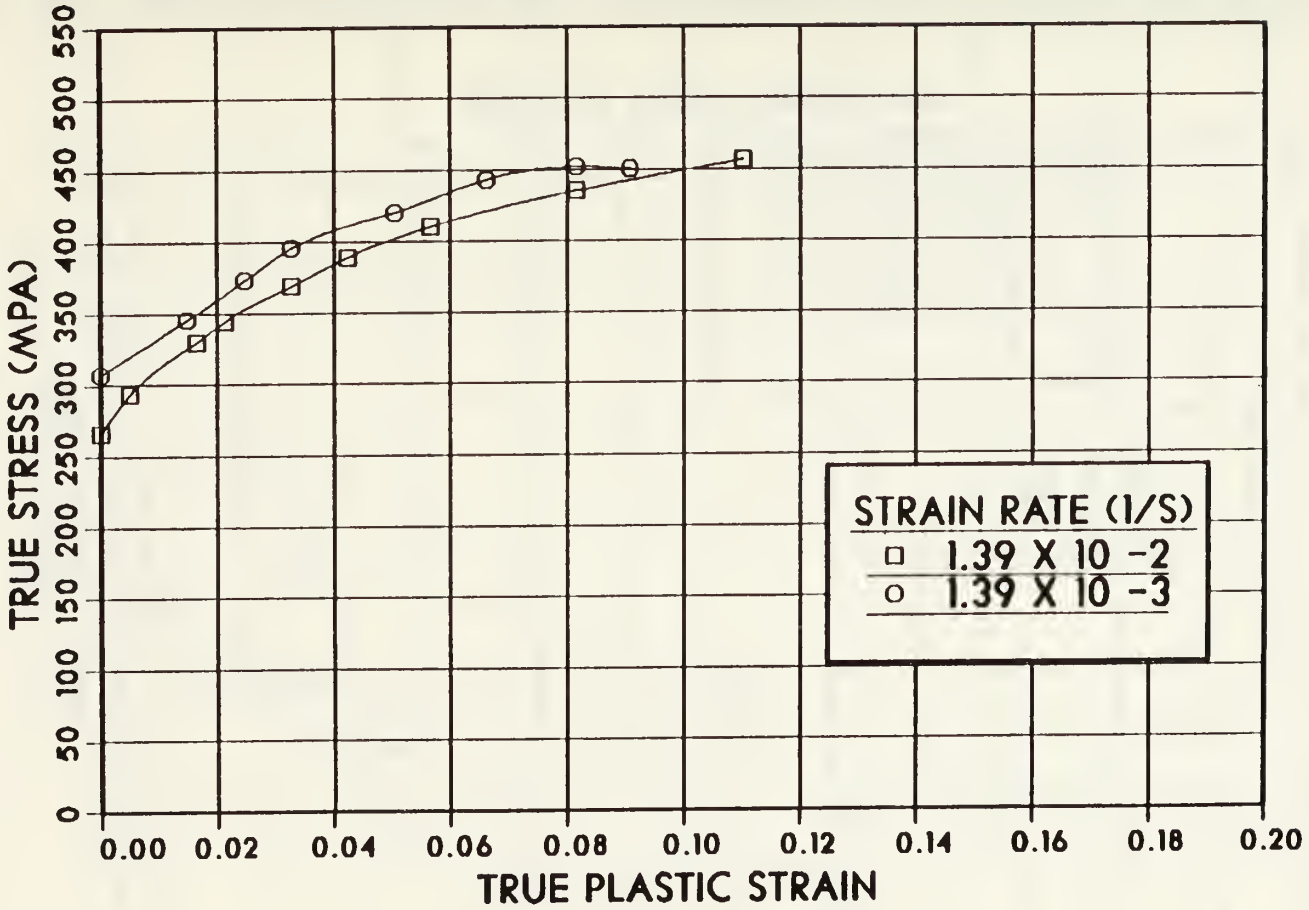

Figure A.5 True stress vs. true plastic strain for tests conducted at 20°C on Al-10%Mg-0.1%Zr. Solution treated, hot worked, oil quenched, and warm rolled at 300°C to 94% reduction. Dashed lines indicate straining beyond the onset of necking.

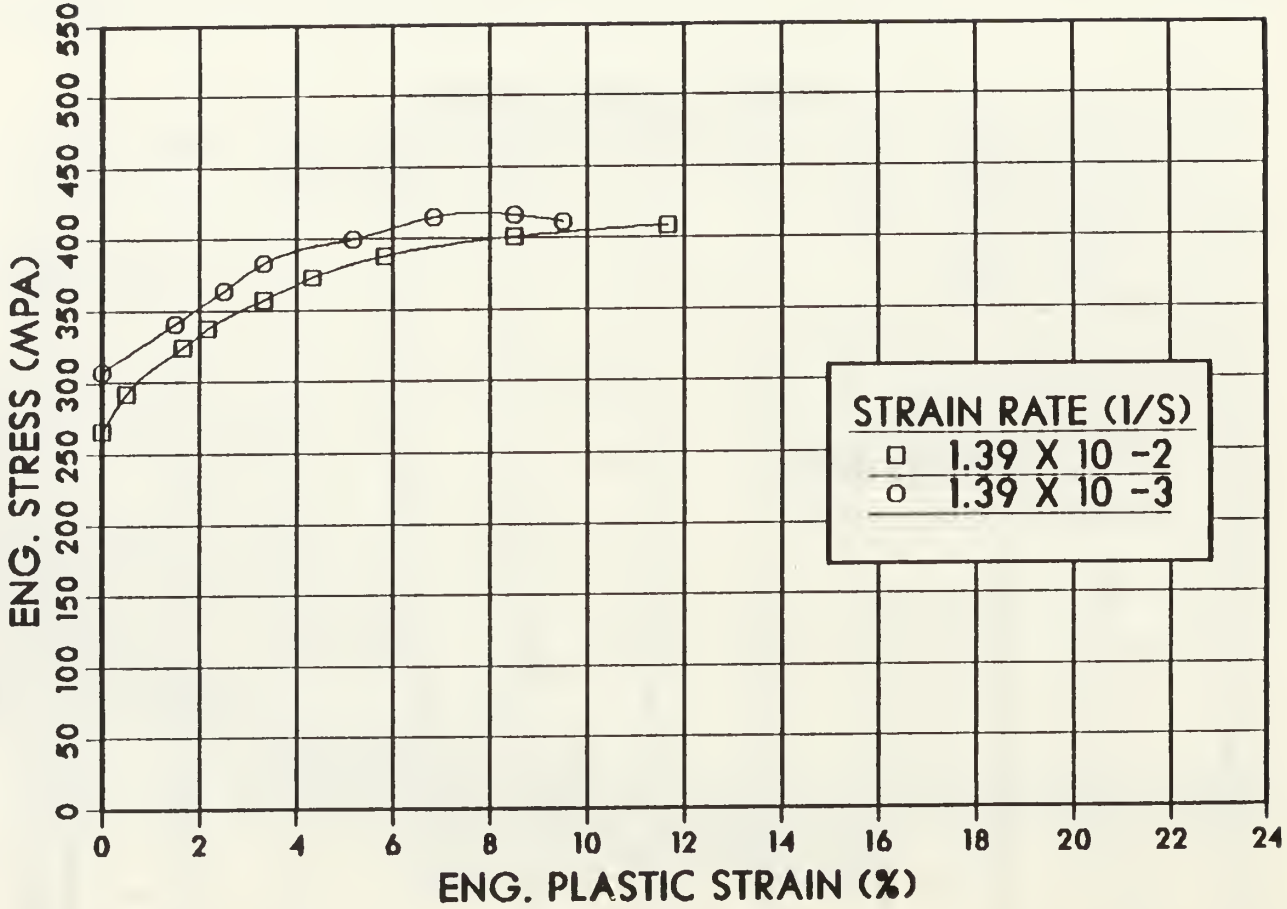

Figure A.6 Engineering stress vs. engineering plastic strain for tests conducted at 20°C on Al-10%Mg-0.1%Zr. Solution treated, hot worked, oil quenched, and warm rolled at 300°C to 94% reduction.

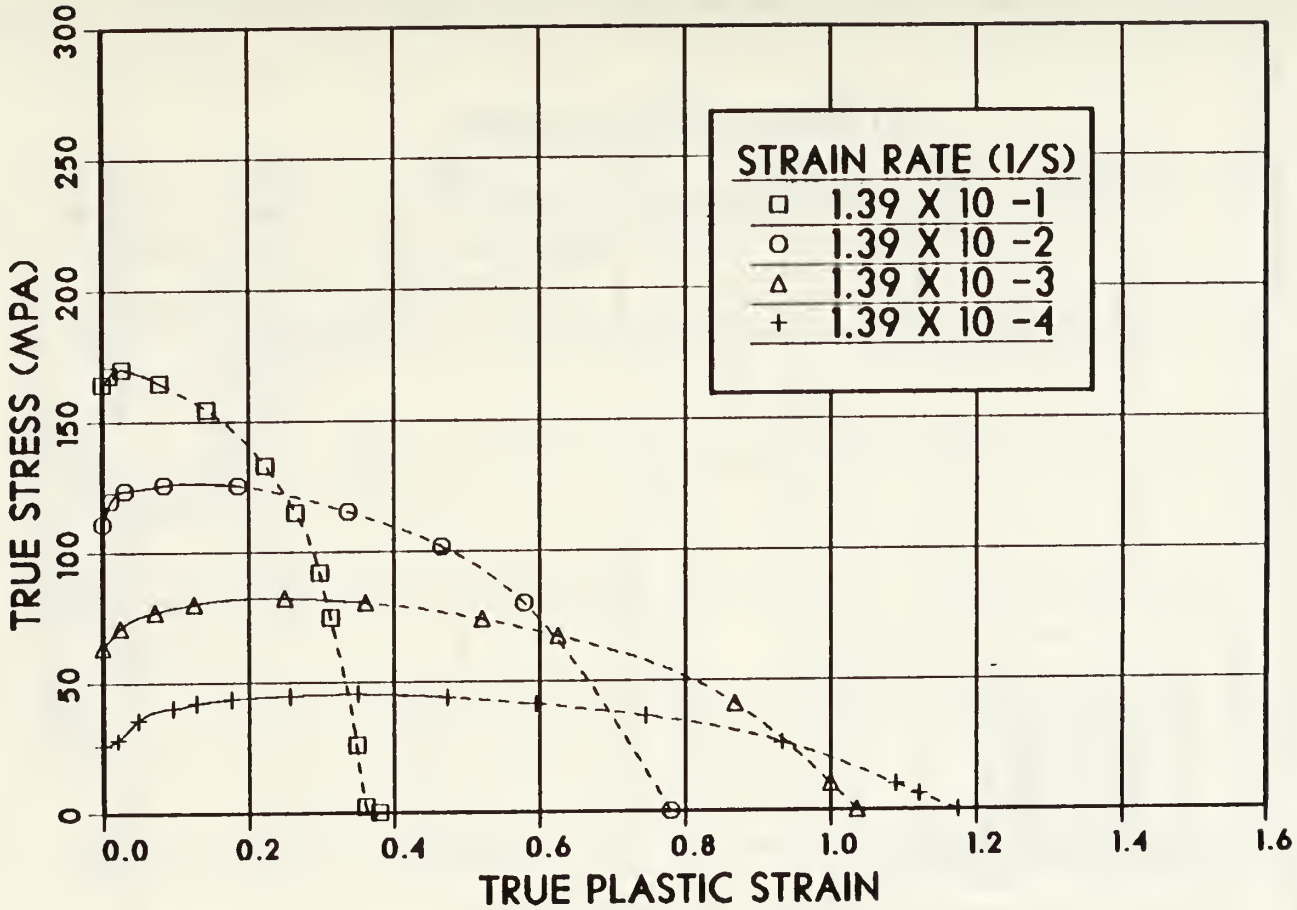

Figure A.7 True stress vs. true plastic strain for tests conducted at 300°C on Al-8%Mg-0.1%Zr. Solution treated, hot worked, oil quenched, and warm rolled at 300°C to 94% reduction. Dashed lines indicate straining beyond the onset of necking.

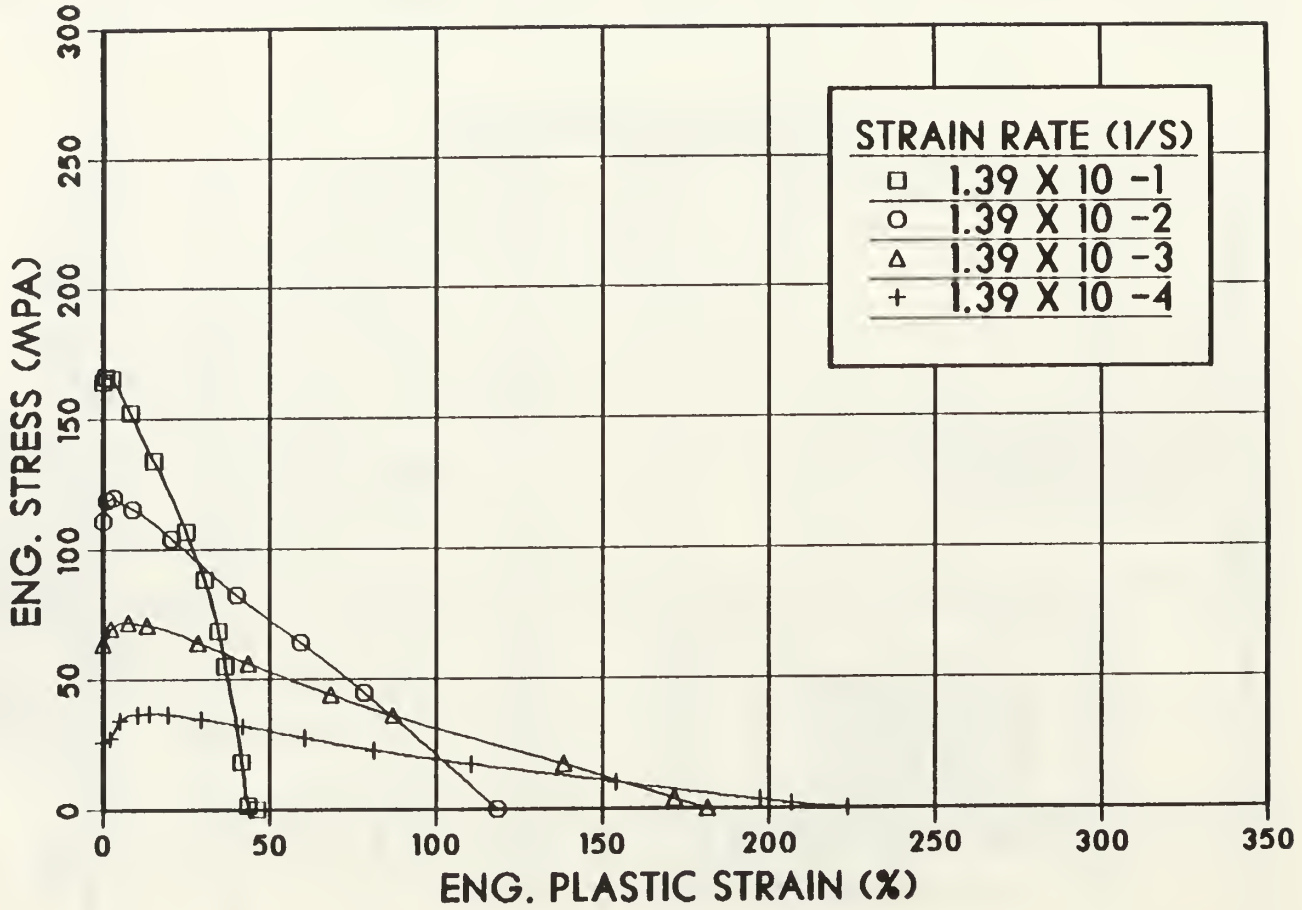

Figure A.8 Engineering stress vs. engineering plastic strain for tests conducted at 300°C on Al-8%Mg-0.1%Zr. Solution treated, hot worked, oil quenched, and warm rolled at 300°C to 94% reduction.

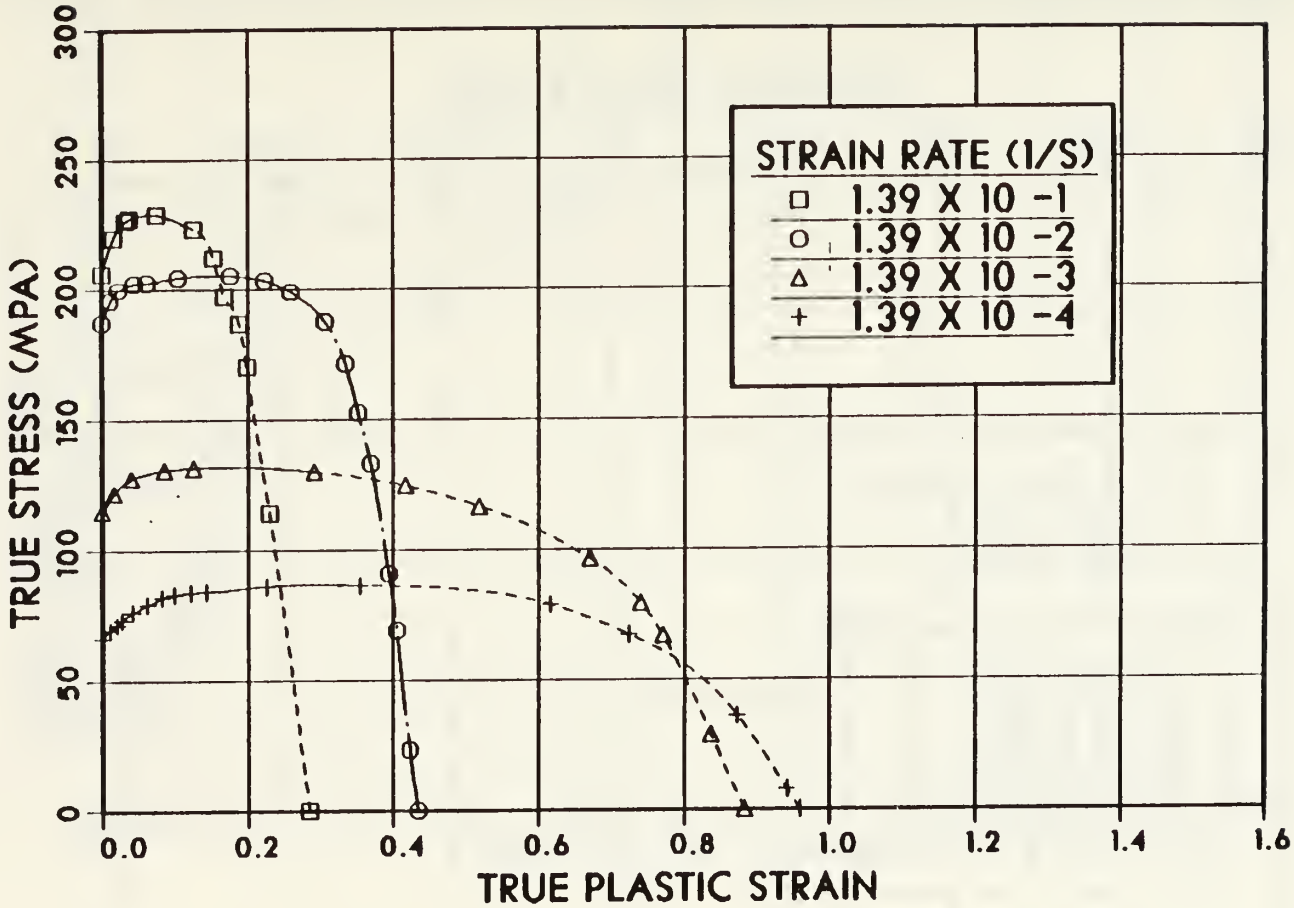

Figure A.9 True stress vs. true plastic strain for tests conducted at 250°C on Al-8%Mg-0.1%Zr. Solution treated, hot worked, oil quenched, and warm rolled at 300°C to 94% reduction. Dashed lines indicate straining beyond the onset of necking.

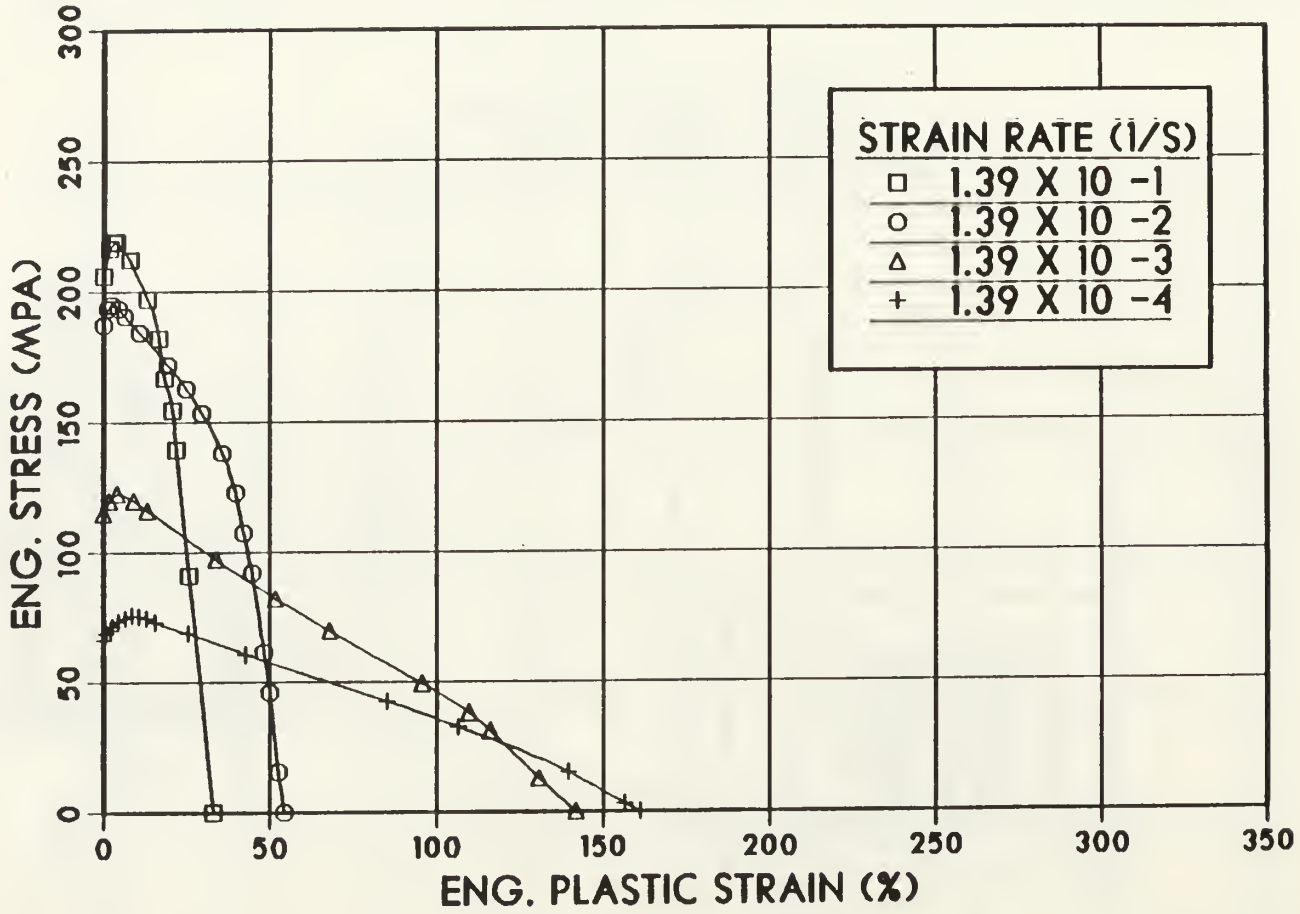

Figure A.10 Engineering stress vs. engineering plastic strain for tests conducted at 250°C on Al-8%Mg-0.1%Zr. Solution treated, hot worked, oil quenched, and warm rolled at 300°C to 94% reduction.

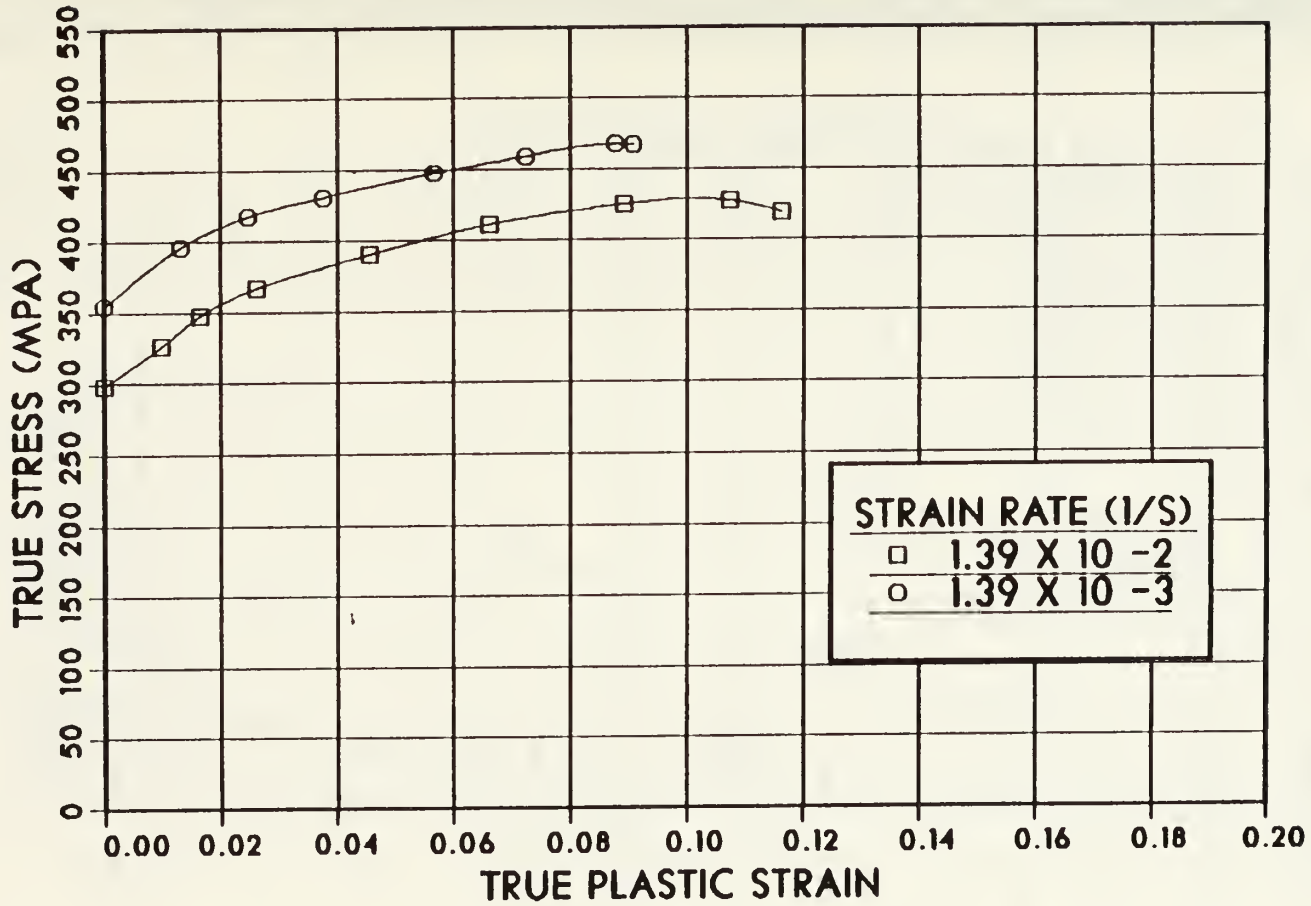

Figure A.11 True stress vs. true plastic strain for tests conducted at 20°C on Al-8%Mg-0.1%Zr. Solution treated, hot worked, oil quenched, and warm rolled at 300°C to 94% reduction. Dashed lines indicate straining beyond the onset of necking.

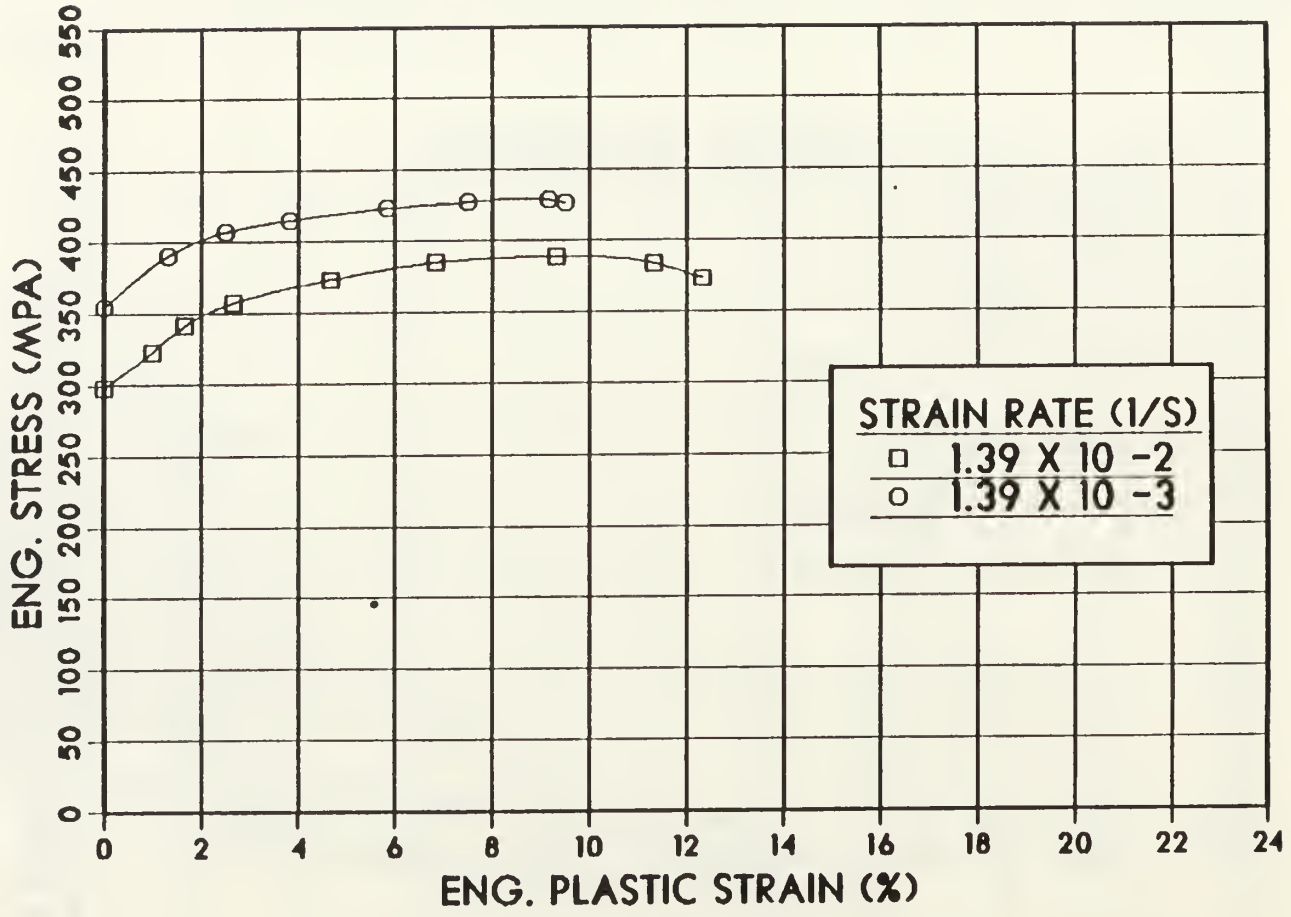

Figure A.12 Engineering stress vs. engineering plastic strain for tests conducted at 20°C on Al-8%Mg-0.1%Zr. Solution treated, hot worked, oil quenched, and warm rolled at 300°C to 94% reduction.

APPENDIX B: GRAPHS FROM TESTING OF AL-10%Mg-0.1%Zr ALLOY AT 300°C

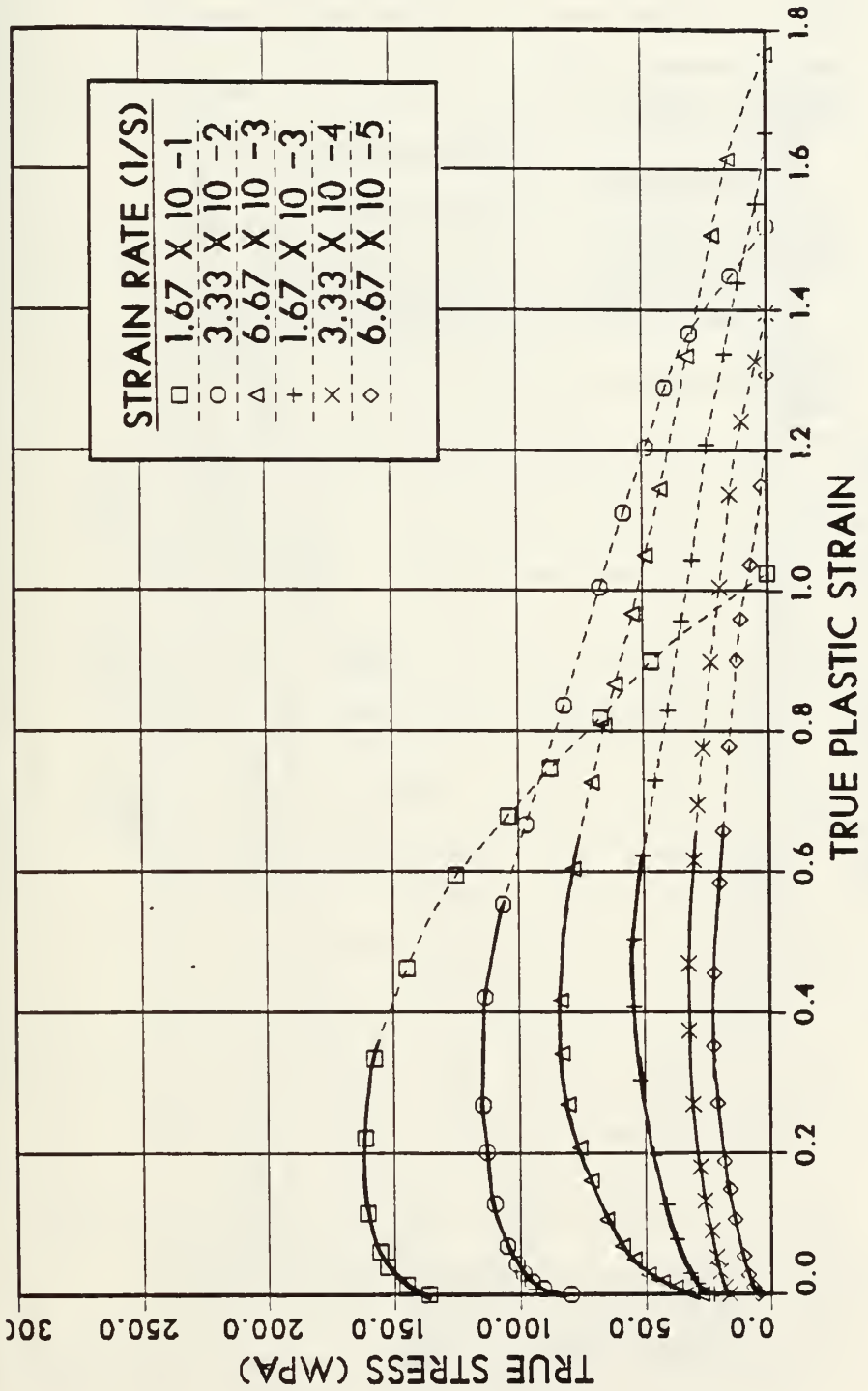

Figure B.1 True stress vs. true plastic strain for tests conducted at 300°C on Al-10%Mg-0.1%Zr. Solution treated, hot worked, oil quenched, and warm rolled at 300°C to 92% reduction. Dashed lines indicate straining beyond the onset of necking.

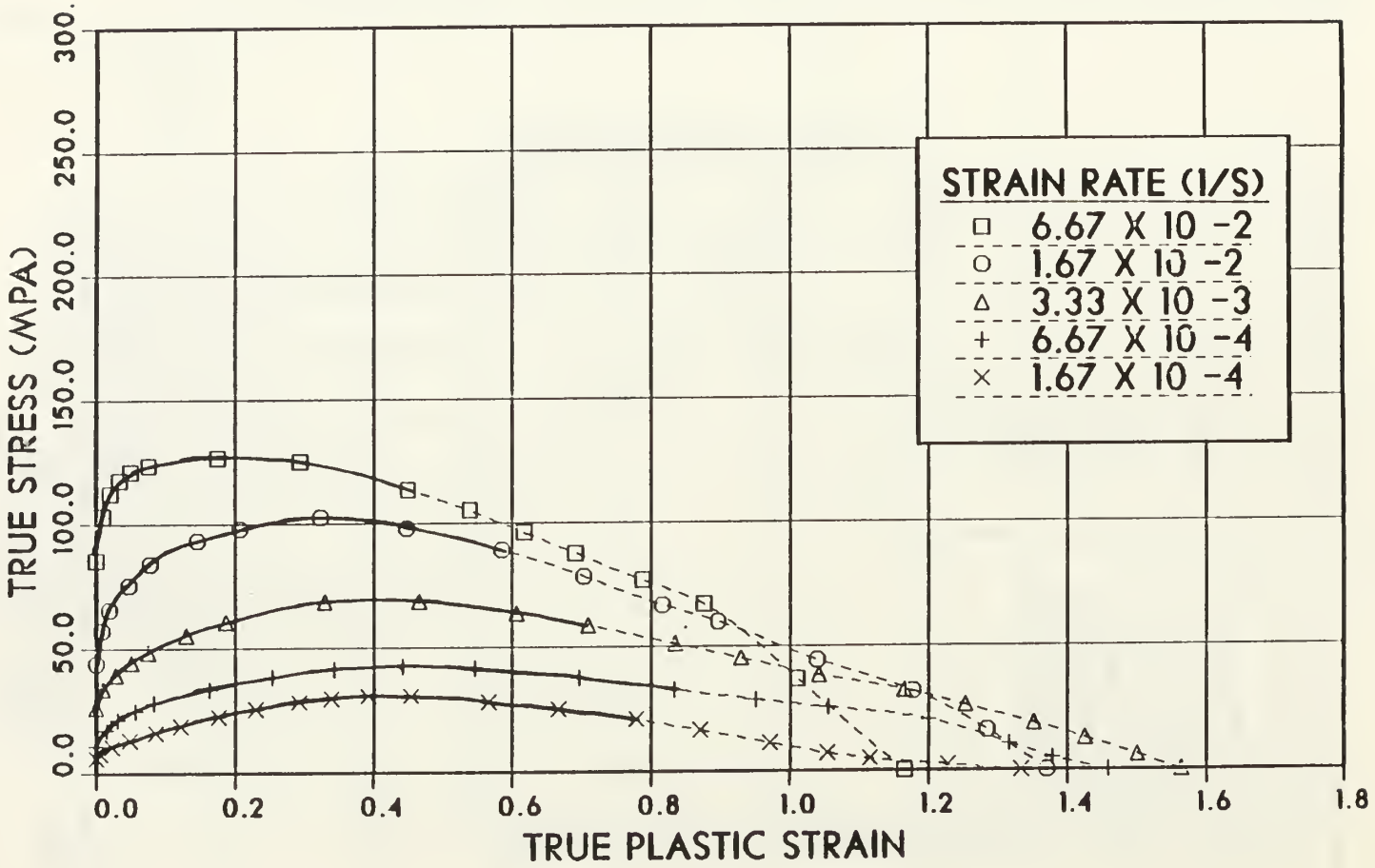

Figure B.2 True stress vs. true plastic strain for tests conducted at 300°C on Al-10%Mg-0.1%Zr. Solution treated, hot worked, oil quenched, and warm rolled at 300°C to 92% reduction. Dashed lines indicate straining beyond the onset of necking.

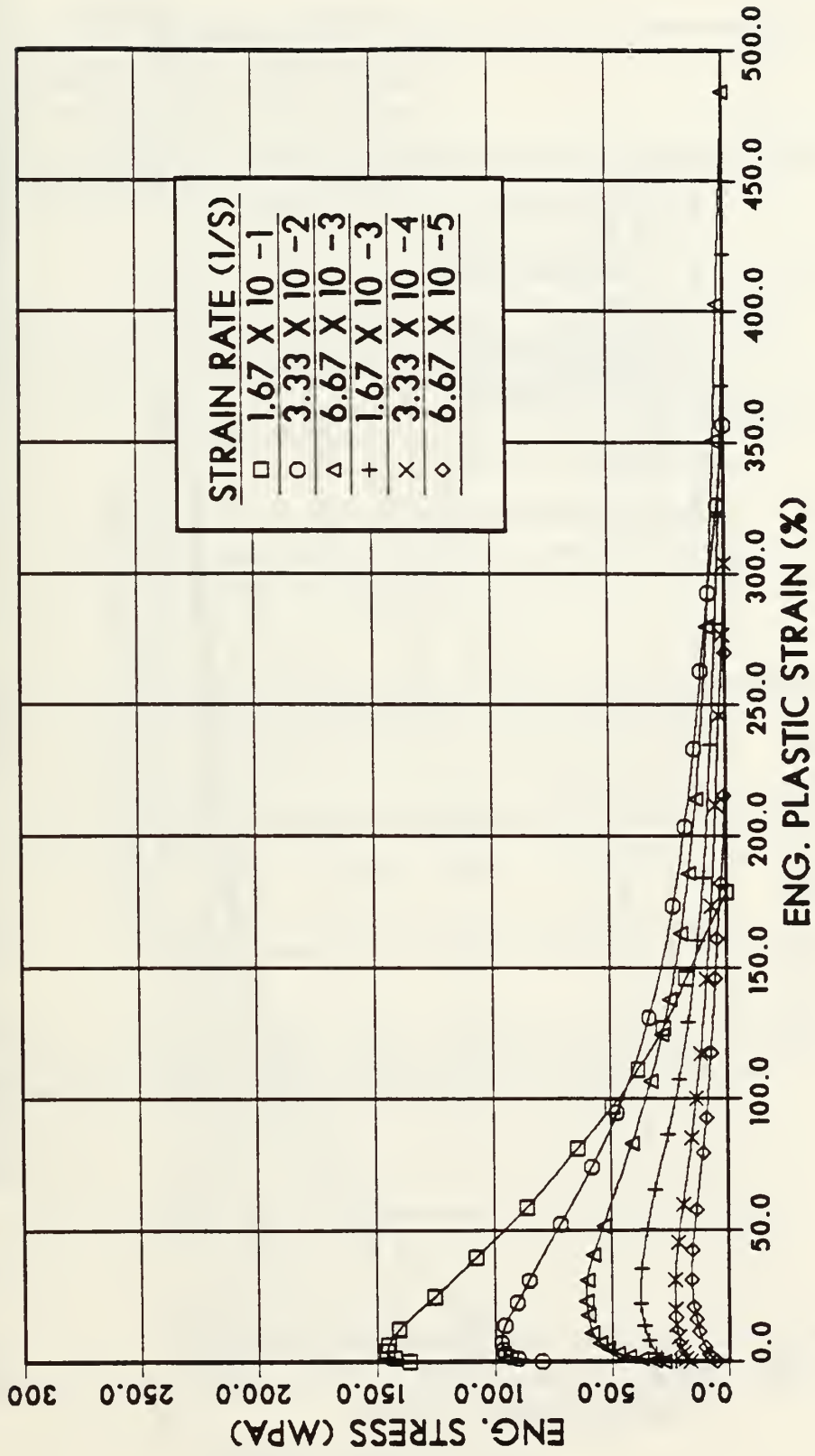

Figure B.3 Engineering stress vs. engineering plastic strain for tests conducted at 300°C on Al-10%Mg-0.1%Zr. Solution treated, hot worked, oil quenched, and warm rolled at 300°C to 92% reduction.

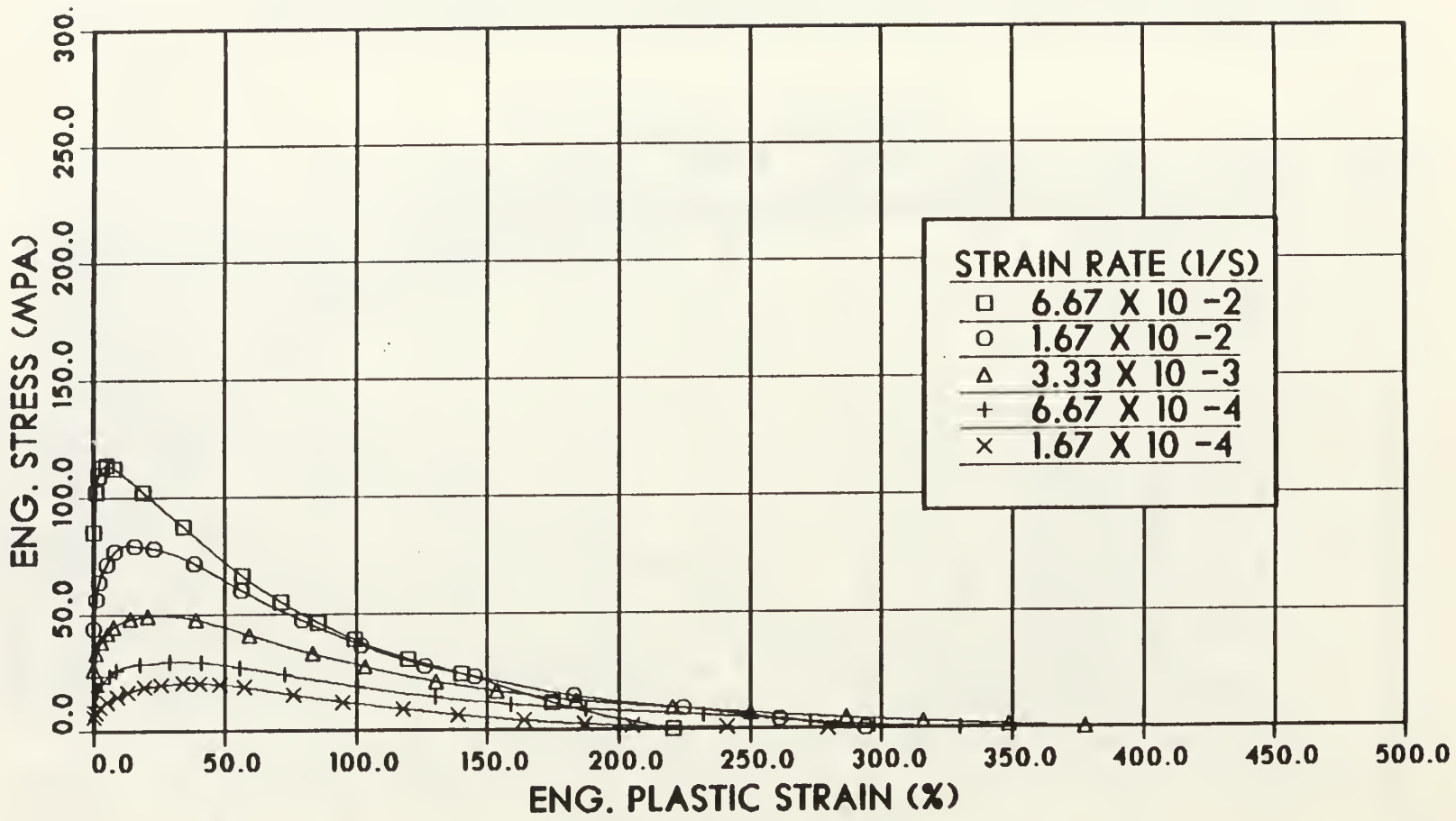

Figure B.4 Engineering stress vs. engineering plastic strain for tests conducted at 300°C on Al-10%Mg-0.1%Zr. Solution treated, hot worked, oil quenched, and warm rolled at 300°C to 92% reduction.

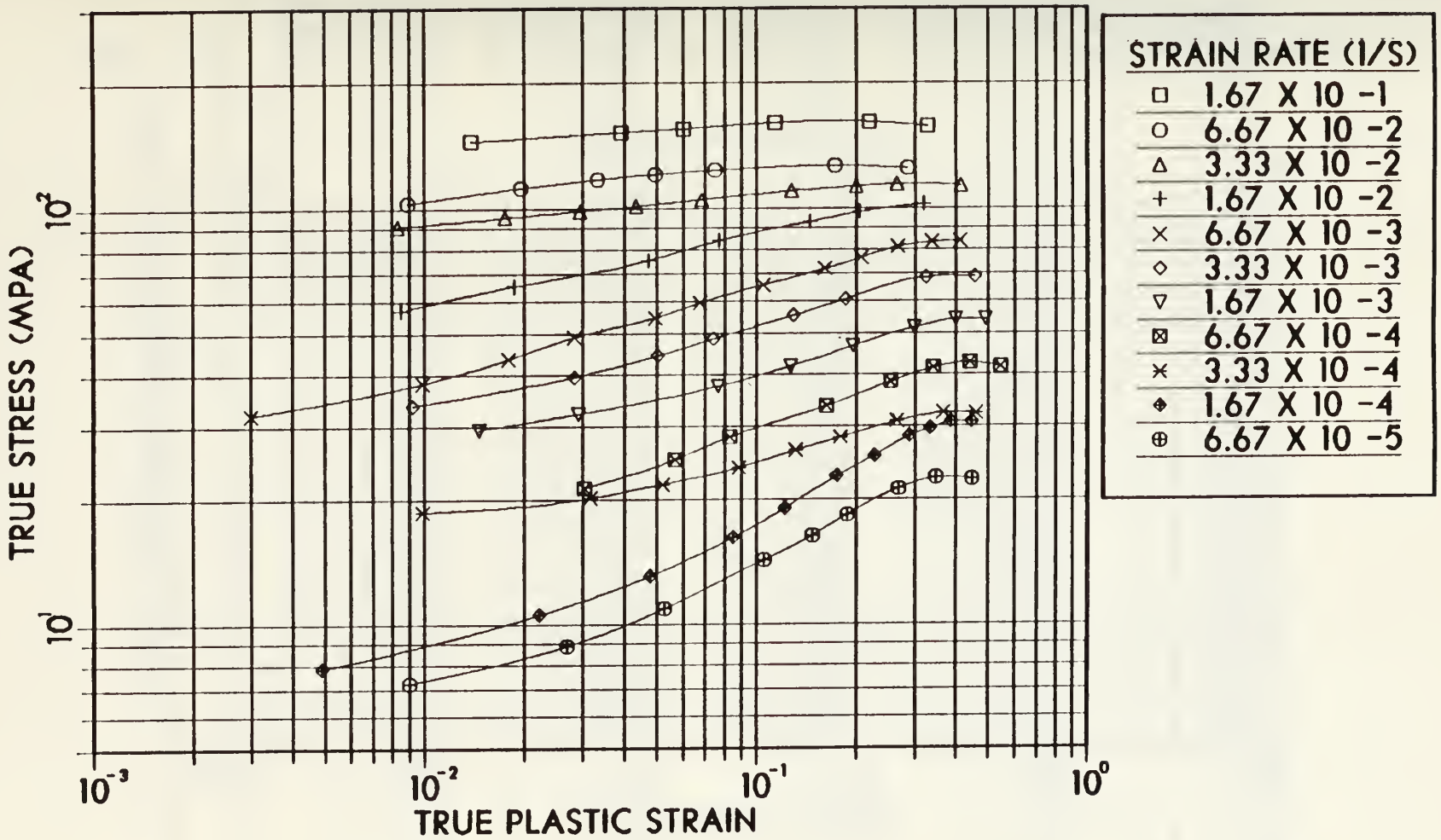

Figure B.5 True stress vs. true strain plotted on logarithmic axes for tests conducted at 300°C on Al-10%Mg-0.1%Zr. Solution treated, hot worked, oil quenched, and warm rolled at 300°C to 92% reduction.

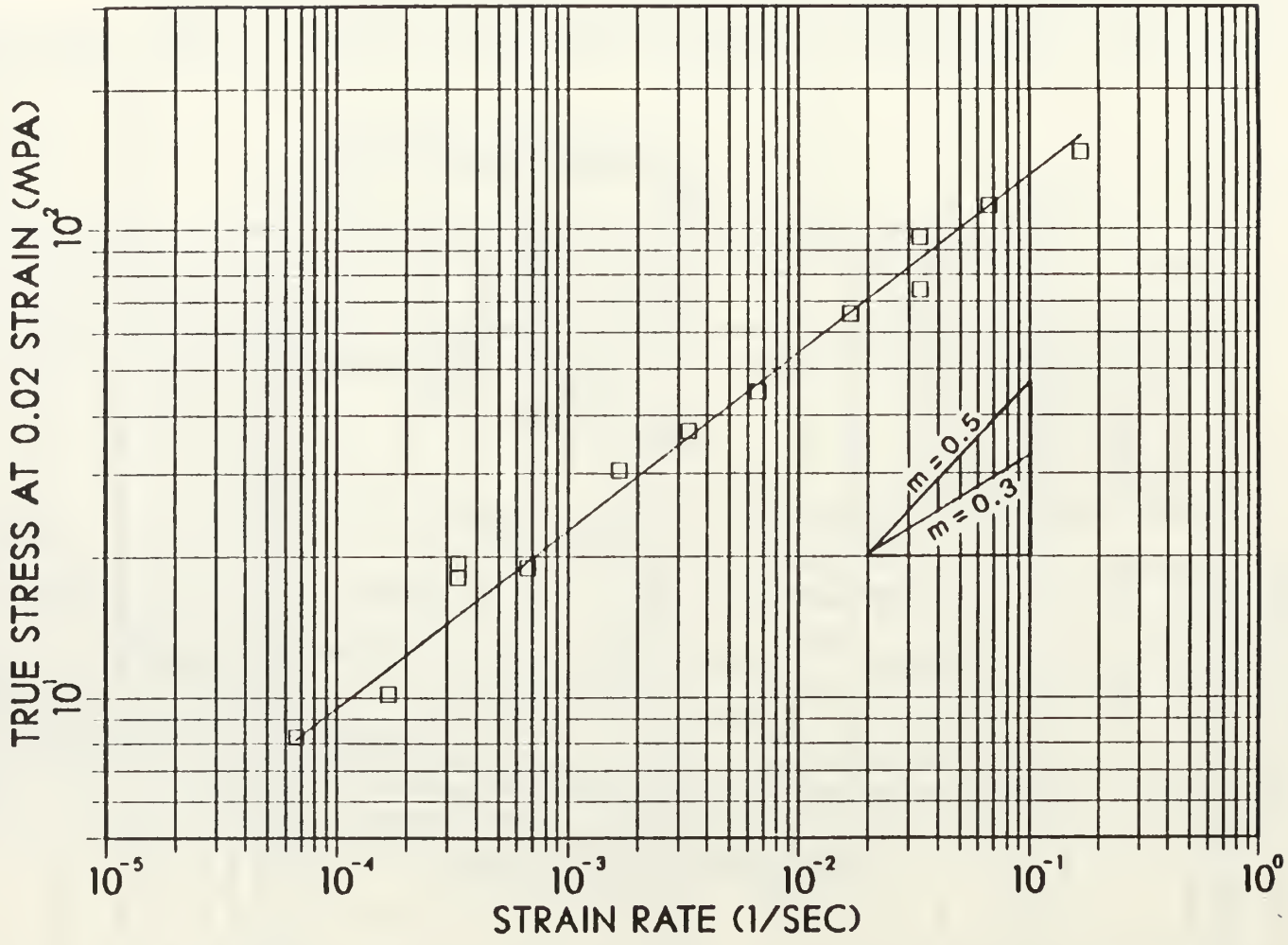

Figure B.6 True stress at 0.02 strain vs. strain rate for tests conducted at 300°C on Al-10%Mg-0.1%Zr. Solution treated, hot worked, oil quenched, and warm rolled at 300°C to 92% reduction.

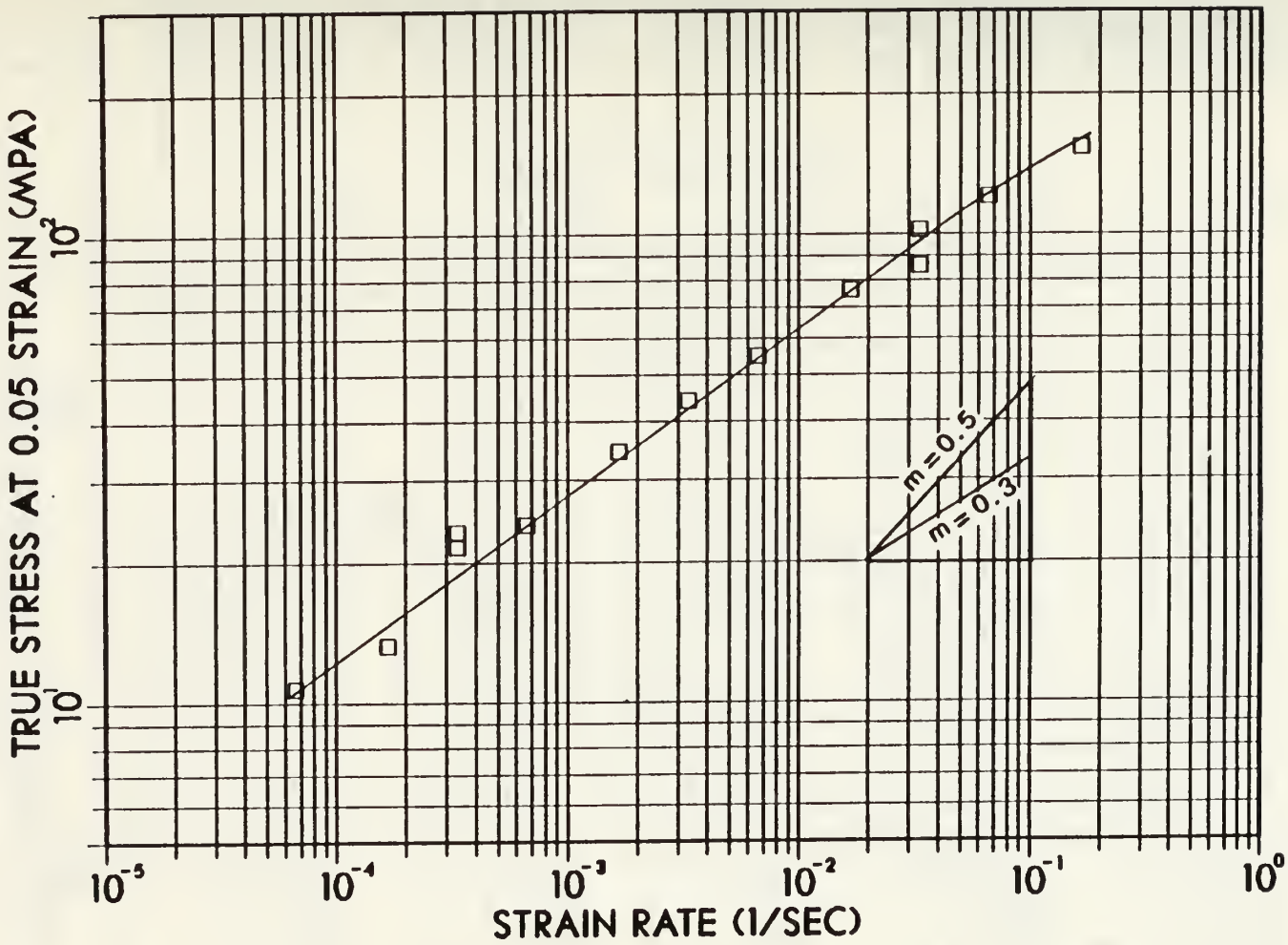

Figure B.7 True stress at 0.05 strain vs. strain rate for tests conducted at 300°C on Al-10%Mg-0.1%Zr. Solution treated, hot worked, oil quenched, and warm rolled at 300°C to 92% reduction.

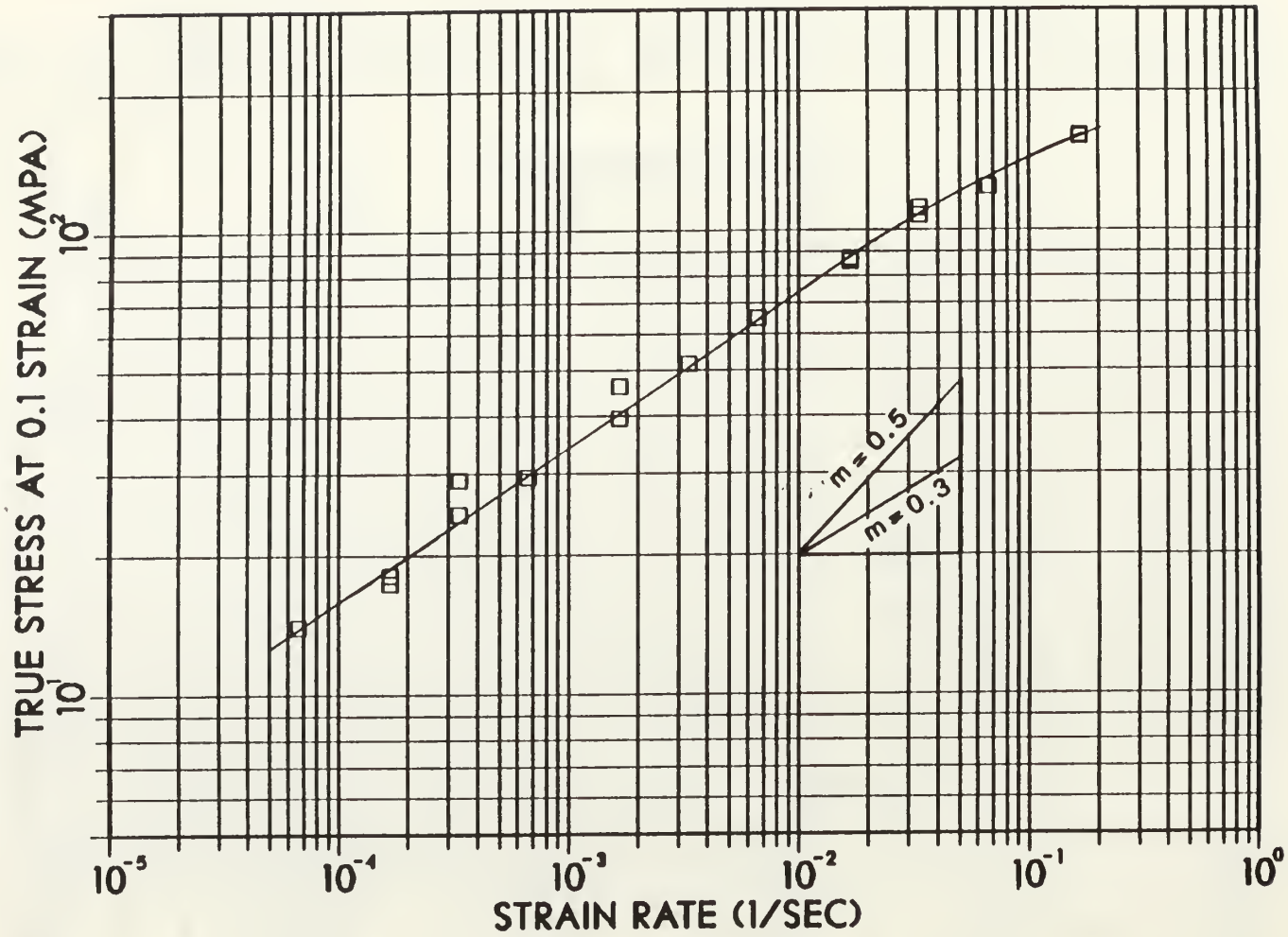

Figure B.8 True stress at 0.1 strain vs. strain rate for tests conducted at 300°C on Al-10%Mg-0.1%Zr. Solution treated, hot worked, oil quenched, and warm rolled at 300°C to 92% reduction.

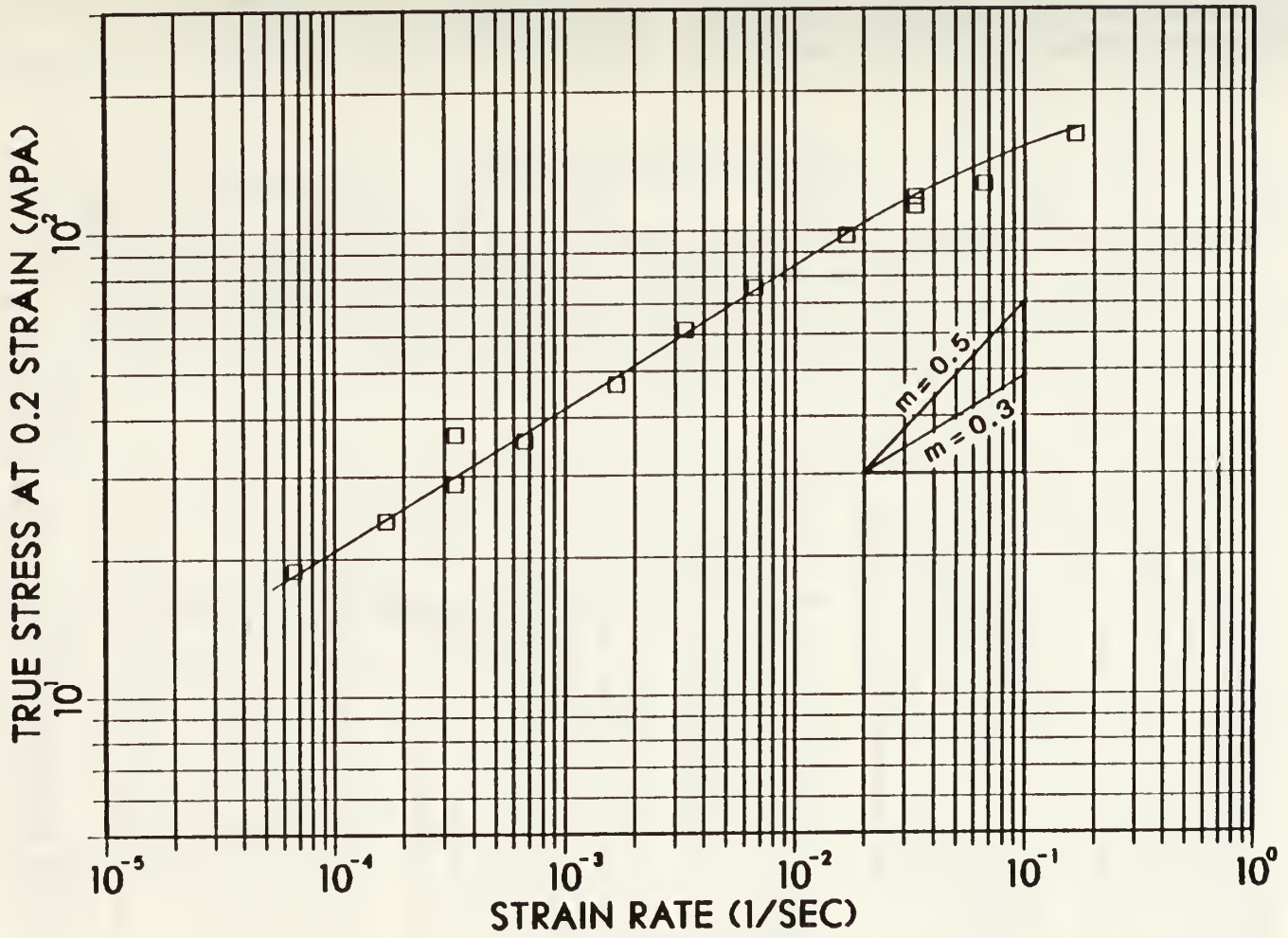

Figure B.9 True stress at 0.2 strain vs. strain rate for tests conducted at 300°C on Al-10%Mg-0.1%Zr. Solution treated, hot worked, oil quenched, and warm rolled at 300°C to 92% reduction.

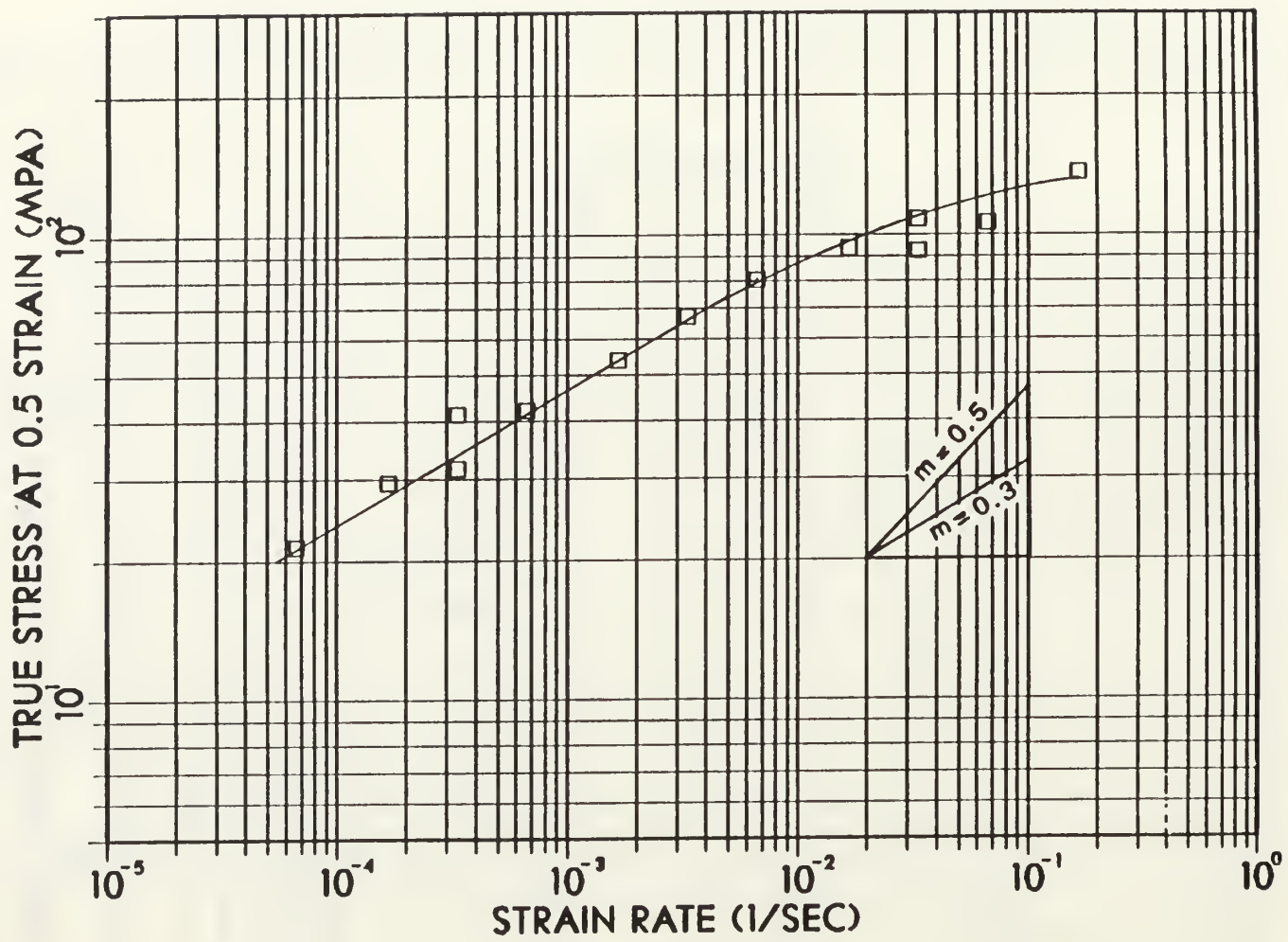

Figure B.10 True stress at 0.5 strain vs. strain rate for tests conducted at 300°C on Al-10%Mg-0.1%Zr. Solution treated, hot worked, oil quenched, and warm rolled at 300°C to 92% reduction.

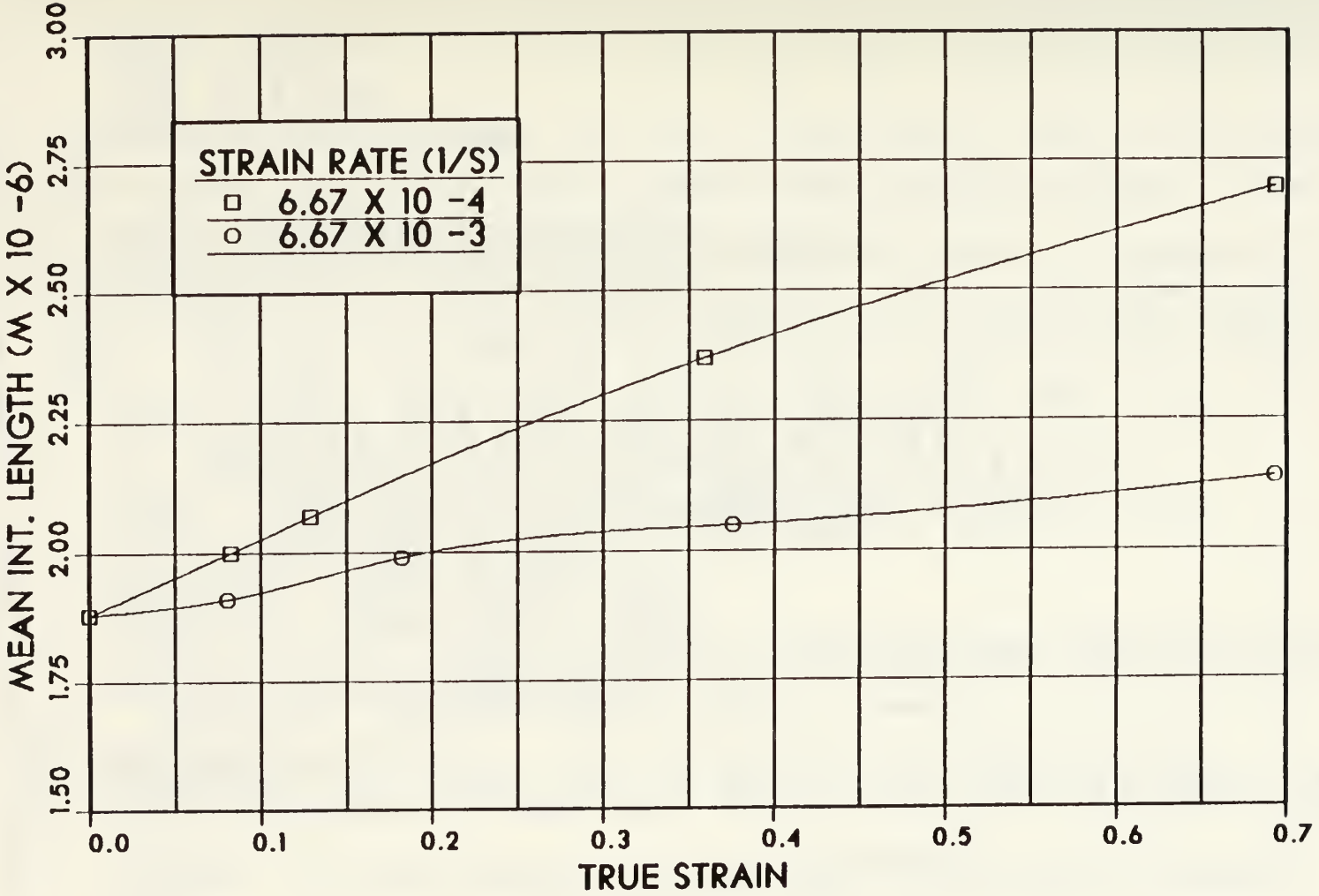

Figure B.11 Mean intercept length vs. true strain for tests conducted at 300°C on Al-10%Mg-0.1%Zr. Solution treated, hot worked, oil quenched, and warm rolled at 300°C to 92% reduction.

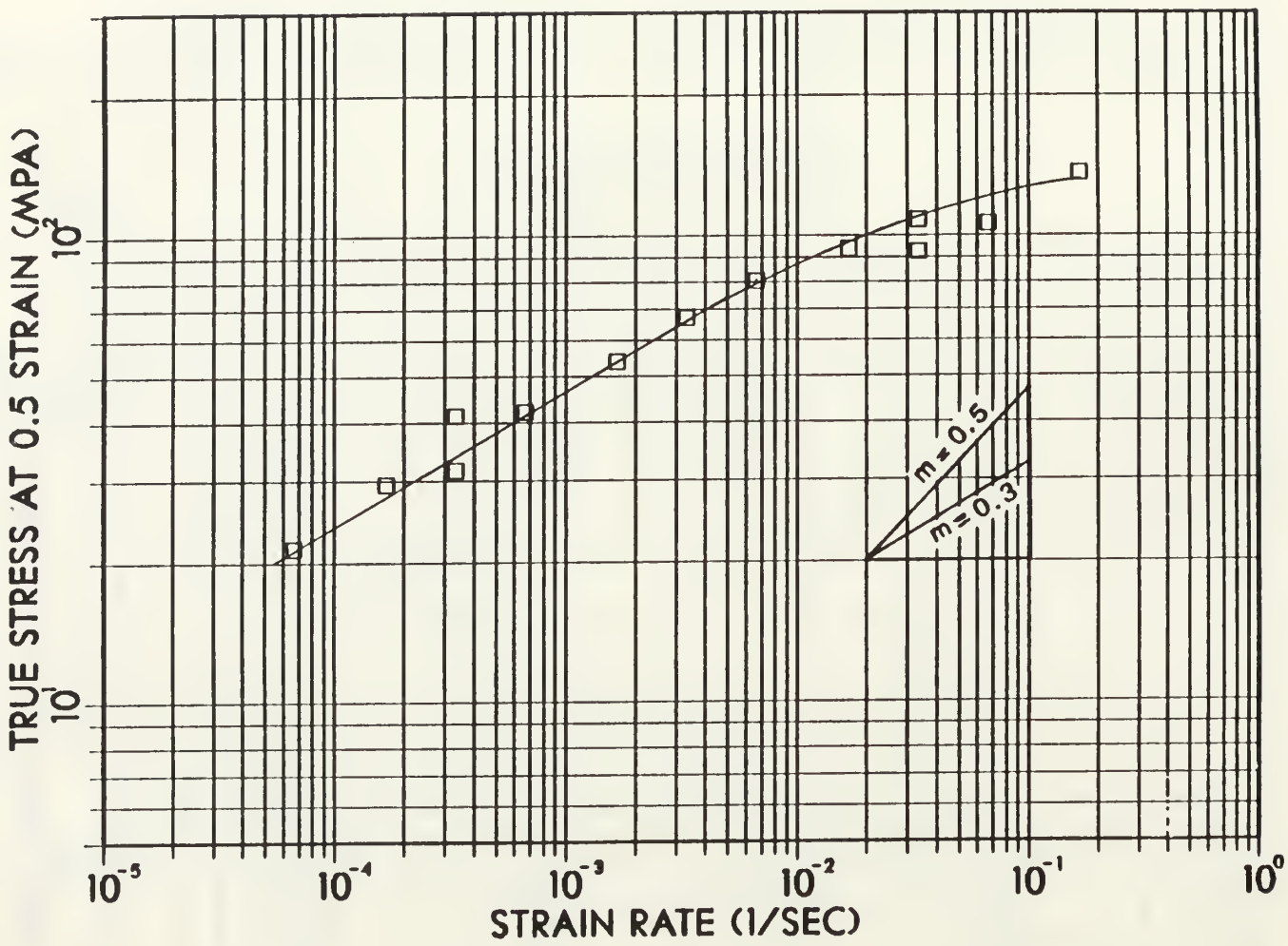

Figure B.10 True stress at 0.5 strain vs. strain rate for tests conducted at 300°C on Al-10%Mg-0.1%Zr. Solution treated, hot worked, oil quenched, and warm rolled at 300°C to 92% reduction.

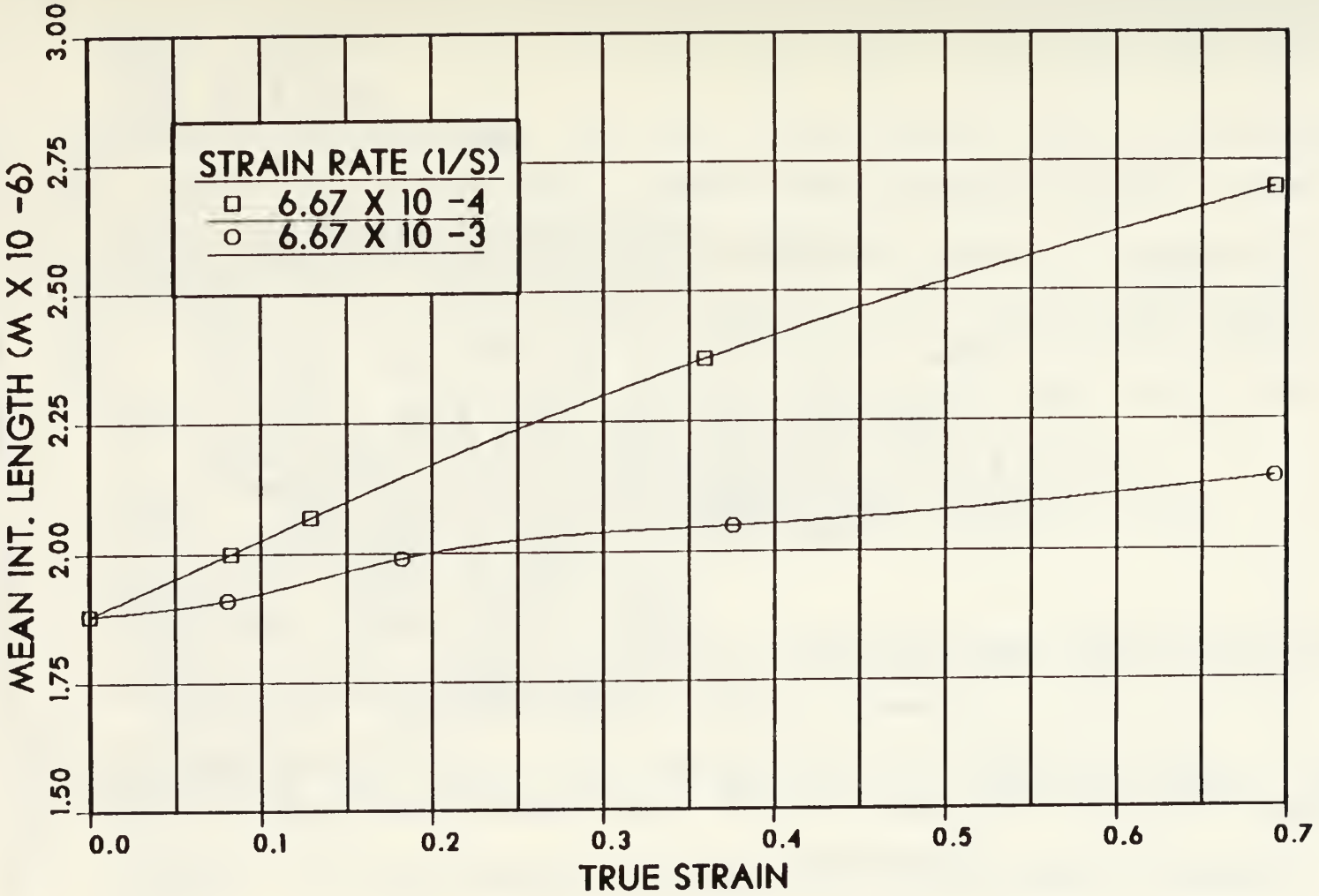

Figure B.11 Mean intercept length vs. true strain for tests conducted at 300°C on Al-10%Mg-0.1%Zr. Solution treated, hot worked, oil quenched, and warm rolled at 300°C to 92% reduction.

FILE: REDOX FORTRAN A

```
C      PROGRAM FOR DATA REDUCTION OF RAW DATA FROM TENSILE TESTING
C                                          13 NOV 1984
C
C     THIS PROGRAM REDUCES DATA CONTAINED IN INPUT FILE "TESTPTS DATA"
C     AND OUTPUTS THE REDUCED DATA TO OUTPUT FILE "REDOXPTS DATA".  THE
C     EXEC "REDOX" IS USED TO RUN THE PROGRAM (FILEDEFS, ETC.).
C
C         *****     VARIABLE DEFINITIONS     *****
C       STR(I) - ENG. STRESS  (PSI)
C       STRN(I) - ENG. STRAIN, CALCULATES WITH DECIMAL, OUTPUTS IN (%)
C       STRMPA(I) - ENG. STRESS  (MPA)
C       TRSTR(I) - TRUE STRESS (PSI)
C       TRSMPA(I) - TRUE STRESS (MPA)
C       TRSTRN(I) - TRUE STRAIN
C       MAG - MAGNIFICATION FACTOR, FROM "TESTPTS DATA"
C       FLOAD - FULL LOAD SCALE OF INSTRON, FROM "TESTPTS DATA"
C       W - SAMPLE GAGE WIDTH (IN.), FROM "TESTPTS DATA"
C       T - SAMPLE GAGE THICKNESS (IN.), FROM "TESTPTS DATA"
C       N - NUMBER OF DATA PTS, FROM "TESTPTS DATA"
C       AREA - SAMPLE GAGE CROSS-SECTIONAL AREA (SQ. IN.)
C
C     ***   VARIABLE AND CONSTANT DECLARATIONS   ***
C
      INTEGER N
      REAL W,T,AREA,FLOAD,MAG,ALOG
      DIMENSION X(30),Y(30),STR(30),STRMPA(30),TRSTR(30),TRSMPA(30)
      DIMENSION STRN(30),TRSTRN(30)
C
C     ***   READ IN INITIAL DATA, COMPUTE AREA, OUTPUT HEADING   ***
C
      READ (5,100)MAG,FLOAD
      READ (5,110)W,T
      READ (5,120)N
      AREA = W*T
C     WRITE (4,135)
```

```
C
C     ***   READ IN INDIVIDUAL DATA PTS & MAKE STRESS CALCS FOR EACH ONE
C
      DO 10 I=1,N
           READ (5,130)X(I),Y(I)
           STR(I) = Y(I)*FLOAD/(10.0*AREA)
C
C     ***   ***   ***   ***   ***   ***   ***   ***   ***   ***   ***   *
C     ***   NOTE: THIS IS FOR A GAGE LENGTH OF 0.5 IN., IF OLD SAMPLE   *
C     ***   GEOMETRY IS USED, THE 0.5 IN THE NEXT LINE MUST BE CHANGED  *
C     ***   TO 0.6.                                                     *
C     ***   ***   ***   ***   ***   ***   ***   ***   ***   ***   ***   *
C
           STRN(I) = X(I)/(MAG*0.5)
           STRMPA(I) = STR(I)*0.006896
           TRSTR(I) = STR(I)*(1.0+STRN(I))
           TRSMPA(I) = TRSTR(I)*0.006896
           TRSTRN(I) = ALOG(1.0+STRN(I))
           STRN(I) = 100*STRN(I)
C
C     ***   WRITE TO OUTPUT FILE   ***
C
           WRITE (4,140)X(I),Y(I),STR(I),STRMPA(I),TRSTR(I),
     *TRSMPA(I),STRN(I),TRSTRN(I)
  10     CONTINUE
 100   FORMAT(F4.0,F6.0)
 110   FORMAT(2(F6.3))
 120   FORMAT(I3)
 130   FORMAT(2(F6.2))
C135   FORMAT('1')
 140   FORMAT(' ',2(F6.2,2X),F8.1,2X,F7.3,2X,F8.1,2X,F7.3,2X,F6.2,2X,
     *F6.4)
       STOP
       END
```

FILE: CORRECT FORTRAN A

```
C     THIS PROGRAM IS USED TO CORRECT ENGR. AND TRUE STRAIN OF REDUCED
C     DATA TO COINCIDE WITH ELONGATION TAKEN OFF THE STRIP CHART.
C                                                        1 APRIL 1985
C
C
C     DATA IS READ IN FROM "ORIGPTS DATA" WHICH IS THE REDUCED DATA
C     FROM A SAMPLE PRECEDED BY A CORRECTION FACTOR PREVIOUSLY COMPUTED,
C     AND THE NUMBER OF DATA POINTS FOUND IN THE FILE. THE CORRECTED
C     DATA IS OUTPUT TO "CORPTS DATA".  THE EXEC "CORRECT" IS USED TO
C     RUN THE PROGRAM (FILEDEFS, ETC.).
C
      INTEGER N
      REAL CF
      DIMENSION A(30),B(30),C(30),D(30),E(30),F(30),G(30),H(30)
      DIMENSION Y(30),Z(30)
C
         READ (5,100)CF,N
         DO 10 I=1,N
              READ (5,110)A(I),B(I),C(I),D(I),E(I),F(I),G(I),H(I)
                   Y(I)=G(I)*CF
                   Z(I)=ALOG(1.0+(Y(I)/100))
              WRITE (4,120)A(I),B(I),C(I),D(I),E(I),F(I),Y(I),Z(I)
   10    CONTINUE
  100 FORMAT(F9.4,I4)
  110 FORMAT(F7.2,2X,F6.2,2X,F8.1,2X,F7.3,2X,F8.1,2X,F7.3,2X,F6.2,2X,
     *F6.4)
  120 FORMAT(' ',F7.2,2X,F6.2,2X,F8.1,2X,F7.3,2X,F8.1,2X,F7.3,2X,F6.2,
     *2X,F6.4)
      STOP
      END
```

FILE: REDOX EXEC A

```
GLOBAL TXTLIB FORTMOD2 MOD2EEH
DEF STOR 1M
I CMS
FILEDEF 04 DISK REDOXPTS DATA (PERM)
FILEDEF 05 DISK TESTPTS DATA (PERM)
LOAD REDOX (START
```


FILE: CORRECT EXEC A

```
GLOBAL TXTLIB FORTMOD2 MOD2EEH
DEF STOR 1M
I CMS
FILEDEF 04 DISK CORPTS DATA (PERM)
FILEDEF 05 DISK ORIGPTS DATA (PERM)
LOAD CORRECT (START
```

FILE: TESTPTS DATA A

```
100.  100.
  0.200  0.082
  18
149.20   0.00
119.00   0.15
100.50   0.55
 89.00   0.95
 80.70   1.15
 65.03   1.65
 51.36   2.15
 43.82   2.55
 31.89   3.25
 23.35   3.65
 17.20   3.75
 11.48   3.55
  8.80   3.30
  6.17   3.03
  3.00   2.45
  1.50   2.05
  0.50   1.70
  0.00   1.25
```

FILE: REDOXPTS DATA A

149.20	0.0	0.0	0.0	0.0	0.0	298.40	1.3823
119.00	0.15	91.5	0.631	309.1	2.132	238.00	1.2179
100.50	0.55	335.4	2.313	1009.5	6.961	201.00	1.1019
89.00	0.95	579.3	3.995	1610.4	11.105	178.00	1.0225
80.70	1.15	701.2	4.836	1833.0	12.640	161.40	0.9609
65.03	1.55	1006.1	6.938	2314.6	15.962	130.06	0.8332
51.36	2.15	1311.0	9.040	2657.6	18.327	102.72	0.7067
43.82	2.55	1554.9	10.722	2917.6	20.120	87.64	0.6294
31.89	3.25	1981.7	13.666	3245.6	22.382	63.78	0.4934
23.35	3.65	2225.6	15.348	3265.0	22.515	46.70	0.3832
17.20	3.75	2286.6	15.768	3073.2	21.193	34.40	0.2957
11.48	3.55	2164.6	14.927	2661.6	18.355	22.96	0.2067
8.80	3.30	2012.2	13.876	2366.3	16.318	17.60	0.1621
6.17	3.03	1847.6	12.741	2075.5	14.313	12.34	0.1164
3.00	2.45	1493.9	10.302	1583.5	10.920	6.00	0.0583
1.50	2.05	1250.0	8.620	1287.5	8.879	3.00	0.0296
0.50	1.70	1036.6	7.148	1047.0	7.220	1.00	0.0099
0.0	1.25	762.2	5.256	762.2	5.256	0.0	0.0

INITIAL DISTRIBUTION LIST

		No. Copies
1.	Defense Technical Information Center Cameron Station Alexandria, Virginia 22304-6145	2
2.	Library, Code 0142 Naval Postgraduate School Monterey, California 93943-5100	2
3.	Department Chairman, Code 69Mx Department of Mechanical Engineering Naval Postgraduate School Monterey, California 93943-5100	1
4.	Professor T. R. McNelley, Code 69Mc Department of Mechanical Engineering Naval Postgraduate School Monterey, California 93943-5100	5
5.	Mr. Richard Schmidt, Code AIR 320A Naval Air Systems Command Naval Air Systems Command Headquarters Washington, DC 20361	1
6.	Dr. Eui-Whee Lee, Code 6063 Naval Air Development Center Warminster, Pennsylvania 18974	1
7.	LT Mark E. Alcamo 2640 Hubbard Dearborn, Michigan 48124	3

Thesis
A3382
c.2

Alcamo
Effect od strain and strain rate on the microstructure of a superplastically deformed Al-10%Mg-0.1%Zr alloy.